BRNO UNIVERSITY OF TECHNOLOGY

Faculty of Chemistry

DOCTORAL THESIS

Brno, 2017

Ing. Adam Hoza

BRNO UNIVERSITY OF TECHNOLOGY
VYSOKÉ UČENÍ TECHNICKÉ V BRNĚ

FACULTY OF CHEMISTRY
FAKULTA CHEMICKÁ

INSTITUTE OF MATERIALS SCIENCE
ÚSTAV CHEMIE MATERIÁLŮ

EFFECT OF ETHYLENE AND PROPYLENE ON PERFORMANCE OF ZIEGLER - NATTA CATALYST IN STOPPED - FLOW POLYMERIZATION

EFFECT OF ETHYLENE AND PROPYLENE ON PERFORMANCE OF ZIEGLER - NATTA CATALYST IN STOPPED - FLOW POLYMERIZATION

DOCTORAL THESIS
DIZERTAČNÍ PRÁCE

AUTHOR
AUTOR PRÁCE

Ing. Adam Hoza

SUPERVISOR
ŠKOLITEL

Ing. Jan Kratochvíla, CSc.

BRNO 2017

VYSOKÉ UČENÍ TECHNICKÉ V BRNĚ
FAKULTA CHEMICKÁ

Zadání dizertační práce

Ústav:	Ústav chemie materiálů
Student:	**Ing. Adam Hoza**
Studijní program:	Makromolekulární chemie
Studijní obor:	Chemie makromolekulárních materiálů
Vedoucí práce:	**Ing. Jan Kratochvíla, CSc.**
Akademický rok:	2016/17

Název dizertační práce:

Effect of Ethylene and Propylene on Performance of Ziegler – Natta Catalyst in Stopped – Flow Polymerization

Zadání dizertační práce:

Cílem práce bude příprava a charakterizace nových typů materiálů na bázi blokových kopolymerů technikou“ stopped–flow“. K tomuto účelu bude zkonstruována experimentální aparatura umožňující technikou“ stopped–flow“ syntézu dostatečného množství materiálu pro cílenou modifikaci vybraného komerčního sekvenčního kopolymeru polypropylenu.

Termín odevzdání dizertační práce: 19.5.2017

Ing. Adam Hoza student(ka)	Ing. Jan Kratochvíla, CSc. vedoucí práce	prof. RNDr. Josef Jančář, CSc. vedoucí ústavu

prof. Ing. Martin Weiter, Ph.D.
děkan

V Brně dne 1.9.2016

ABSTRAKT

Výzkum v této práci byl zaměřen na přípravu a charakterizaci blokových kopolymerů typu polypropylen-*blok*-poly(propylenu-co-ethylenu) (dále jen PP-*blok*-EPR). Tyto materiály jsou považovány za účinné kompatibilizátory mezi semi-krystalickou polypropylenovou (PP) matricí a amorfními doménami statistického kopolymeru propylenu a etylenu (EPR) v rázuvzdorném sekvenčním kopolymeru (ICP) a proto byl výzkum zaměřen na zkoumání vlivu přídavku blokového kopolymeru PP-blok-EPR na vlastnosti komerčního ICP. Blokové kopolymery byly připraveny za použití techniky „stopped-flow". Pro tento účel byla zkonstruována vysokotlaká polymerační „stopped-flow" aparatura, která umožňuje syntézu kopolymerů PP-*blok*-EPR za podmínek blízkých podmínkám v průmyslových reaktorech pro výrobu komerčních ICP materiálů. Aparatura umožňuje vyrábět PP-*blok*-EPR polymer v množství dostačující na jeho charakterizaci a následnou přípravu směsí s komerčním ICP. Velmi krátké polymerační časy (obvykle kolem 0.2 s) kterých bylo dosaženo v kapilárním reaktoru aparatury „stopped-flow" zajišťuje, že aktivní centra Ziglorova-Nattova katalyzátoru produkují polymer řetězce skládající se z bloku semikrystalického polypropylenu a bloku amorfního EPR kopolymeru. Takovéto molekuly jsou v literatuře popsány jako „skutečné blokové kopolymery PP-blok-EPR".

Kopolymery syntetizované v aparatuře „stopped-flow" byly frakcionovány preparativní TREF (Temperature Rising Elution Fractionation) metodou a získané frakce byly následně analyzovány pomocí DSC, ^{13}C-NMR a GPC/SEC. Tyto analýzy odhalily přítomnost amorfního EPR ve vysoce krystalické frakci (100-140 °C). Toto zjištění potvrdilo, že významná část polymerních řetězců, připravených v aparatuře „stopped-flow" jsou blokové kopolymery skládající se z bloku semikrystalického PP homopolymeru a bloku amorfního EPR kopolymeru v jednom polymerním řetězci.

Kopolymery získané metodou „stopped-flow byly v tavenině smíchány s komerčním rázuvdorným kopolymerem ICP. U takto připravených směsí byly vyhodnoceny mechanické vlastnosti, DTMA a reologické vlastnosti a výsledky byly srovnány s vlastmi původního komerčního ICP kopolymeru. Dále byly studovány rozdíly v morfologii a umístění EPR domén v matrici PP prostřednictvím SEM.

Zřetelný vliv kopolymeru PP-blok-EPR na vlastnosti ICP byl pozorován zejména v morfologických změnách EPR domén dispergovaných v PP matrici. Tyto změny mají pozitivní vliv na rovnováhu mezi modulem v ohybu a rázovou pevností ICP materiálu. Vliv kopolymeru PP-blok-EPR na reologické vlastnosti ICP byl nevýznamný. Podobně také v případě DTMA nebyl pozorován významný vliv kopolymeru PP-blok-EPR na vlastnosti ICP.

KLÍČOVÁ SLOVA

Stopped-flow, blokový kopolymer, polypropylén

ABSTRACT

The research presented in this thesis focused on the preparation and characterization of polypropylene-block-poly(propylene-co-ethylene) (hereinafter referred to also as PP-block-EPR). These materials are considered to be efficient compatibilizers between a semi-crystalline polypropylene (PP) matrix and amorphous ethylene/propylene rubber (EPR) domains in impact-resistant polypropylene copolymers (ICP). The effect of prepared PP-block-EPR copolymers on properties of commercial ICP materials was investigated. The unique PP-block-EPR copolymers were prepared by using the "stopped-flow" technique. For this purpose a high-pressure stopped-flow polymerization apparatus was constructed. This apparatus allowed the synthesis of PP-block-EPR copolymers under conditions comparable to conditions applied in industrial reactors for the production of standard ICP materials. The apparatus also enabled the production of sufficient amounts of materials for characterizing and subsequent blending with ICP. Very short polymerization times (typically around 0.2 s) applied in stopped-flow capillary reactors ensured that the active sites of a Ziegler-Natta catalyst produced polymer chains consisting of a block of semi-crystalline polypropylene (PP) and a block of amorphous ethylene/propylene random copolymer (EPR). Such macromolecules are described in the literature as real PP-block-EPR copolymers.

Copolymer materials synthesized in the stopped-flow apparatus were fractionated by the preparative means of Temperature Rising Elution Fractionation (TREF). The fractions obtained were subsequently analysed by DSC, ^{13}C-NMR and GPC/SEC methods. These analyses revealed the presence of EPR, also in a crystalline fraction (100 – 140 °C). This finding confirmed that a noticeable portion of polymer chains, produced in the stopped-flow polymerization, were real block copolymers consisting of semi-crystalline PP homopolymer and amorphous EPR copolymer in one polymer chain.

The prepared samples were blended in melt with a commercial ICP material. Tensile properties, DTMA and oscillation rheology were evaluated on the prepared blends and the results compared with the properties of the original ICP copolymer. Furthermore, the differences in EPR domain morphology and location in the PP matrix were studied by SEM.

The obvious influence of the PP-block-EPR copolymer on ICP properties was observed mainly in morphological changes of the EPR domains dispersed in the PP matrix. These changes showed a positive influence on the balance between the flexural modulus and the impact strength of ICP material. The influence of the PP-block-EPR copolymer on ICP rheology was insignificant. Similarly, also in the case of DTMA no obvious influence of PP-block-EPR copolymer on the dynamic-mechanical properties of ICP was observed.

KEYWORDS

Stopped-Flow, block copolymer, polypropylene

HOZA, A. *Effect of Ethylene and Propylene on Performance of Ziegler - Natta Catalyst in Stopped - Flow Polymerization.* Brno: Vysoké učení technické v Brně, Fakulta chemická, 2017. 113 s. Vedoucí dizertační práce Ing. Jan Kratochvíla, CSc.

PROHLÁŠENÍ

Prohlašuji, že jsem dizertační práci vypracoval samostatně a že všechny použité literární zdroje jsem správně a úplně citoval. Dizertační práce je z hlediska obsahu majetkem Fakulty chemické VUT v Brně a může být využita ke komerčním účelům jen se souhlasem vedoucího dizertační práce a děkana FCH VUT v Brně.

.....
podpis studenta

ACKNOWLEDGEMENTS

I would like to thank to the company UNIPETROL RPA, s.r.o. - POLYMER INSTITUTE BRNO, odštěpný závod for their support of my research and opportunity to work with their sophisticated equipment.

Furthermore, I thank to the W.R. Grace & Co. company for providing the catalyst for the research.

I would like to express sincerely thanks to my supervisors and Jan Kratochvíla, Igor Cejpek for their help, encouraging support and great interest in my work.

I would like to thank my colleagues Miroslav Skoumal and Jan Grůza for their support and useful advices.

My thanks belong also to Zdeněk Buráň, Jiří Sadílek, Petra Zbořilová, Martin Vik, Klára Jindrová, Radek Matuška Pavla Bartášková and Zlata Vrátníčková for providing me with measurement and analyzes.

Finally I want to thank to my family for support and encouragements over the all years of my studies. This work is dedicated mainly to them.

CONTENTS

1 INTRODUCTION

Despite several decades of research efforts since 1953, many aspects of active site structure and polymerization mechanisms in Ziegler-Natta catalysis still remain unclear. Comprehension of the fundamental mechanisms has therefore apparently progressed more slowly than the commercial development of the polymerization catalysts [1].

The complexity of the polymerization mechanism in Ziegler-Natta catalysis could be demonstrated on a comparison of Ziegler-Natta catalyst performance in presence of ethylene and propylene monomers. Figure 1 demonstrates the kinetics of propylene and ethylene homopolymerization reactions with the same catalyst system at the same temperature. The figure indicates that active sites in the ethylene polymerization reaction are formed at a lower rate, but are apparently more stable than active sites formed in the propylene polymerization reaction [2]. The active sites are formed relatively slowly in the ethylene homopolymerization, but when the maximum of polymerization rate is reached, the sites remain stable for several hours [2].

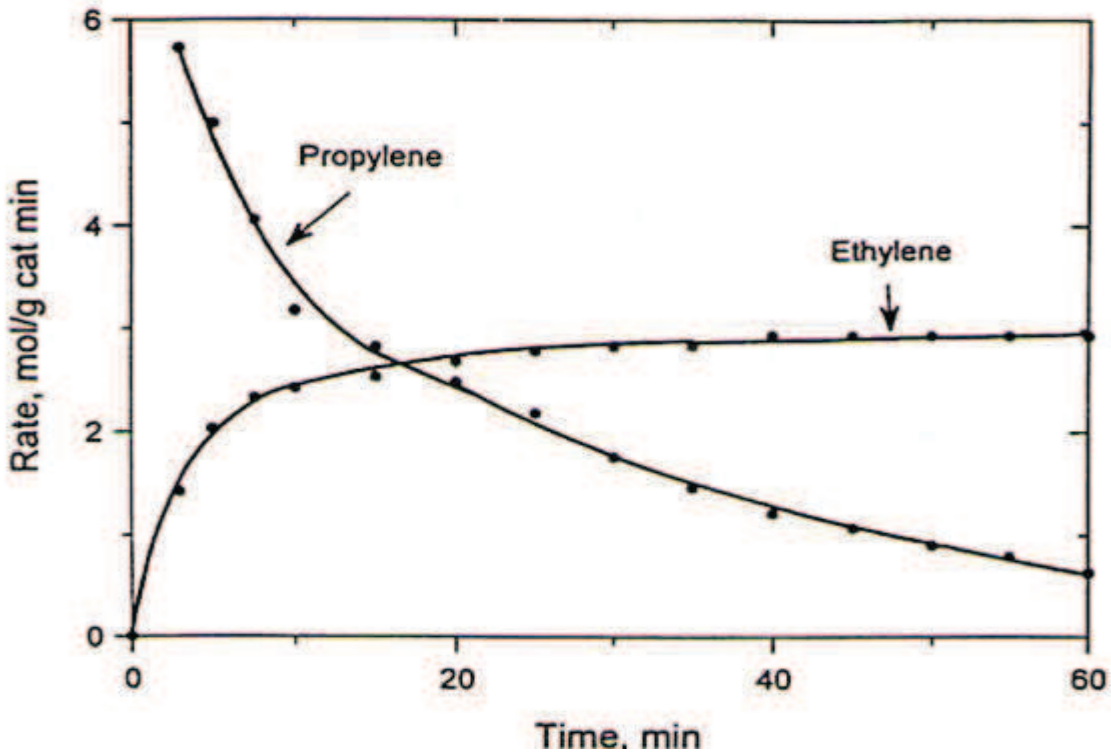

Figure 1: Comparison of ethylene and propylene homopolymerization kinetics with catalyst system $TiCl_4$/DBP/$MgCl_2$-TEA/$PhSi(OEt)_3$ in n-heptane at 70 °C. The monomer concentrations are 1.24 M (ethylene) a 1.12 M (propylene) [2].

1.1 STOPPED-FLOW TECHNIQUE FOR 1-ALKENE POLYMERIZATION

In a conventional process of propylene or ethylene polymerization with a $MgCl_2$-supported Ziegler-Natta catalyst, the polymerization is usually performed for 1 – 3 hours during which the polymerization rate varies. The change, typically a

decrease, in polymerization rate over time is caused by various chain-transfer reactions together with changing the active sites performance [3].

Conversely stopped-flow polymerization is conducted within an extremely short time period (tenths of second). The most predominant feature of the stopped-flow technique is its quasi-living polymerization characteristic, as demonstrated in Figure 2. The polymerization time in the stopped-flow apparatus is shorter than the average lifetime of the growing polymer chain, which ensures that the states of active sites are not significantly influenced by time-dependent changes and chain-transfer reactions [1, 4].

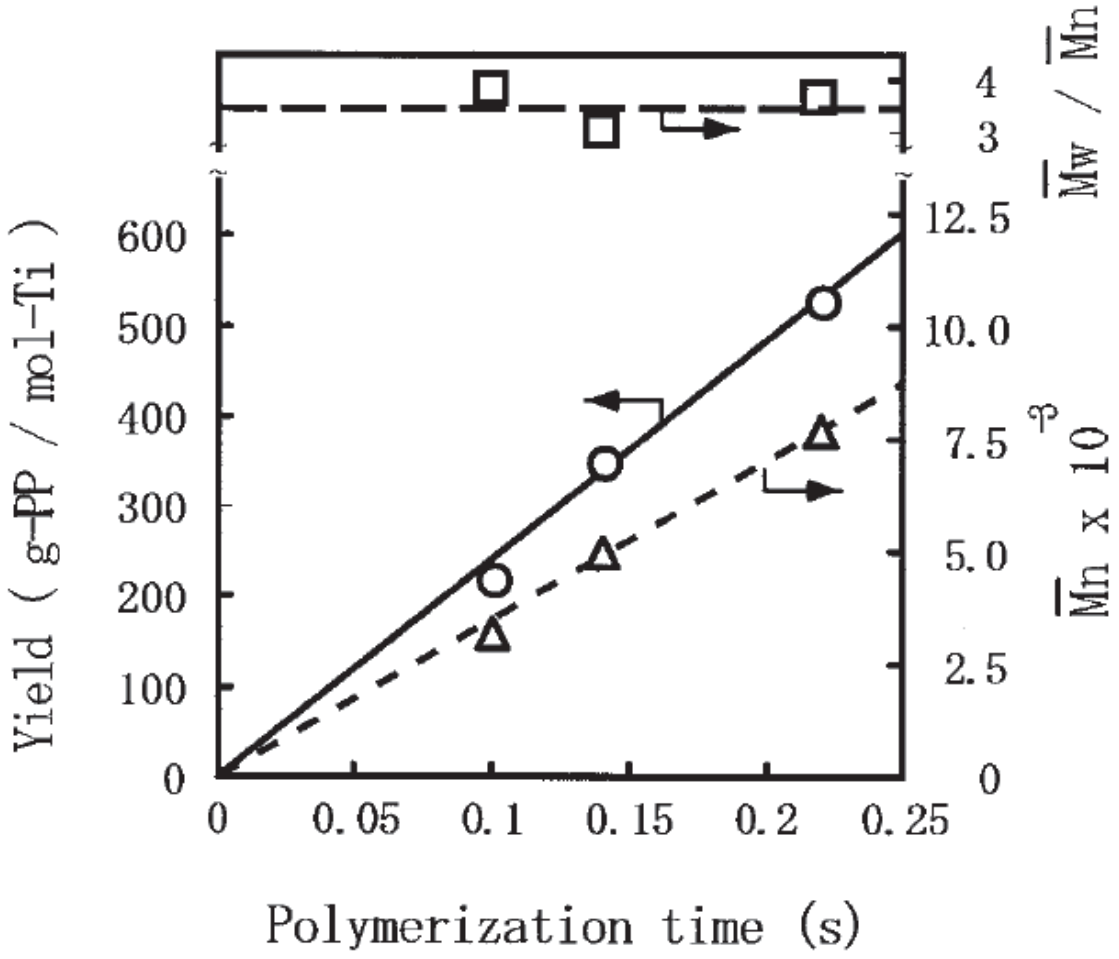

Figure 2: Dependence of yield, $\overline{M_n}$ and $\overline{M_w}/\overline{M_n}$ on polymerization time. $MgCl_2$/EB/$TiCl_4$ catalyst: 1.1 g, TEA: 14 mmol, Al/Ti molar ratio: 30, heptane: 200 ml, [propylene] = 0.50 mol/l, temperature: 30 °C [1].

One of the most attractive features of this method is the ability to obtain the polymer produced in the initial polymerization stage, which directly reflects the nature of the active sites just after their formation. Accordingly, the method was found to be useful for the study of the nature of the active sites, as well as for the assessment of their kinetic parameters [5, 6].

Characteristics such as the constant polymerization rate and negligible chain-transfer reactions within an extremely short period of time cannot be achieved by any other polymerization technique used for investigation of Ziegler-Natta catalysts [1].

The stopped-flow technique has been proven to be a powerful tool for elucidating kinetic mechanisms and polymer particle morphology [3, 6]. Keii and Terano were the first who utilized the stopped-flow method to follow the kinetics of propylene polymerization with an $MgCl_2$-supported Ziegler–Natta catalyst, in 1987 [7]. This technique was originally developed by Chance in the early forties for studying fast enzyme reactions [8].

In its basic form a principle of stopped-flow technique is as follow: Two reagents are driven through tubes to come into contact, then the reagents flow mixed together for a certain time into a flask containing a quenching agent. In order to be able to utilize the stopped-flow technique, it is necessary to meet the following requirements [1]:

- The active sites on the catalyst have to be formed by interaction with the co-catalyst instantaneously. Thus perfect mixing of catalyst and co-catalyst is required.
- The time required for the formation of the active sites at the beginning of the polymerization must be negligible compared with the polymerization time.
- Stirring of the catalyst slurry in the vessel should be efficient in order to avoid temperature and concentration gradients.
- During polymerization the flow velocity has to be constant.
- Monomer conversion has to be kept below ca. 10 % so as to be able to ignore the changes in monomer concentration and polymerization temperature.
- Polymerization has to be terminated immediately and completely after the reaction in order to avoid deviations in polymerization time and to be able to ignore the unfavourable side reactions induced by slow and/or reversible termination reactions.
- A sufficient amount of polymer has to be obtained to perform all the required analytical measurements.

1.1.1 Stopped-Flow Polymerization Apparatus

The basic stopped-flow polymerization system with two vessels has been extensively applied to study the homopolymerization and non-block-type copolymerization of olefins. A schematic drawing of the stopped-flow apparatus is shown in Figure 3. In the case of a typical polymerization procedure, the catalyst slurry and the co-catalyst solution, both saturated with monomer, flow simultaneously through a Teflon tube from vessels A and B into flask C containing a quenching agent. Polymerization is running in the PTFE tube from point X to point Y, and then the reaction is terminated in the quenching vessel. The time of polymerization can be adjusted by changing the length of the polymerization tube or by changing the flow rate of catalyst components [1, 4, 9, 10].

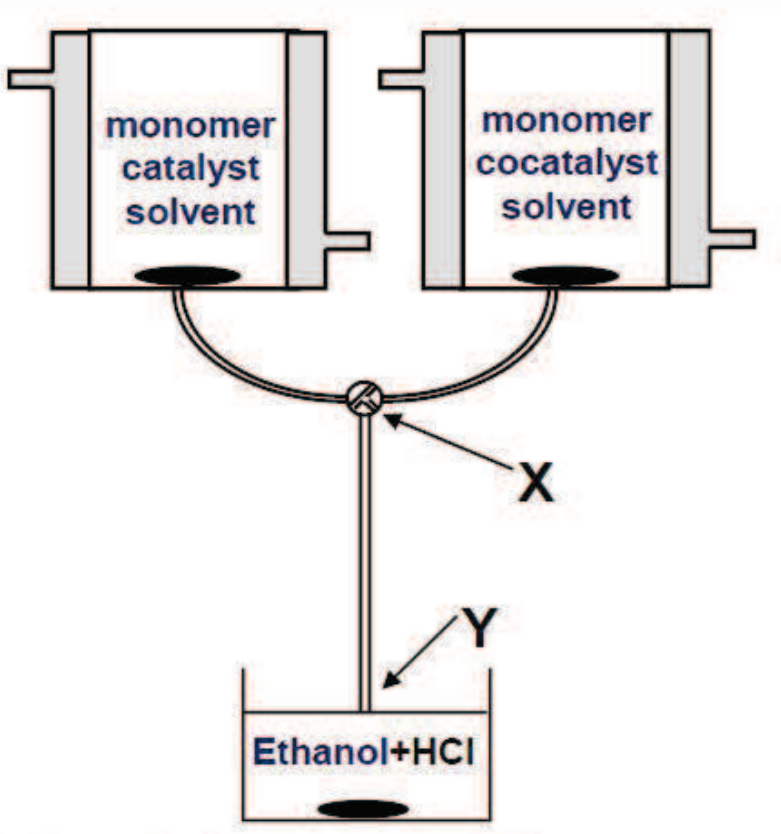

Figure 3: Schematic illustration of Stopped-Flow polymerization apparatus [1].

One of the most important features of the stopped-flow technique, quasi-living polymerization, can be utilized to synthesize olefin block copolymers with well-defined structures [1]. Research on catalyst pre-treatment within a very short period and synthesis of special block copolymers is performed using a three-vessel stopped-flow apparatus, which is schematically illustrated in Figure 4. Here, the catalyst slurry and the co-catalyst solution with propylene are placed in vessels A and B, respectively. The solution saturated with ethylene is in vessel C. The polymerization of propylene proceeds in the Teflon tube between points X and Y, then the subsequent copolymerization of propylene with ethylene takes place between points Y and Z. At point Z the polymerization is terminated [1, 9].

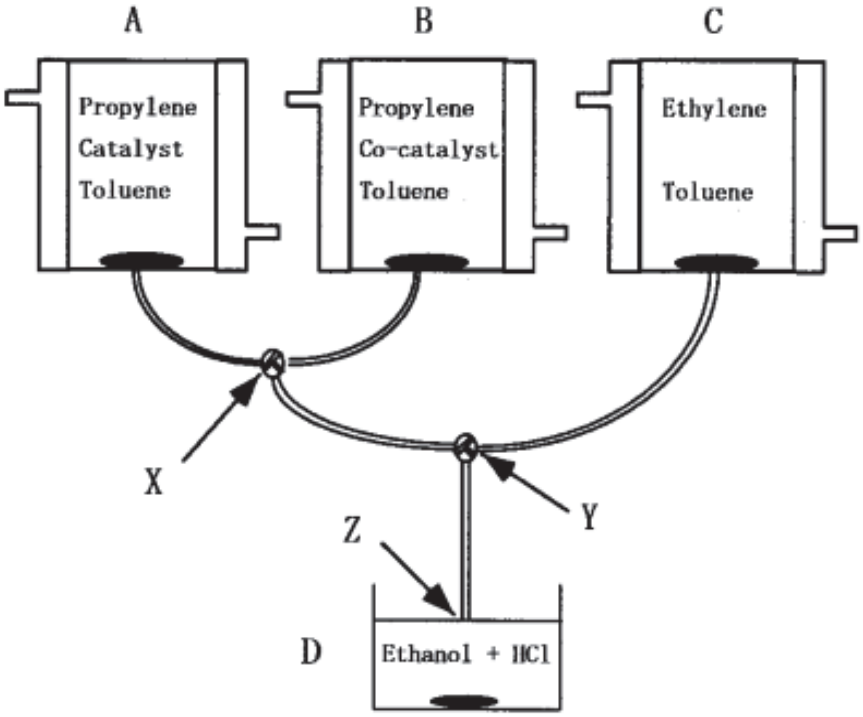

Figure 4: Three-vessel-type Stopped-Flow apparatus for synthesis of block copolymers [1].

1.2 KINETICS OF 1-ALKENE POLYMERIZATION WITH $MgCl_2$-SUPPORTED CATALYST

The stopped-flow technique has been proven to be one of the powerful methods for studying the state of the active site and elucidating the complex mechanism of coordination polymerization [1, 4, 5, 3, 6].

Di Martino et al. [11] performed an experiment with polymerization times up to 1.4 s in a quenched-flow reactor. They observed a rapid increase of polymerization rate to a maximum value of over 60 kg/(g*h), followed by a rapid decay to a ‘‘steady-state’’ rate of 9 kg/(g*h) after about 1 s of reaction.

Terano et al. [10] proved that active site formation was completed within 0.1 s. Mori et al. [4] obtained results indicating that the formation of active sites occurs even faster, within ca. 0.01 s.

A wide range of plausible mechanisms have been proposed as an explanation for catalyst decay during the polymerization [12, 13]:

Kissin [2, 14] suggested that highly isospecific Ti-based Ziegler–Natta catalysts contain five types of active site [15] divided into two families:

The sites of the first family (sites I–III in Figure 5) are able to polymerize and copolymerize α-olefins and ethylene. During copolymerization these sites produce random ethylene/α-olefin copolymers. These sites are relatively unstable from a kinetic point of view. In the case of $TiCl_4/MgCl_2$ catalysts activated by $AlEt_3$ and modified by silanes, most of these sites are isospecific. The active sites of the first family are formed significantly faster and decay faster in comparison with active sites

of the second family. The rate constant of deactivation k_d is ca. 5 to 15 times higher than the k_d of the second family sites [2].

The second family sites (sites IV and V in Figure 5) can efficiently polymerize only ethylene, and, when exposed to mixtures of ethylene and 1-alkene, they incorporate 1-alkene molecules into polymer chains very poorly. These sites are not able to homopolymerize 1-alkenes, but from a kinetic point of view they are relatively stable [2].

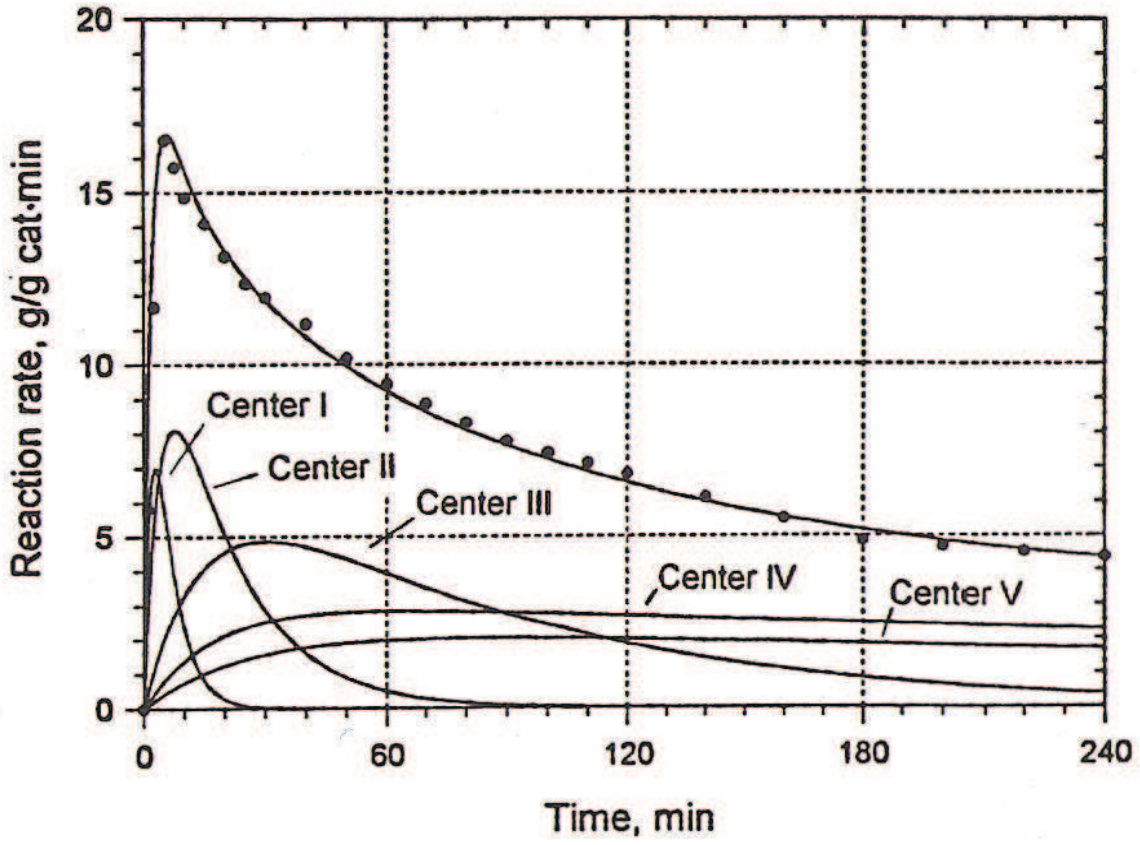

Figure 5: Deconvolution of the kinetic curve in ethylene/1-hexene copolymerization at 85 °C with the $TiCl_4$/DBP/$MgCl_2$-TEA system (without hydrogen). Points: experimental data, lines: calculated kinetic profiles for each site [16].

This theory has been supported by other authors [17, 18, 19, 20]. Chien et al. [12] reported that deactivation occurs regardless of the presence of a monomer, and it is caused by the interaction of the catalyst with an alkyl-aluminium compound. Alkyl-aluminium reduces Ti^{3+} to lower oxidation states, mainly Ti^{2+} [12]. Busico et al. [13] observed that the Ti^{2+} and lower oxidation states were inactive in propylene polymerization. The presented explanation of activity deceleration is suitable for 1-alkene polymerization, but in the case of ethylene it was proven that the Ti^{2+} species were still active [13, 17, 18, 21, 22].

Luo et al. [23] determined that during the 5 h period of polymerization the fraction of Ti^{3+} active sites decreased rapidly to zero and Ti^{2+} active sites reached a

maximum value of ca. 24 % after 2 h of polymerization. The fraction of Ti^{2+} active sites then declined to ca. 5 % in the next 4 h of polymerization.

The irregular (2,1)-monomer insertion into the growing chain (Figure 6) is considered a major reason for activity decay in propylene polymerization [2, 21, 24, 25, 26, 27, 28]. This irregular (2,1)-monomer insertion causes the highly isospecific active sites to be practically incapable of further propylene insertion, mainly due to the relatively high stability of the formed complex and also for steric reasons. Hydrogen converts the $Ti–CH(CH_3)_2$ group into a Ti–H group, which reactivates the polymerization site. This could explain the hydrogen-activation effect observed in propylene polymerization. It is known that the reactivation of irregular (2,1)-inserted propylene units is up to 1000 times slower than regular (1,2)-insertion [2].

Busico et al. [26] determined that in the case of an $MgCl_2$-supported catalyst ca. 10 – 30 % of all active sites are for a certain time in a “dormant” state.

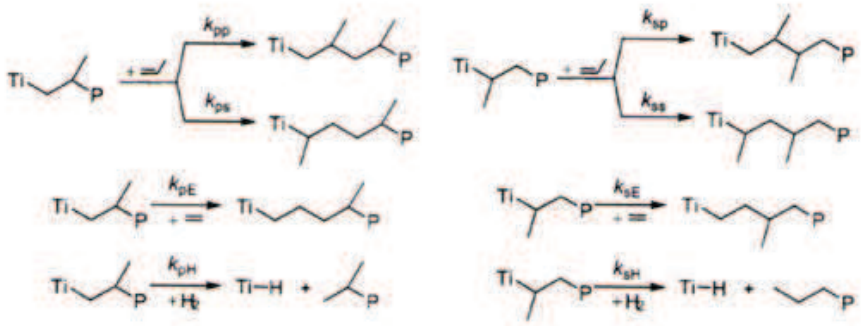

Figure 6: Regular (1,2) and irregular (2,1) insertion of propylene and subsequent reactivation with ethylene or hydrogen [26].

Another explanation of dormant site formation was proposed by Guyot et al. [29]. They suggest that the dormant site arises from a monomer transfer reaction. This transfer reaction leads to a stable dormant π-allyl structure (Figure 7), and it is dominant mainly after the (2,1)-insertion.

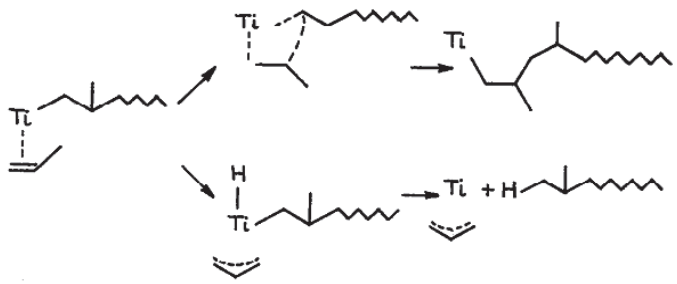

Figure 7: Proposed mechanism of dormant π-allyl site formation [29].

Some researchers assume that the rapid polymerization rate decrease could be caused by a physical phenomenon based on limitation of monomer diffusion due to encapsulation of the catalyst by the polymer layer [12, 21, 30, 31].

Han-Adebekun [19] determined that during the polymerization the polymer was partially melted at relatively high reaction temperatures. The resulting limitation of the diffusion is believed to be partially responsible for the observed activity decrease at such elevated temperatures.

A novel insight into catalyst deactivation was presented by Lim and Choung [32]. They assumed that catalyst deactivation was caused by a combination of chemical and physical phenomena, such as reduction of titanium active sites and monomer diffusion resistance.

Kisin et al. [33] proposed a plausible explanation of catalyst deactivation in the case of ethylene polymerization. They assumed that the relatively stable Ti–C_2H_5 complex is formed in ethylene polymerization reactions each time after ethylene insertion into the Ti–H bond as well as after each step of the chain transfer with the monomer (Figure 8). When modelling kinetics they estimated that the relative stability of the Ti–C_2H_5 complex keeps a large fraction of the active sites in ethylene polymerization (70 – 75 %) in the "dormant" state [2]. The frequency of Ti–H bond formation (followed by generation of the Ti–C_2H_5 complex) is significantly increased in the presence of hydrogen. This mechanism is considered as a suitable explanation of why the addition of hydrogen decreases the rate of ethylene polymerization. In ethylene/1-alkene copolymerization reactions, the 1-alkene molecule is inserted into the Ti–H bond and this reaction by-passes the stage of the stable Ti–C_2H_5 complex, and thus the polymerization rates (copolymerization of ethylene with 1-alkene) are apparently higher in comparison with ethylene homopolymerization performed under the same conditions [26, 33].

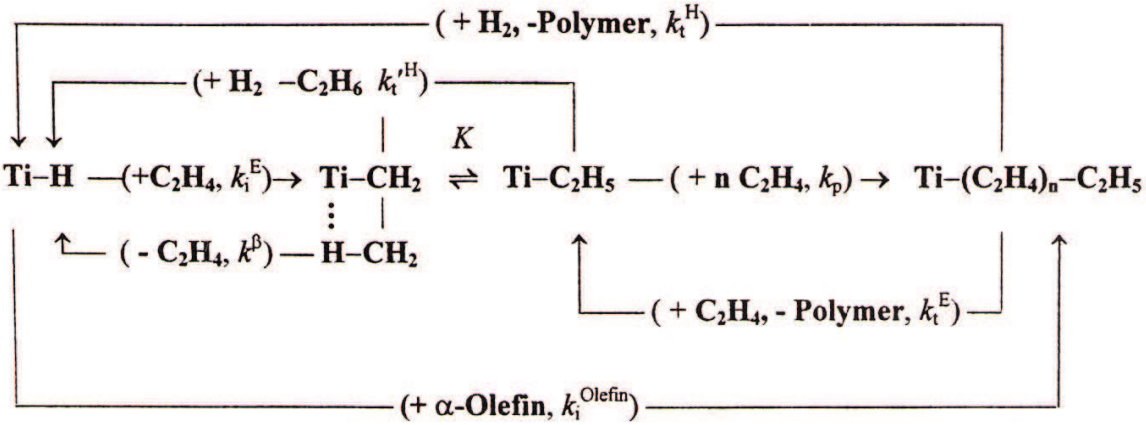

Figure 8: Schematic illustration of the equilibrium between active and dormant sites in ethylene polymerization [33].

The promoting effect of comonomer on 1-alkene polymerization is well-known. It is known that addition of a 1-alkene comonomer to ethylene apparently enhances the polymerization rate even at relatively small concentrations of the 1-alkene comonomer. This effect is well described in the literature [13, 16, 18, 24, 34, 35, 36, 37, 38].

The described effect depends on the nature of the catalyst system and on the length of the carbon chain of the 1-alkene comonomer. The effect could be attributed to various chemical and physical factors [35]:

- modification of the propagation rate constant (formation of a new type of active site by a reaction involving 1-alkene molecules) [12, 13, 18, 21, 22, 23, 29]
- an increase in the amount of active sites (activation of new sites or reactivation of dormant sites by comonomer) [2, 26]
- diffusion phenomena (change of monomer concentration in the vicinity of the active site) [32, 30]

1.2.1 Polymerization Kinetics

Several theories have been postulated to clarify the kinetics of catalyst deactivation during 1-alkene polymerization [33, 38].

Kissin [39] considers first-order decay to be satisfactory for the characterization of kinetic curves. He proposed that the polymerization system contains two types of active site, stable ones and highly unstable ones. Then the total amount of active sites in the polymerization can be expressed as follows:

$$[C^*] = [C_1^*] + [C_2^*] \qquad (1)$$

The concentration of the stable active sites $[C_2^*]$ remains almost unchanged during the polymerization and corresponds to the stationary part of the kinetic curve. The unstable sites$[C_1^*]$, which undergo rapid deactivation, are responsible for the activity decay.

Assuming that the active site deactivation rate depends only on catalyst concentration, the decrease in the concentration of active sites $[C_i^*]$ could then be defined as a first-order reaction with a deactivation rate constant k_{di} [21, 39, 40, 41].

$$-\frac{d[C_i]}{dt} = k_{di} \cdot [C_i^*] \qquad (2)$$

After integration, $[C_i^*]$ at varying time t is given as:

$$[C_{i,t}^*] = [C_{i,0}^*] \cdot \exp(-k_{di} \cdot t) \qquad (3)$$

where $[C_{i,0}^*]$ is the initial concentration of the active sites.

The overall polymerization rate Rp could be described by the following equation [41]:

$$R_p = k_p \cdot [M] \cdot [C^*] \qquad (4)$$

where [M] is monomer concentration and k_p the propagation rate constant.

So combining equation (3) and (4) gives the kinetic equation:

$$R_{p,t} = k_p \cdot [M] \cdot [C_i^*] \cdot \exp(-k_{di} \cdot t) \qquad (5)$$

The equation can also be rewritten in the form:

$$R_{p,t} = R_{p,0} \cdot \exp(-k_{di} \cdot t) \qquad (6)$$

where $R_p(t)$ and $R_p(0)$ are the polymerization rates at time t and t = 0, respectively.

Thus, the catalyst system with more types of active site, deactivating with different rate constants, could be expressed as the sum of kinetic equations:

$$R_{p,t} = \sum R_{pi,0} \cdot \exp(-k_{di} \cdot t) \qquad (7)$$

Some of the models use the Langmuir-Hinshelwood adsorption isotherms, assuming the competitive reversible adsorption reaction of monomer and alkyl-aluminium to the active sites [38, 10]. The overall polymerization rate is given as:

$$R_p = k_p \cdot [C^*] \cdot \frac{K_M \cdot [M]}{1 + K_A \cdot [A] + K_M \cdot [M]} \qquad (8)$$

where k_p represents the propagation rate constant, [A] is the concentration of co-catalyst, [M] is the concentration of monomer, and K_M and K_A are the equilibrium adsorption constants of monomer and alkyl-aluminium

As the activation of unstable sites occurs over a very short period (<0.1 s), only the deactivation profile could be determined by the techniques applied.

Skoumal [42] constructed a kinetic function on the basis of a commonly used kinetic model expressed by equation (4) combined with the kinetic equation of the *n-th* order of deactivation described by Al-Haj Ali [43]:

$$-\frac{d[C_i]}{dt} = k_{di} \cdot [C_i^*]^n \qquad (9)$$

However, the presented equation (9) has only an empirical meaning. Then the combination of expressed equations gives the general function for the description of fast deactivation of unstable sites according to *n-th* order deactivation reaction kinetics:

$$R_{p,t}\mathrm{f} = \left[R_{p,0}\mathrm{f}^{1-n} + (n-1) \cdot K_D \cdot [M]^{1-n} \cdot t\right]^{\frac{1}{1-n}};\ K_D = k_p^{1-n} \cdot k_{df} \qquad (10)$$

The integral form is expressed as the dependence of yield on polymerization time:

$$Y_t\mathrm{f} = \frac{R_{p,0}\mathrm{f}^{2-n} - \left[R_{p,0}\mathrm{f}^{1-n} + (n-1) \cdot K_D \cdot [M]^{1-n} \cdot t\right]^{\frac{2-n}{1-n}}}{(2-n) \cdot K_D \cdot [M]^{1-n}};\ n \neq 1, n \neq 2 \qquad (11)$$

To describe the stable active sites a kinetic function with first order activation followed by first order deactivation (subsequent reactions) was applied. Then the derivative and integral form could be expressed:

$$R_{p,t}\mathrm{s} = \left(1 - \exp(-k_a \cdot t)\right) \cdot \left(R_{p,0}\mathrm{s} \cdot \exp(-k_{ds} \cdot t)\right) \qquad (12)$$

$$Y_t\mathrm{s} = \frac{R_{p,0}\mathrm{s}}{(-k_{ds})} \cdot \left(\exp(-k_{ds} \cdot t) - 1\right) - \frac{R_{p,0}\mathrm{s}}{(-k_a - k_{ds})} \cdot \left(\exp\left((-k_a - k_{ds}) \cdot t\right) - 1\right) \qquad (13)$$

where k_a is the activation rate constant of stable sites.

Finally, a linear combination of integral functions (11) and (13) was applied for the overall characterization of polymerization kinetics with the high-activity $MgCl_2$-supported $TiCl_4$ catalyst.

1.3 BLOCK COPOLYMER

1.3.1 Block Copolymer Structure

The impact resistant copolymer of propylene and ethylene is sometimes called a “block-type copolymer”, but actually it does not have a true block-type structure, because the lifetime of the growing polymer chain is extremely short compared with the residence time in industrial polymerization reactors.

As mentioned in Chapter 1.1, the stopped-flow technique can be utilized for the synthesis of real olefin block copolymers. As was mentioned above this cannot be accomplished by the traditional sequential polymerization process, even on laboratory scale [1].

Real block copolymers (BCP) are composed of two or more chemically distinct blocks of polymers, which are covalently bound together [45, 44, 46, 47] in a single macromolecule. The simplest architecture is the linear AB-diblock copolymer shown in Figure 9, in which a polymer chain of type A monomers is covalently linked to a polymer chain of type B monomers. The linear AB-diblock copolymer is usually prepared by the repeated addition of monomers of B to the end of a previously synthesized chain of homopolymer A [48].

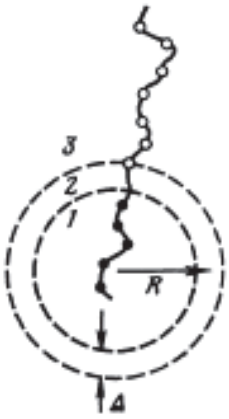

Figure 9: Linear AB diblock copolymer in an isolated micelle: 1-core (domain), 2-surface layer, 3-shell (matrix) [49].

The covalent linkages between these individual blocks prevent macroscopic phase separation even when the polymer blocks are thermodynamically incompatible. Instead of this the individual blocks can separate into micro-phases forming domains with sizes comparable to the dimensions of the individual blocks within the polymer chains (1-100 nm), see Figure 9 [48, 44, 51].

In bulk, the minority block is segregated from the majority block forming regularly-shaped and uniformly-spaced nano-domains. The shape of the segregated domains in the AB-diblock copolymer system is governed by the volume fraction of the minority block and by the incompatibility of polymers forming the AB-diblock copolymer [48, 45, 50]. The phase diagram for a conformationally symmetrical diblock copolymer is illustrated in Figure 10.

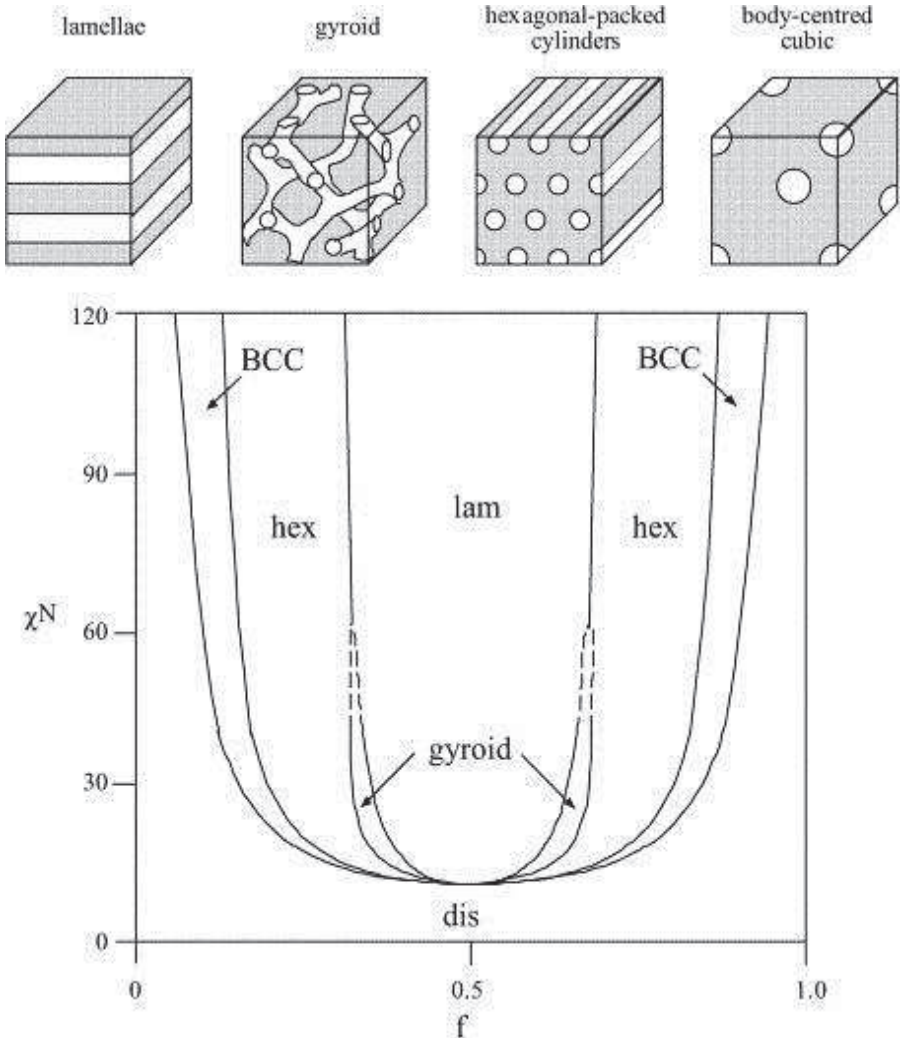

Figure 10: Phase diagram for a conformationally symmetrical diblock copolymer illustrating the equilibrium morphologies: lamellar (lam), hexagonally-packed cylinder (hex), gyroid (gyr) and body-centred cubic (BCC) spheres [47].

Since the individual blocks can be combined to provide distinct chemical or physical properties for block copolymers, extensive industrial applications of AB-diblock copolymers have been found, including their use as structural plastics, blend stabilizers, emulsifiers and contact sensitive adhesives [45]. Many applications mainly utilize the ability of block copolymers to suppress macroscopic phase separation [44].

Generally, phase separation (micro- or macroscopic) is an equilibrium process, which represents a balance between repulsive and attractive forces between different entities. These forces are specified by a minimum in potential energy with distance apart. This assumption is useful for understanding and modelling the microphase separation of a BCP. The thermodynamics of the self-assembly process can be represented by a simple Gibbs free energy equation [52]:

$$\Delta G = \Delta H - T\Delta S \qquad (14)$$

where the phase separation is a spontaneous process if ΔG is negative. Δ*H* is the enthalpy change of the process and is determined by the potential energy and

intermolecular forces between the assembling entities. ΔS is the change in entropy associated with the formation of the ordered or hierarchical arrangement. Since the organization is generally (but not always) accompanied by an entropy decrease, for spontaneous phase separation the enthalpy has to be negative and in excess of the entropy itself. Equation 14 shows that the self-assembly process is less efficient, when the magnitude of $T\Delta S$ approaches the magnitude of ΔH and the temperature during the process increases above a critical temperature. In such a case spontaneous self-assembly will not occur [52].

The morphologies of BCPs are driven by three main parameters [44, 45]:

- total degree of polymerization N (= N_A + N_B),where N_A, N_B are the degrees of polymerisation of each block such that $f_A = N_A/(N_A+N_B)$.
- volume fractions of the blocks (f_A and f_B, f_A = 1 - f_B), where f_A is the volume fraction of block A and f_B is the volume fraction of block B
- strength of interaction parameter (χ) between two segments of BCP (Flory-Huggins parameter, which defines the incompatibility between these blocks)

Assuming a simple AB-diblock copolymer consisting of units A and B, the value of the χ parameter, which defines the interactions between block A and block B can be written as [52]:

$$\chi = \frac{z\Delta w}{kT} \qquad (15)$$

where, χ is the exchange energy per molecule normalised by the thermal energy kT and is dimensionless, z is the number of neighbouring chains surrounding one block, Δw is the exchange energy per block A and block B contact. The interaction parameter χ can directly be related to the change in molar enthalpy during mixing, ΔH_m, by:

$$\Delta H_m = f_A \cdot f_B \cdot \chi RT \qquad (16)$$

where f_A and f_B are the volume fractions of the blocks.

Assuming no volume change during mixing, the value of the interaction parameter χ can be estimated from the Hildebrand solubility parameters δ_A and δ_B:

$$\chi = \frac{V_m(\delta_A - \delta_B)^2}{RT} \qquad (17)$$

where δ_A and δ_B are the Hildebrand solubility parameters of blocks A and B. The solubility parameter δ is a numerical estimate of the degree of interaction between materials. Materials with similar values of δ are likely to be miscible. V_m is the molar volume of one of the components of the mixture.

Therefore:

$$\Delta H_m = f_A \cdot f_B \cdot V_m(\delta_A - \delta_B)^2 \qquad (18)$$

These equations show that any block copolymer system, where the blocks have different solubility parameters (i.e., different strengths and forms of intermolecular interaction) will have positive enthalpy of mixing and will thus have a tendency to microphase separation and self-assembly. This is provided by the entropy change, which in the case of BCP self-assembly systems is always a decrease, as discussed

above. The entropy change associated with the process should not be so large as to overcome the enthalpy contribution.

The Flory-Huggins theory has been considered the basis for modelling of the behaviour of block copolymers since their discovery, and remains the most frequently used model, providing a suitable basis for the prediction of the morphology of BCP microphase separated systems (Figure 10).

1.4 HIGH IMPACT RESISTANT POLYPROPYLENE COPOLYMER

The isotactic polypropylene homopolymer has various excellent properties, such as high stiffness and good thermal and chemical resistance. However, on the other hand it has rather low toughness (impact resistance) and is brittle at low temperatures. Impact resistant PP material was developed as a partial solution to this problem. This material is prepared by a sequential polymerization process, which comprises of propylene homopolymerization followed by random copolymerization of propylene with ethylene [53, 38].

Isotactic polypropylene (iPP) and ethylene-propylene rubbers (EPR) are generally incompatible and their mixtures are thus heterogeneous. Phenomena such segregation, stratification and phase inversion could therefore be expected as in other multiphase polymer systems [54].

It was observed that when iPP and EPR components are mixed only mechanically, the dispersion of the copolymer phase is not uniform and the desired mechanical properties are not achieved [55].

The first impact copolymer polypropylene (ICP), a designation commonly used for the "*in-situ*" blend of iPP and EPR, made directly during the polymerization, was prepared by the Montell Company in 1960 [56]. They found that "*in-situ*" blends apparently exhibited better properties than similar blends prepared by simple mechanical mixing of iPP and EPR components. ICP is typically prepared by a two-step polymerization [57]. Firstly the homopolymerization of propylene is performed in the first reactor followed by ethylene/propylene copolymerization in the second one.

The performance of ICP is closely related to its heterophasic structure. Synthesis of ICP with good dispersion of both phases is designed by several parameters, such as composition, chain structure, interfacial interaction between the phases and viscosity ratio between the dispersed phase and the matrix [58].

SEM investigations showed that the EPR phase segregates into irregularly-shaped domains. It was found that the segregation of EPR increases with increase of the ratio between the viscosity of EPR and iPP matrix [59]. It was also determined that the dispergation of EPR in iPP became finer and more uniform, when the EPR phase has a melt viscosity lower or equal to iPP matrix [54].

Caballero et al. [60] utilized a metallocene catalyst system for the synthesis of EPR samples covering the whole composition range of ethylene and propylene ratio. The analyses revealed that E/P copolymers, which contained from 10 to 80 mol. % ethylene comonomer are essentially amorphous, whereas copolymers with an ethylene content outside of this range are semicrystalline. It was calculated that

heterogeneous copolymers that contain polymer chains with domains of at least 5 consecutive units of the same monomer will be able to crystallize. The average molecular weight (M_w) of the produced E/P copolymer directly depends on comonomer content, where the lowest values were observed for E/P copolymers that contained 20 to 60 mol. % of ethylene.

1.4.1 Influence of Dispersion and Size of EPR Domains

It is well known that the size of EPR domains and their dispersion in the iPP matrix have a crucial influence on the physical and mechanical properties of final ICP material [61]. To achieve the best stiffness-toughness balance the EPR domains have to be homogeneously dispersed in the iPP matrix. Also the size of domains should be well controlled.

The iPP particles produced in the first step of sequential polymerization contain a significant number of micropores partially filled with low tacticity polypropylene [61, 62]. In the second step, these micropores are completely filled with amorphous EPR produced during the copolymerization [63]. Jing et al. [61] determined that after polymerization the size of EPR domains in polymer particles is smaller than 1 μm. This indicates that the majority of copolymer material was formed inside the particles [61, 62].

Furthermore, Tong et al. [62] observed two kinds of ICP particle with different ethylene content by SEM and TEM microscopies. The first kind, with an ethylene content of 7.4 mol. % represents ICP formed at the beginning of the copolymerization stage (in the second reactor) during ICP preparation. The second kind, with an ethylene content of 26.7 mol. % represents ICP formed at the late stage. The results indicate that during the early stage of copolymerization, with lower content of copolymerized ethylene (7.4 mol. %), the EPR phase is produced exclusively in a surface layer of iPP particle. In the late stage of copolymerization, with higher content of copolymerized ethylene (26.7 mol. %), the EPR phase is developed also in the inner part of the particle. Jing et al. and Tong et al. [61, 62] ascribed this phenomenon to a mass transfer barrier. They proposed that the mass transfer barrier originated in loosely agglomerated inclusions of low tacticity PP, produced during the first polymerization step within the semi-filled micropores inside the iPP particles. These inclusions inside the micropores resist the diffusion of comonomer into the particle.

Debling et al. determined that even with 70 wt. % of EPR the iPP particle still contains enough pores to prevent monomer diffusion limitations [37].

Katayama et al. [55] studied the dispersion of the EPR phase in iPP. Based on the results they suggested a hypothesis that EPR formed in particles fills the gaps between subglobule particles of polypropylene homopolymer. Microscopic Fourier transform infrared spectroscopy revealed that ethylene is homogeneously dispersed throughout the whole ICP particle.

Comparison of EPR dispersion before and after injection moulding revealed a significant increase of the EPR domains' size after injection moulding. This

observation implies that in melt the EPR phase has a strong tendency to separate from the iPP matrix, which results in the increase in EPR particle size [61].

Jing et al. [61] found that after injection moulding, the particle size of EPR and atactic PP domains is larger than 1 μm. Other authors [58, 64, 65, 66] utilized scanning electron microscopy and determined that the particle size of the dispersed EPR phase is in the range from 0.5 to 2.5 μm.

Jang et al. [67] proposed that 0.5 μm is a critical diameter for EPR domains in an iPP matrix. Only EPR domains with a diameter bigger than the critical diameter could improve the fracture resistance of polymeric materials. Obviously, the majority of EPR domains in ICP have a size beyond this critical level. In addition, it was determined that a broader distribution of EPR domains sizes also facilitates the improvement of ICP impact strength. Therefore it is believed that the excellent toughness of ICP copolymers results from the good dispersion and appropriate size of EPR domains.

On the other hand, morphological studies performed by Mahdavi and Nook [68] on commercial ICP samples show that the dispergation of EPR domains in the iPP matrix is not satisfactory, with an evident tendency to aggregate. In such a case the EPR domains are very large with rather a small interface between EPR phase and iPP matrix. The smaller interface between EPR domains and the iPP matrix further decrease the ability of EPR to improve the toughness of ICP materials.

1.4.2 Influence of Chain Structure

Mirabella [69] fractionated commercial ICP using TREF and subsequently characterized the fractions by ^{13}C-NMR, and DSC. These techniques were used for the structural analysis of commercial ICP. It was found that the ICP is composed of 75 wt. % isotactic homopolymer PP, 17 wt. % amorphous EPR and 8 wt. % ethylene-rich semi-crystalline E/P copolymers. The results were used to determine the distribution function of the composition of the copolymer produced in the second reactor during the preparation of commercial ICP.

The theory, which describes the composition of EPR copolymer in ICP material, is well developed only for ICP produced on homogeneous catalyst systems.

In the case of ICP copolymers produced on heterogeneous catalysts, such as $MgCl_2$-supported $TiCl_4$, the situation is more complicated. It is known that these systems often produce EPR copolymers with broad and multimodal compositional distributions. This is the main reason why a suitable theory allowing the calculation of copolymer composition distributions for the copolymers produced on heterogeneous catalysts still does not exist.

Nevertheless, the function developed for the calculation of the theoretical composition distribution for copolymers produced on homogeneous catalyst systems could be helpful also in the rough estimation of the composition of E/P copolymer produced in the second reactor during the production of impact copolymers on standard heterogeneous catalyst systems. The following function was proposed for

the calculation of E/P copolymer composition distribution produced on a homogeneous catalyst system [69]:

$$W(y)dy = \frac{3(\lambda / 2a_0 b_0 k)^{1/2}}{4(1+\lambda y^2 / 2a_0 b_0 k)^{5/2}} dy \qquad (19)$$

where λ is the number-average dispersed phase of growing chains, and a_0, b_0 represent average molar copolymer composition. The parameter k is calculated using the equation:

$$k = \frac{a_0 r_2 A}{B} + \frac{b_0 r_1 A}{B} \qquad (20)$$

where r_1, r_2 are reactivity ratios, A, B represent the molar composition of monomer feed, $y = a - a_0 = b_0 - b$ is a composition deviation parameter, and a, b represent the variable molar copolymer composition.

This function is the composition distribution for all chain lengths and is calculated from basic polymerization parameters such as feed composition, reactivity ratios, number-average chain length and average copolymer composition. The calculated composition distribution function for the second reactor in the production of ICP is presented in Figure 11. The important point to illustrate in Figure 11 is that the central portion highlighted with cross-hatching represents copolymers that contain a large fraction of ethylene and propylene and, therefore, are expected to be rubber-like and exhibit negligible crystallinity. The extremities of the curve on the other hand represent copolymers that are rich in one of the monomers with only a small fraction of the other monomer. These copolymers are supposed to be semicrystalline [69].

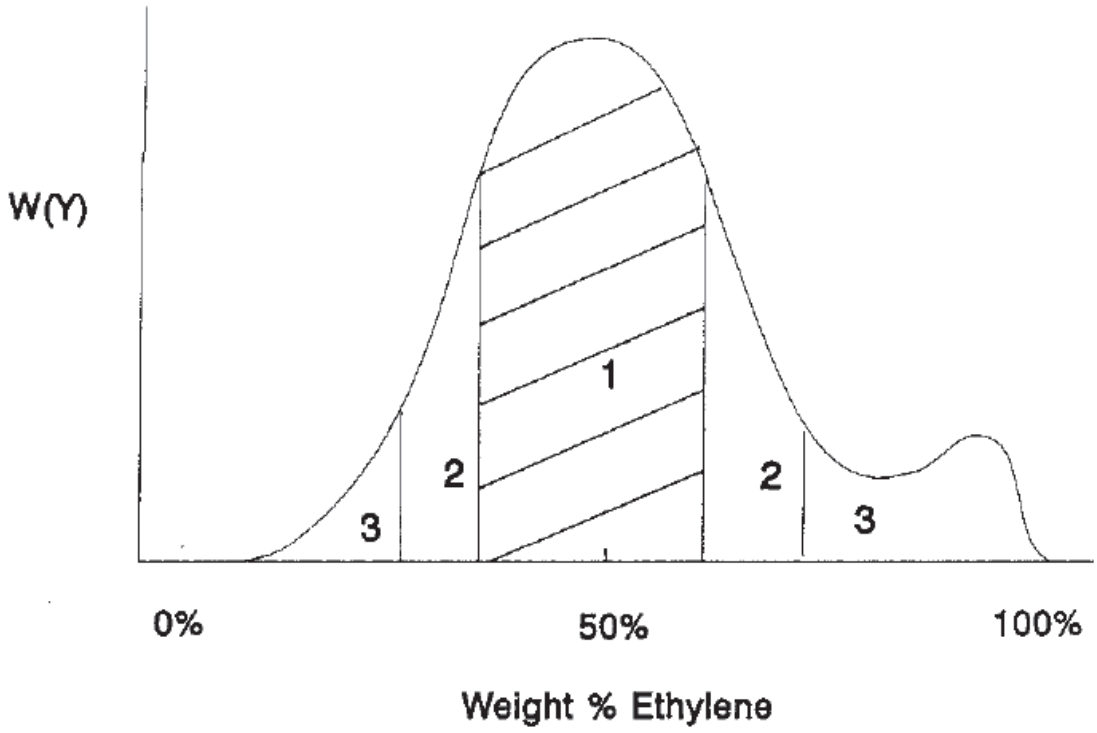

Figure 11: Qualitative representation of the composition distribution function (weight percentage of ethylene) of the second reactor polymer in ICP [69].

Nitta et al. [70] determined that EP copolymers with a propylene content higher than 84 mol. % were miscible with iPP and crystallizable PP sequences present in these EP copolymers were incorporated into crystalline iPP. The rest of the EP copolymer chains were in the amorphous phase. The EP chains containing crystallizable PP sequences acted as tie molecules, which bound together the adjacent lamellae and enhanced the toughness of iPP. On the other hand, the EP copolymers with a propylene content below 77 mol. % were incompatible with iPP. These iPP/EP blends showed phase-separated morphology.

Xue et. al. [57] compared two commercial ICP materials with similar ethylene content, MFI, tensile yield strength and flexural strength. However, one of the samples exhibited higher impact strength at low temperature (80 kJ/m^2 versus 68 kJ/m^2). The samples were fractioned and individual fractions were characterized using FTIR. The results indicated that the sample with higher impact strength contained more room-temperature soluble fractions (amorphous EPR) and also more fractions with higher isotacticity eluted at 120 and 140 °C (isotactic polypropylene). The second sample contained more fractions with partly crystallizable segments of polypropylene and polyethylene. The authors proved that the difference in microstructure distribution resulted in observable differences in their mechanical properties.

1.4.3 Model of Multiphase Structure of ICP

It is known that ICP produced by a multistage polymerization process forms a multiphase system [64].

Phase separation in ICP occurs especially during the crystallization process of ICP after injection moulding resulting in a multiphase morphology [58, 63].

The experimental results [68, 71, 72, 73] indicate that ICP materials also contain, in addition to polypropylene (PP) and amorphous ethylene-propylene random copolymer (EPR), crystallizable ethylene-propylene copolymers. Some authors have also observed a small amount of polyethylene (PE) [58, 65, 72, 74]. Crystallizable ethylene-propylene copolymers can further be divided into ethylene-propylene segmented copolymer (EsP) with short sequences of PE and PP segments, and ethylene-propylene block copolymer (EbP) with long sequences of PE and PP blocks [58, 57, 68].

The multiphase morphology of ICP has been investigated by many authors [20, 57, 64, 65, 66, 68, 75, 76, 77].

Recently, the advanced analysis of ICP was performed for the clarification of multiphase morphology by Cheruthazhekatt et al. [76, 75]. He utilized a sophisticated technique, where ICP material was first fractionated according to molecular weight by SEC and subsequently these fractions were further fractionated by TREF according to their ability to crystallize. The obtained fractions were analysed by fast scanning DSC with scan rates of 10 – 1000 °C/s, which allowed the analysis of the obtained infinitesimal amounts (nanogrammes) of each fraction. They detected a complex

mixture of ethylene-propylene copolymers with varying ethylene and propylene content and sequence length distributions, as well as iPP homopolymer.

Theoretical models based on interfacial free energy and spreading coefficient explain well the observed core-shell morphology of ICP. It was found that interfacial interaction (or interfacial tension) between different phases is a major factor, which controls phase separation and structure [58]. Based on the results of multiple fractionation several theories for ICP structure description were postulated [58, 78].

As shown in Figure 12, in the steady state the structure of ICP exhibits phase separated morphology [78]. Different components can form a multi-layered structure, as shown in the globe left-down in Figure 12. The EPR together with PE are separated from the iPP matrix. However, by removing EPR, as in the case of the F_a xylene insoluble fraction of the ICP copolymer, the original multi-layered structure disappears (see the globe right-down in Figure 12). It was observed that after removing EPR from ICP the rate of iPP matrix crystallization was higher. This effect is explained on the presumption that after the extraction of EPR the crystallizable PE segments come into contact with the iPP matrix. The authors assume that faster crystallization of iPP matrix after EPR extraction is attributed to a faster nucleation rate of linear PE segments, which subsequently could serve as stable nuclei for iPP crystallization [78].

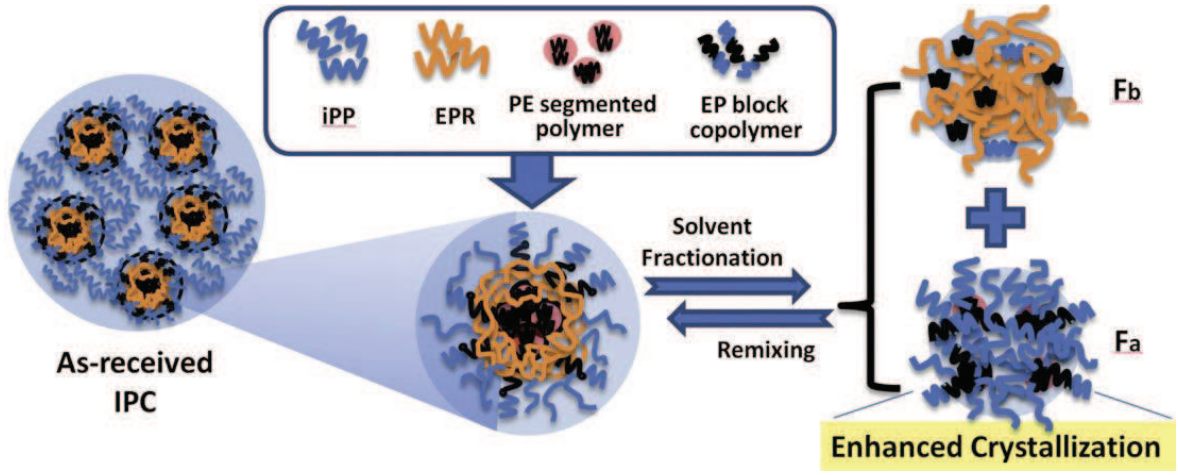

Figure 12: Schematic model depicting the relationship between phase structure and crystallization behaviour in ICP. (F_a is the xylene insoluble fraction and F_b is the xylene soluble fraction) [78].

It was determined that crystallizable PE segments are located in the inner core of the ICP copolymer particle and are surrounded by an amorphous EPR phase [74, 65, 64]. In a stable multi-layered ICP structure, the crystallizable PE segments are entangled with EPR chains, which prevent crystallizable PE segments from contact with the iPP matrix [78]. However, when this structure is disturbed, either by shear or solvent fractionation, the overall crystallization in the ICP copolymer can be noticeably affected. As mentioned above, crystallizable PE segments released from

the amorphous EPR phase can form stable nuclei and enhance the subsequent crystallization rate of the iPP matrix [65].

Tong et al. [72] suggested, that crystallizable ethylene-propylene copolymers, including EsP and EbP, play different and important roles in the formation of a multi-layered core-shell structure in the ICP material. EsP forms a hard inner core, which increases the rigidity of the dispersed phase. On the other hand, EbP creates a hard outer shell, which not only increases the rigidity of the dispersed EPR phase, but also enhances the adhesion between the dispersed EPR phase and the PP matrix.

Zhang et al. [64] proposed a modified core-shell model of EPR domain in ICP as shown in Figure 13. In this model, the EPR domain consists of the EbP core and two layers, where the outer layer is EbP and the inner layer is EPR. Furthermore, Zhang et al. [64] assume that some EbP also passes through the EPR layer and forms bridges, which connect the core of the EPR domain with the outer EbP layer. Besides this Zhang et al. [64] defined four kinds of EbP chain (in Figure 13 marked as I, II, III and IV). The chains with more polypropylene segments are defined as type I. It is assumed that these chains tend to be located in the interface layer between the iPP matrix and EPR, playing the role of a compatibilizer. Then the chains with more polyethylene segments are denoted as type II. These chains tend to be located inside the EPR domains forming a PE-rich core. The chains with equivalent PP or PE content are defined as type III. These chains could be found in the EbP layer and also in the PE-rich core. Zhang et al. [64] assume that these chains can also pass through the EPR shell and form EbP bridges as shown in Figure 13. Finally, the chains containing some E/P random sequences are defined as type IV, and could be found anywhere in the EbP phase.

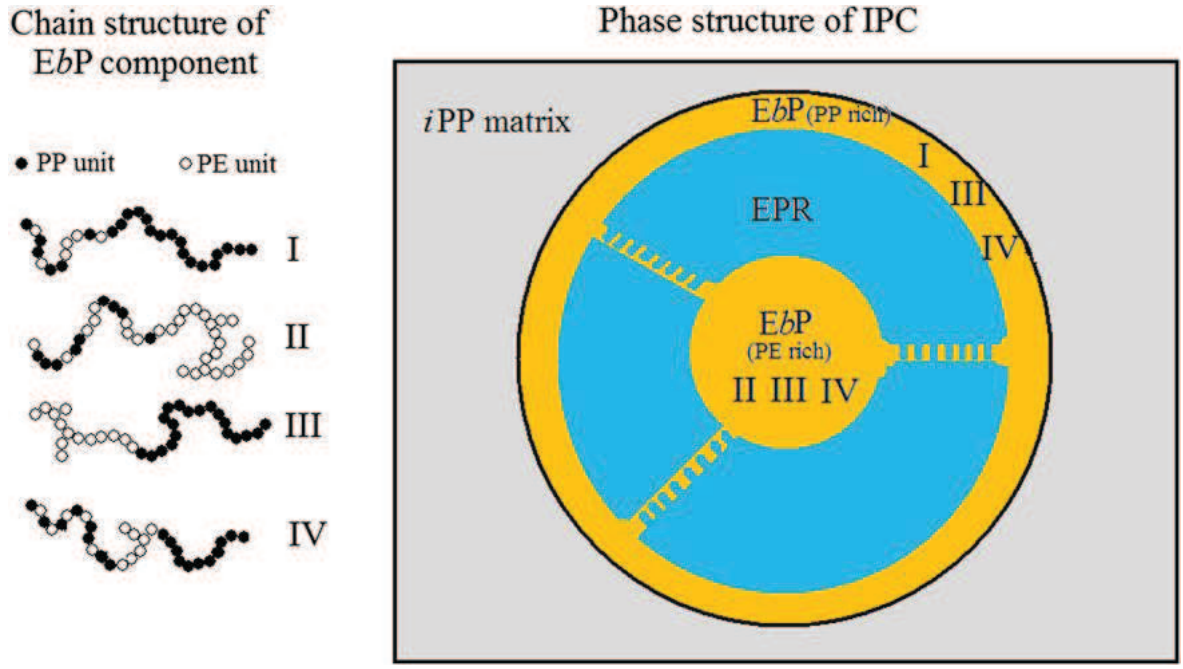

Figure 13 Schematic drawing of chain structures of block copolymers and their placement inside EPR domain. [64].

The core-shell model of the ICP domain was also promoted by Remerie and Groenewold [66]. They obtained results indicating that the most critical parameter, which determines the location of each component inside the EPR domain, is the content of ethylene. Their results demonstrated the formation of stratified domain structure in which ethylene content decreases from the centre of the domain towards the interface with iPP. Based on the presented results, Remerie and Groenewold [66] proposed the presence of three basic shells: the centre one consisting of the highest ethylene content (98 and 96 wt. %), the intermediate one containing intermediate composition (ethylene content 85 and 83 wt. %) and the material with 37 wt. % ethylene, which forms the outer layer. The degree of blending of neighbouring layers is determined by molecular weights of components and differences in ethylene content.

Fan et al. [71] observed that the impact strength of iPP matrix at room temperature can be apparently improved by the presence of segmented copolymer structures (i.e. EsP and EbP). On the other hand, the random copolymer is necessary for increasing iPP matrix impact strength at low temperatures (- 30 °C).

Mahdavi and Nook [68] fractionated several commercial ICP samples using the TREF method. They determined that the amounts of the EsP and EbP fractions in the commercial ICP are very low (1.4 and 3.0 wt. %, respectively). As the EsP fraction is important for adhering the EPR to the iPP matrix and the EbP fraction makes it compatible with the matrix, and the low content of these fractions in ICP strongly reduces the effect of the elastomeric phase on the properties of final ICP. They concluded that in order to obtain the best balance between toughness and rigidity of ICP materials, the content of these fractions in commercial products has to be increased and precisely controlled.

1.5 INFLUENCE OF BLOCK COPOLYMER ON IMPACT COPOLYMER PROPERTIES

Lot of studies have focused on the investigation of the influence of EbP diblock copolymers on the properties of ICP [20, 58, 64, 65, 71, 78, 79, 80, 81, 82].

It is known that during crystallization of the iPP matrix the EbP fractions are segregated from the iPP matrix cumulating mainly on the interfaces between previously formed EPR domains and crystalline iPP matrix. This process results in the multi-layered core–shell morphology of ICP copolymers. It is known that EbP fractions can behave as compatibilizers, which can enhance the interfacial adhesion between the EPR and iPP phases. Thus, the outer shell of the multi-layered core-shell structure can be considered as a compatibilizing layer binding the EPR phase (intermediate layer) with the iPP matrix [58, 64, 65, 71, 78, 79, 82]. The similar phase morphology formed in the bulk ICP copolymer indicates that this multiphase separation of different components of ICP occurs also in the polymer melt. This process together with the morphology of the multiphase also determines the mechanical properties of ICP material [58].

Fan et al. [71] observed that the interaction between the EPR and iPP phases is important for the effective absorption of energy by the tough EPR phase mainly at low temperatures. The significantly better impact-resistant properties of in-situ ICP blends in comparison with mechanically prepared blends can be explained by the presence of the segmented copolymer, which is produced only during the two-stage synthesis of ICP.

Tan et al. [81] compared two ICP materials prepared in the same industrial equipment using different spherical Ziegler–Natta catalysts. The samples had similar ethylene content, molecular weights and MWD, but different impact toughness at low temperature. The results revealed that poor interfacial adhesion between the dispersed EPR phase and iPP matrix, larger dimensions of EPR domains and their non-uniform distribution within the iPP matrix, which is due to a low content of EsP, were the main reasons for the low impact resistance of ICP samples.

Tian et al. [83, 77] utilized a technique called the Atmosphere-Switching Polymerization Process (ASPP) for the preparation of series of block copolymers with different propylene/ethylene content and molecular structures. They found that the increase of EbP content and length of PP block in EbP lead to a decrease in size of EPR phase domains and interfacial tension between EPR and iPP. The results published by Tian et al. [83, 77] again confirmed that the EbP copolymer behaves as a compatibilizer between the EPR phase and the iPP matrix.

Extensive research focused on the evaluation of ICP structure was performed by the research group around Terano [9, 70, 84, 85, 86, 87]. They utilized the stopped-flow technique for the preparation of special PP-b-EPR diblock copolymers.

Mori et al. [85] specially developed a high-pressure type of stopped-flow polymerization apparatus for the synthesis of PP-b-EPR diblock copolymers with controlled crystalline-amorphous microstructure. Consequently, Nitta et al. [84] investigated the miscibility of this type of block copolymer with iPP/EPR blends. They surprisingly observed that the PP-b-EPR diblock copolymer is not compatible with the EPR copolymer, but is compatible with the iPP matrix. They found that in blends of iPP with EPR the PP part of the PP-b-EPR diblock copolymer is incorporated into the crystalline iPP phase and the EPR part is trapped in the inter-lamellar space of the iPP. According to their results, PP-b-EPR added to PP/EPR influences the morphology of the final blend, glass transition temperature and tensile properties. However, they also determined that in the presence of PP-b-EPR diblock copolymers better compatibility of EPR and iPP was not achieved despite the fact that the chemical structure of these diblock copolymers simulates well the anticipated structure of material produced during the transition from iPP to EPR production. It is apparent that not all the block copolymers could act as compatibilizing agents between the iPP and EPR phases. This may be due to the fact that the PP-b-EPR molecule prepared by Nitta et al. has higher mobility, which results from its apparently lower molecular weight (M_w = 42 000) in comparison with pure iPP or EPR.

The crystalline structure of the ICP copolymer could be changed by the block copolymer [88, 80, 71, 64]. The prepared blends showed that the isothermal crystallization kinetics of PP/EbP binary blends have a lower Avrami exponent and a slower crystallization rate than the PP/EbP/EPR ternary blends [88]. The size of iPP spherulites could be reduced [89, 80] or the spherulite structure could even be destroyed [71] by the presence of segmented EsP or block EbP copolymers which are compatible with the PP homopolymer. Since both the EPR and the EbP fractions decrease the crystallization rate of iPP in PP/EPR and PP/EbP binary blends, it is speculated that the miscibility of EPR and EbP can weaken the influence of EbP on the crystallization of neat PP [88]. This hypothesis was supported by Hongjun et al. [80], who observed that the non-crystalline parts of EbP copolymer introduce defects into the crystallizable part of ICP copolymer, which enhance the impact strength of final ICP.

It is known that a crystalline block copolymer with both crystallizable PP and PE segments could exist as an interphase between the dispersed amorphous EPR phase and the iPP matrix. It is believed that crystallizable PP segments are inserted into the crystalline iPP matrix, while PE segments are trapped inside the amorphous EPR phase. In a solid state the multi-layered phase structure of ICP is stable. However, in the molten state an external shear can destroy the multi-layered phase structure by pulling out PE homopolymers as well as the PE segments of block copolymers from amorphous phase. This extraction of PE from the amorphous phase causes that the PE segments gather and form stable nuclei. Song et al. [65] assume that this effect subsequently enhances the crystallization rate of ICP copolymers.

Due to the presence of polyethylene component in ICP copolymer, the glass transition temperature (Tg) of EPR present in ICP is apparently lower than Tg determined on EPR fraction, which was extracted from ICP. The glass transition temperatures determined for EPR/EbP blends imply that these two components have a good compatibility [64].

Addition of EPR to PP/EbP blends leads to an increase in multiphase domain number and size. This indicates that the block component EbP is partially miscible with both PP and EPR fractions. Chen et al. [89] found that without the EbP component the dimensions of the mechanically dispersed EPR phase are noticeably smaller than the domains of EPR in ICP prepared by two-stage polymerization. These mechanically dispersed EPR domains are typically no bigger than 0.2 μm. It is obvious that EPR is better dispersed in ICP in comparison with mechanically prepared iPP/EPR blends. Fan et al. [71] proposed that the main reason is the presence of EbP in ICP.

Feng et al. [90] studied the influence of EbP addition on the mechanical properties of ICP material. They observed that a suitable amount of EbP diblock copolymer added into the iPP/EPR blend increases toughness and decreases the glass transition temperature. Another advantage of the addition of EbP diblock copolymer into iPP/EPR blend is the increase in tensile strength. This effect was also

accompanied by a reduction of the decrease of tensile strength which typically accompanies the toughening of plastics with elastomers.

Investigation of PP/EbP/EPR ternary blends revealed that these blends consist of two main phases (iPP and EPR) and the EbP in these blends behaves as a compatibilizer and also as a nucleation agent as well as an emulsifying agent. All these effects of EbP increase the toughness and tensile strengths of the PP/EbP/EPR blend. This effect was directly proved by a detailed SEM analysis of specimens after the tensile test [90].

Some other polyolefin elastomers have also been published as suitable compatibilizers for improving the mechanical properties of iPP and PE materials. It was found that ethylene-1-butene (EB) and ethylene-1-hexene (EH) copolymers are miscible with the amorphous phase of iPP, however the content of 1-alkene (i.e. 1-butene and 1-hexene) in the copolymer have to be above 50 mol. %. On the contrary, if the EB and EH copolymers contain more than 50 mol. % of ethylene, they become immiscible with the amorphous phase of iPP and form microheterogeneous structures in iPP matrix [91].

2 OUTLINE OF THESIS

This thesis will focus on the preparation and characterization of a new type of polymer material based on polypropylene-block-poly(propylene-co-ethylene) (PP-block-EPR). The unique PP-block-EPR copolymers were prepared by using the “stopped-flow” technique. For this purpose a new experimental apparatus suitable for carrying out very short polymerization experiments with a maximum yield will be built.

The synthesized polymer will be characterized in details to confirm the predicted presence of block copolymers. Subsequently, this material will be used for the targeted modification of commercial impact-resistant polypropylene copolymers (ICP) and the effect of block copolymer addition on the properties of the resulting mixture will be studied.

3 EXPERIMENTAL PART

Several procedures employed in this work have been developed within this study, namely all procedures pertaining to stopped flow apparatus and procedures of using it.

Simultaneous research targeted the characterization of the special products of the stopped flow experiments has also been carried out by our colleagues, namely the SSA method, EPR size distribution and TREF analysis. The methods utilized within this study are described in this chapter only informatively because their continuous development has not been completed yet by relevant publications.

3.1 CHEMICALS AND MATERIALS

All polymerization experiments were performed in liquid propylene using a commercial high-activity $MgCl_2$/phthalate/$TiCl_4$ catalyst, supplied by W.R. Grace & Co. The catalyst concentration in *n*-heptane was ca. 20 wt. % (content of titanium in dry catalyst 1.6 wt. %). The catalyst slurry was stored in a glass vessel covered by a permanent flow of pure nitrogen.

Polymerization grade propylene obtained from the PP plant (Unipetrol RPA a.s., Litvínov, Czech Republic) was used. Propylene was further purified by passing through six purification columns. The content of critical impurities (CO, COS) was less than 10 ppb vol., and water and oxygen levels were under 0.1 ppm vol.

Polymerization grade ethylene was purchased from SIAD Czech spol. s r.o. (Czech Republic).

The isopentane used as medium for dissolving ethylene was obtained from the PE plant (Unipetrol RPA a.s., Litvínov, Czech Republic).

The triethylaluminum (TEA) co-catalyst with ultra-low aluminium hydride content (<0.05 wt. %, TEA-ULH grade) originated from Chemtura GmbH (Germany). Neat TEA was diluted with *n*-hexane to a concentration of 20 wt. % and kept in 1-litre stainless steel vessels under the nitrogen.

The surface active agent N,N-bis(2-hydroxyethyl)-C_{13-15} alkyl amine was purchased from Croda International as Atmer 163. Before application into the reactor Atmer 163 was purged by bubbling with nitrogen for 60 min at 100°C for oxygen and water removal.

Nitrogen was supplied by Linde Gas a.s. (Czech Republic). It was further purified passing through purification columns with Cu catalyst and a 3A molecular sieve. The content of O_2 and H_2O in the nitrogen were under 0.1 ppm vol.

The reference sequential impact resistant copolymer (ICP) powder was produced at the PP plant of Unipetrol RPA a.s., Litvínov, Czech Republic. The basic properties of this material are summarized in Table 1

Table 1: Properties of commercial ICP material.

	MFR 21N [g/10min]	X.S. [wt%]	C2 (FT-IR) [wt%]	RCC2 (FT-IR) [wt%]	RC (FT-IR) [wt%]	intrinsic viscosity (X.S.) [ml/g]
ICP	30.6	12.6	7.0	55.8	12.5	229

3.2 STRUCTURAL ANALYSIS METHODS

3.2.1 GPC/SEC – Molecular Mass Distribution Determination

The Size Exclusion Chromatography (SEC) used in this study consisted of a Polymer Laboratories PL-GPC 220 analyser equipped with PL-220DRI (differential refractive index detector) and Viscotek model 220R differential bridge VD (viscometer detector). All the detectors were installed in the column oven compartment together with a set of columns. The set of applied columns consisted of three PL gel 10 µm, MIXED-B, 300 x 7.5 mm.

All sample solutions were prepared in filtered 1,2,4-trichlorobenzene containing 0.05 wt. % of Santonox R antioxidant ($C_{22}H_{30}O_2S$ - 4,4'-Thiobis(6-tert-butyl-m-cresol) to prevent oxidative degradation of polymer samples. Typically 10 mg of polymer was used for sample preparation. The same solvent was used as the SEC eluant. A sample concentration of 0.5 mg/mL and an injection volume of 200 µL were employed. The measurements were performed with a flow rate of 1.0 mL/min at 165°C.

The columns were calibrated using 14 polystyrene standards supplied by Waters with molecular weights M_w ranging from 2 350 to 3 700 000. Data handling was accomplished using Viscotek TriSEC software – a Universal Calibration Module was used for calculation.

3.2.2 ^{13}C-NMR – Propylene/Ethylene Structure Determination

^{13}C-NMR analysis was utilized for the determination of a propylene/ethylene copolymer structure in ICP and the composition of E/P copolymers synthesized in a stopped-flow apparatus. For the analysis 100 mg of polymer material was dissolved in a mixture of 1,2,4-trichlorobenzene (1.7 mL) and deuterated benzene (0.4 mL) and homogenized for 8 h at 130 °C under a nitrogen atmosphere.

Prepared samples were analysed with a 500 MHz Bruker DRX NMR instrument at 120 – 125 °C. Pulses were applied at a 77° angle with 15 s time delays.

In the case of samples where the isotactic polypropylene is the prevailing polymer, peak identification was performed on the basis of the chemical shifts described by Di Martino et al. [92]. The triad distribution and co-monomer content was computed according to the procedure described by Kakugo et al. [93].

Evaluation of sequential impact resistant copolymer structure was performed according to 1st order Markovian statistics published by Randall [94].

3.2.3 FTIR - Fourier Transform Infrared Spectroscopy

The presence and content of comonomer in the polymer was determined using a Nicolet Nexus FT-IR spectrometer. Transmittance spectra were measured at a resolution of 2 cm^{-1} with 32 scans.

3.2.4 DSC - Differential Scanning Calorimetry

DSC analysis was carried out according to ISO 11357. The DSC measurement of 1^{st} melting, crystallization and 2^{nd} melting was done on a DSC Q 100 TA Instruments calorimeter (TA Instruments, USA). A 5 – 10 mg sample was heated within the temperature range -70 – 200 °C at a rate of 10 °C/min. The sample was maintained at 200 °C for 8 min and then cooled to 50 °C at the same rate. Immediately after this a second melting cycle at the same temperature interval was carried out.

Subsequently, the polymer crystallinity was calculated from the enthalpy of the second melting:

$$\alpha = \frac{\Delta H_m}{\Delta H_m^*} \cdot 100 \qquad (21)$$

where α is the percentage content of crystalline PP in the sample, ΔH_m is the melting enthalpy of crystalline PP in the sample and ΔH_m^* is the theoretical melting enthalpy of 100 % crystalline PP (207 J/g) [95].

3.2.5 SSA - Successive Self-nucleation Annealing

SSA is a method of structural analysis using isothermal crystallization. It is based on different abilities of crystallizable sequences (segments between structural defects) in a polymer chain to crystallize at variable temperatures according to their length. The principle of stepwise cooling and subsequent measurement by using DSC is shown in Figure 14.

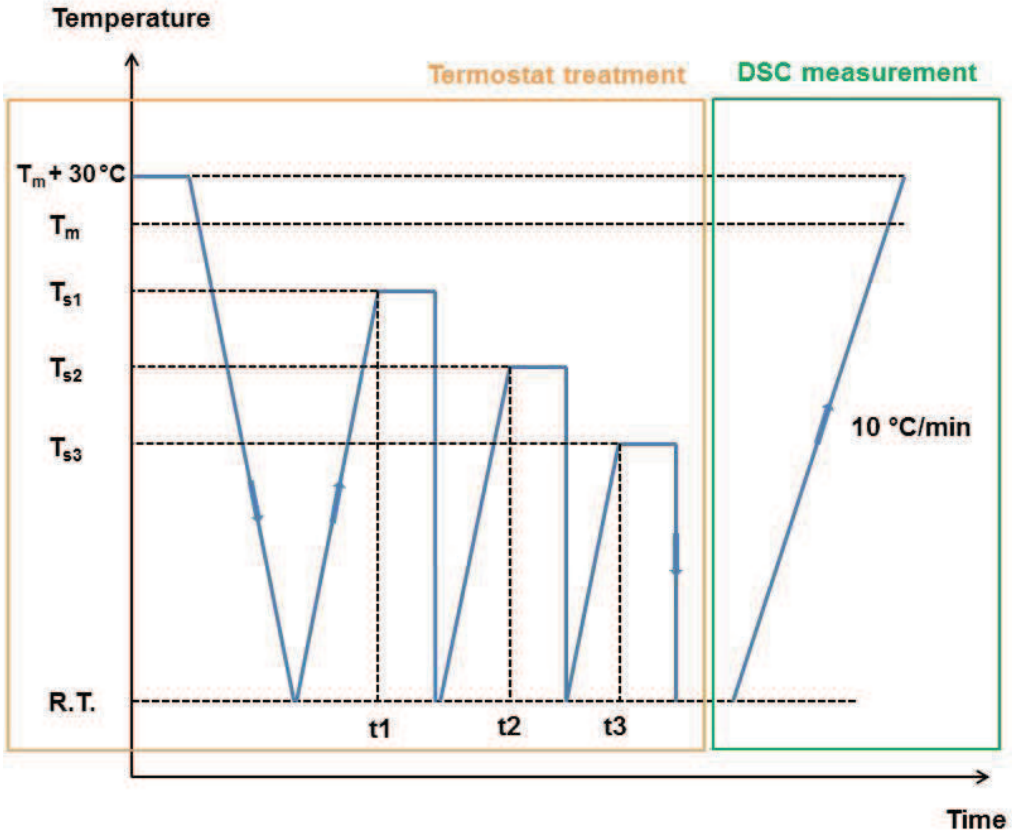

Figure 14: Scheme of temperature profile of stepwise cooling and subsequent measurement by using DSC [redrawn 96].

Differential scanning calorimetry (DSC) and successive self-nucleation annealing (SSA) were used to determine melting and crystallization temperatures of copolymer samples prepared in a stopped-flow apparatus.

Segment length can be calculated from the equation [96]:

$$l_i = \frac{2\sigma_e T_m^0}{\Delta H_u \left(T_m^0 - T_{m,i}\right)} \qquad (22)$$

where σ_e is the basal surface energy of ethylene polymer crystals (for PP = 122 mJ/m^2 [97]), T_m^0 is the equilibrium melting temperature (192 °C [98]), ΔH_u and ΔH_i are the heats of fusion for repeating monomer units (196 J.cm^{-3} [99]) and for each melting peak and $T_{m,i}$ is the melting temperature of each melting peak.

Quantity of segment length can be calculated [96]:

$$Q_i = \frac{\rho_c \Delta H_i}{14.03 \Delta H_u} \cdot \frac{0.2534}{2 l_i} = \frac{0.2534 \rho_c \Delta H_i \left(T_m^0 - T_{m,i}\right)}{56.12 \sigma_e T_m^0} \qquad (23)$$

where ρ_c is a density of PP crystals (0.936 g/cm^3 [99, 100]).

The DSC analyses were carried out using a DSC Q 100 TA instrument in the temperature range of 30 – 200 °C.

The development of SSA analysis was not the subject of this study as it has been carried out separately. In this chapter, application of SSA analysis is demonstrated on a representative sample from stopped-flow apparatus.

Figure 15 shows the DSC profile after the SSA of the sample prepared in the stop-flow apparatus. According to current knowledge [101], the area of temperature from 150 °C (this correspond with segments longer than 15 nm in the SSA profile in Figure 16) are mainly crystalline PP homopolymer chains with a low number of stereospecific errors. In the case of the block copolymer there are interesting peaks at the temperature range 40 - 150 °C. These peaks correspond to lengths of segments of up to 10 nm. Unfortunately, present configuration of the SSA apparatus (isothermal crystallization thermostat) does not enable evaluation of peaks lower than 75 °C. Therefore, it was not possible to investigate origin of peak near the temperature of 50 °C in Figure 15.

The peaks in the temperature range 100 - 150 °C probably contain chains with shorter crystalline segments. However, it is not absolutely clear what parts of the sample these peaks belong to [101]. It is likely that these peaks are represented by the homopolymer polypropylene with a low isotacticity or chains with longer polyethylene sequences. These chains contain shorter crystalline segments because of the fact that a significant part of these macromolecules is not able to crystallize (consists of amorphous EPR copolymer). We assume that these macromolecules are the PP-*block*-EPR copolymers, which are constituted of relatively short crystalline homopolymer blocks connected by a covalent bond with a long amorphous EPR block.

The peak at the temperature 50 °C (evaluation of which by SSA was not possible as described below) corresponds to melting of a polymer chain with a large amount of stereospecific defects. It is likely that the block copolymer with short polypropylene blocks also melts in this area.

Figure 16 shows a comparison of the SSA profile of a block copolymer synthesized on the stopped-flow apparatus and commercial ICP. The area under the peaks corresponds to the crystallinity of the samples. Because of the presence of large amounts of PP homopolymer produced in the first reactor, the ICP sample has a significantly higher main peak. The comparison in the range of peak sizes ranging from 5 to 10 nm is interesting. In this area, the higher sample representation is that prepared by the stopped-flow method. This may be due to the higher content of homopolymer PP with stereospecific errors caused by the presence of the EPR block.

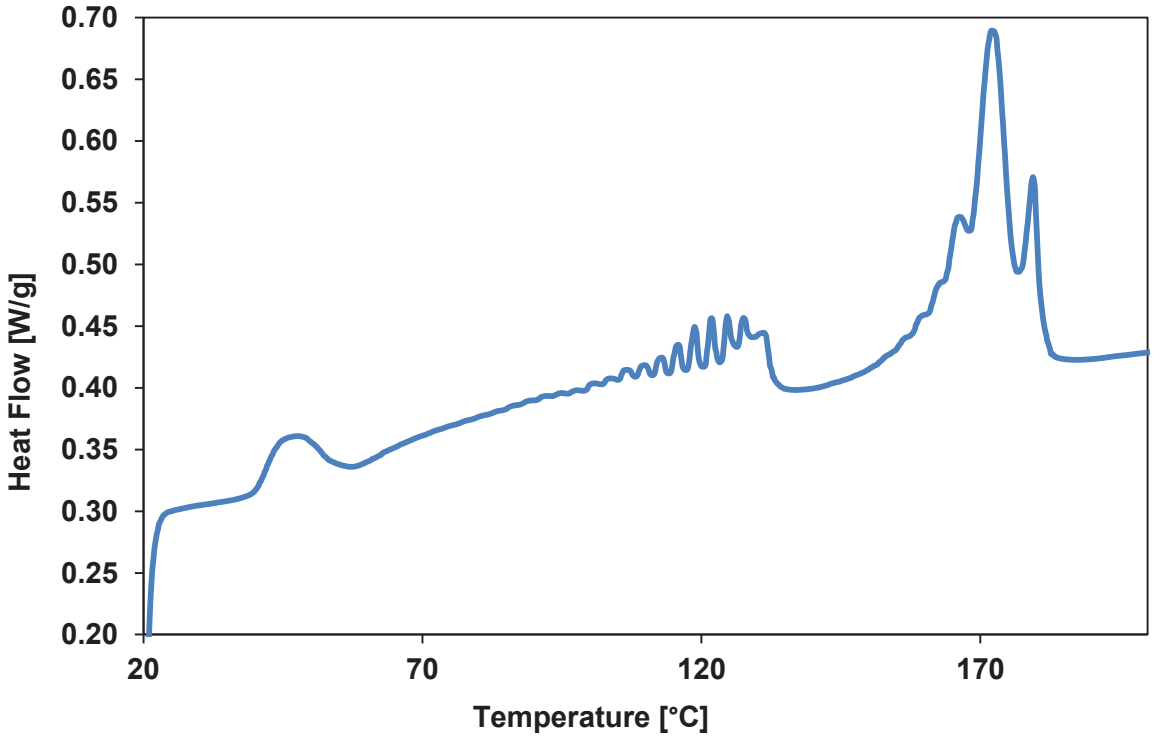

Figure 15: DSC profile of the sample copolymer prepared by the stopped-flow technique.

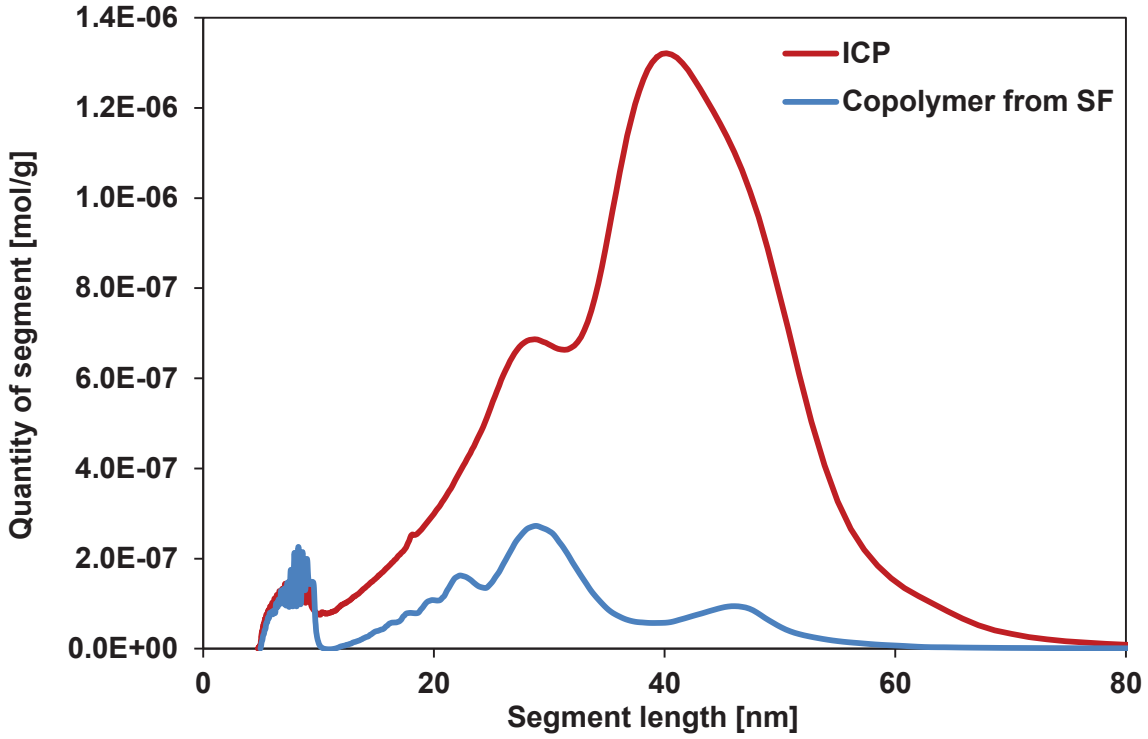

Figure 16: SSA profile of the commercial ICP and the copolymer prepared by the stopped-flow technique.

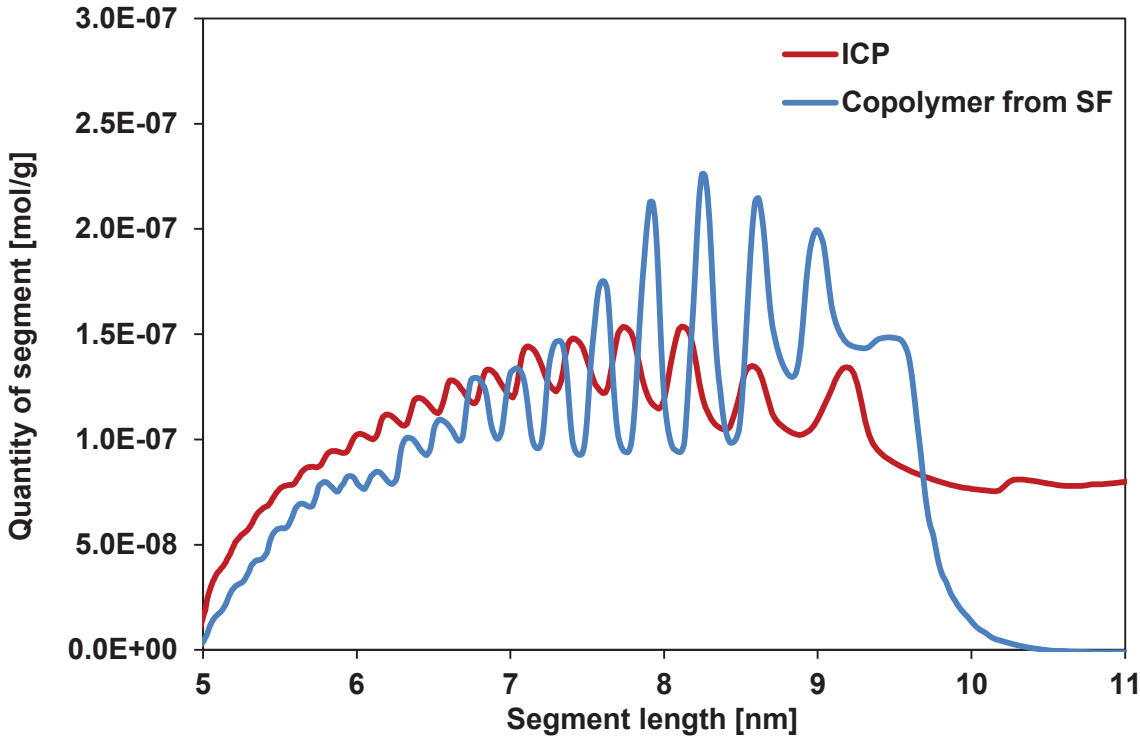

Figure 17: Details of segment length distribution between 5 to 10 nm in the SSA profile of the sample K79SF.

3.2.6 TREF - Temperature Rising Elution Fractionation

Temperature Rising Elution Fractionation (TREF) is a technique suitable for the analysis of semicrystalline polymers. TREF analysis is based on the principle that different components of polymer blend crystallize at different temperatures. There are two main TREF methods: Analytical TREF (ATREF), which provides information about a polymer's ability to crystallize and Preparative TREF (PTREF), which makes it possible, in addition to ATREF, to fractionate polymeric material into separate components suitable for other analytical methods.

Fractionation is performed in a column. The sample is dissolved at 140 °C, injected into a column heated to a temperature of 140°C and then cooled to 40 °C. During the slow cooling, specific polymer fractions crystallize at specific temperatures. The TREF apparatus consists of a solvent reservoir from which the solvent is pumped at a constant flow through the column with the sample. The column with the sample is placed in an oven. The fractions are detected by an infrared detector and the detected signal is processed. The result of TREF analysis is a fractiogram, which typically consists of several peaks depending on the number of the fractions present in the sample. The fractiogram is expressed as a concentration dependence on increasing temperature.

Analytical TREF was used to characterize the block copolymer prepared by the stopped-flow technique. The 0.04 wt. % polymer sample solution in 1,2,4-trichlorobenzene was prepared and 2.0 mL of this solution were injected into the SS column 300×10 (ID) mm containing an inert support (Chromosorb P 60/80). The

initial temperature was 140 °C and the sample was cooled to 40 °C at a rate of 6 °C/h. Afterwards the sample was heated from 40 °C to 140 °C at a rate of 4 °C/min applying 1 mL/min solvent flow through the column.

Preparative TREF was used for fractionation of block polymer samples into three fractions. The preparative column SS 300x20(I.D.) mm was filled with an inert support (Chromosorb P 60/80). The 1 – 2 wt. % solution of the sample in 1,2,4-trichlorobenzene was cooled at a rate of 2 °C/h from 140 °C down to 20 °C. The fractions obtained at 40, 100 and 140 °C were subsequently precipitated by cold methanol, filtered through a sintered glass frit and dried.

3.2.7 Rheological Measurement

The viscoelastic properties were measured on a Bohlin Gemini rotational rheometer with plate-plate geometry (diameter 25 mm). PP sample used for measurement was in the form of a hot pressed disc (2 mm thick with 21 mm diameter). Before the measurement the sample was preheated to 200 °C for 5 min, and then carefully pressed in order to completely fill the gap between the two plates. Two types of measurement were performed:

1) Prior to oscillatory frequency sweep measurement, an amplitude sweep test was performed. The amplitude sweep test was carried out for the purpose of determining the limit of the linear viscoelastic range (LVA). This test was performed with a constant frequency, usually of 6.28 rad/s (1Hz) and deformation (strain) in the range of 0.5 – 100 %. From this measurement a deformation limit was obtained at which modulus and complex viscosity began to decrease. When the LVA range exceeded a certain level, the structure of the sample was irreversibly changed or completely destroyed.

If the elastic modulus (G') was higher than the viscous modulus (G") the material exhibited the character of a gel. The structure showed a certain rigidity.

On the contrary, if G' was lower than G", the material exhibited the character of a liquid.

2) A frequency sweep test was performed within a linear viscoelastic range with the deformation below the limiting value of deformation. Usually one third of the deformation limit was used in the frequency sweep test. Dependence of the loss (G´´) and the storage (G´) modulus, the complex viscosity (η^*) and the phase angle on frequency was usually determined at 200 °C with a constant strain of 5 % and an angular frequency in the range 0.05 – 250 rad/s.

The rotational test was performed in order to obtain the dependence of shear viscosity on shear rate. A geometry cone-plate (diameter 25 mm, cone 2.5°) was used. Before the measurement, the sample was preheated to 200 °C for 5 min, and then pressed to 70 μm, which corresponds to a theoretical tip of the cone of 2.5° at the zero position). The gap between the cone and the plate was completely filled. The measurement was performed at 200 °C in the range of shear rates 0.001 – 5 s^{-1}.

The crossing point of elastic and viscous modulus (G'=G") can be used for comparison of the average molar mass and molar mass distribution as shown in

Figure 18. The position of the crossing point on the x-axis gives information about the average molecular weight. The position of the crossing point on the y-axis determines the value corresponding to the distribution of molecular weight, usually termed the rheological polydispersity index (PI).

Generally, polymers with the same molar mass distribution can be compared from the perspective of average molecular weight; the crossover point G'=G" is found at lower frequencies for the polymer with a higher average molecular weight. On the other hand, comparison of molecular weight distribution can be applied for polymers with the same average molecular weight. In this case a crossover point G'=G" at lower G values means the polymer has a wider distribution.

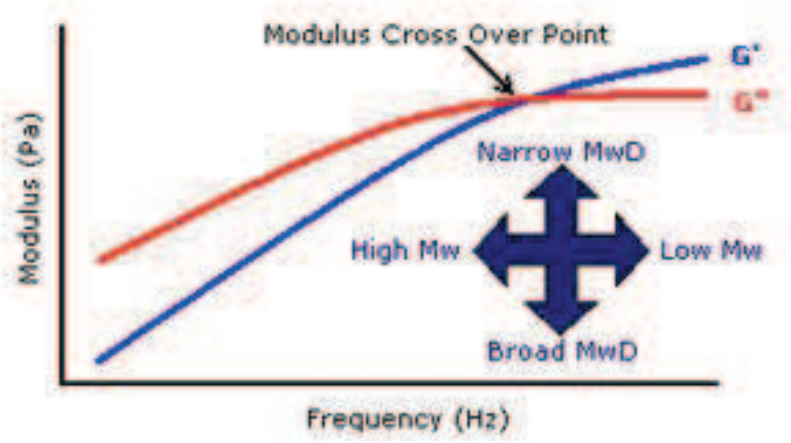

Figure 18: Dependence of the viscous and elastic modulus at a frequency [102].

3.2.8 DMA - Dynamic Mechanical Analysis

Dynamic-mechanical analysis was carried out on samples prepared via hot pressing according to ISO 293. Measurements were performed on a DMA DX04T instrument (RMI, Czech Republic). A temperature range -88 °C to +120 °C with a rate of heating of 2 °C/min and a single cantilever mode were used.

3.2.9 XS - Xylene Solubility

The solubility assessment was carried out according to ISO 6427. The polymer sample was completely dissolved during 1 h in 125 ml of o-xylene at its boiling point of 144.4 °C. The solutions were cooled to 23 °C, and kept at that constant temperature for 18 h. After centrifugation, the insoluble fraction was collected by filtration.

3.2.10 SEM - Scanning Electron Microscope

The test specimen was cooled to the temperature of liquid nitrogen. After 30 min of cooling the test specimens were broken using a Charpy pendulum. The fracture surface was cut with a sharp broken piece of glass under liquid nitrogen. Then

amorphous EPR rubber was etched with xylene (80 °C, 45 min). The etched surface was observed with a Philips XL 30 scanning electron microscope.

The distribution of EPR domains in ICP material was evaluated on three independent SEM pictures.

The sizes of the individual EPR domains were obtained by analysing the image of the SEM microscope through the ATLAS programme (Tescan, Czech Republic). The cavities were marked in the programme. The software evaluates the area, the equivalent diameter (diameter of a circle equal to the same area), the circuit and the position of the frame of the individual cavities. The output is a text file that contains all the values in pixels. The text file has been loaded into the programme AnalyzaCastice, created by Dr Žídek (Faculty of Chemistry, Brno University of Technology, Czech Republic). This software was required to convert the scale (pixels to micrometres). In the next step, the file is copied to an Excel file, which is evaluated by the frequency of the individual particle size.

The final EPR domain distribution profile is the average of these three SEM pictures.

3.2.11 μ-CT - X-Ray microtomography

The X-Ray microCT (micro-computed tomography) imaging is a high resolution technology allowing the visualization of measured samples in spatially 3D representation without any destructive sample preparation (cutting, etching, etc.). The basic principle is schematically displayed in Figure 19 where the sample is placed on the rotating stage and is irradiated by X-rays from the X-ray source. The beam transmitted through the sample continues to the scintillation layer where the X-Rays are transformed into visible or near infrared light. Then the light beams proceed through the microscope optics towards the CCD camera. The data are collected for the selected angle of sample rotation in the form of transmitted images during the scanning and are reconstructed into the final 3D model of the sample morphology. A detailed description of the X-Ray microCT technique, including possible artefact identification and limitations can be found in [103, 104]. The general principle of X-Ray imaging is photon absorption by a sample depending on the sample's chemical nature. Basically, a specimen containing atoms with high atomic numbers (large atomic nuclei) absorb more X-Rays [105]. X-Ray absorption also depends on sample density and its effect becomes more important when scanning samples containing similar atoms (e.g. polymers). More dense samples absorb more X-rays which can be applied for heterophase polymer visualization. The phase contrast can be enhanced by a larger sample-detector distance, which on the other hand prolongs the scanning time [103].

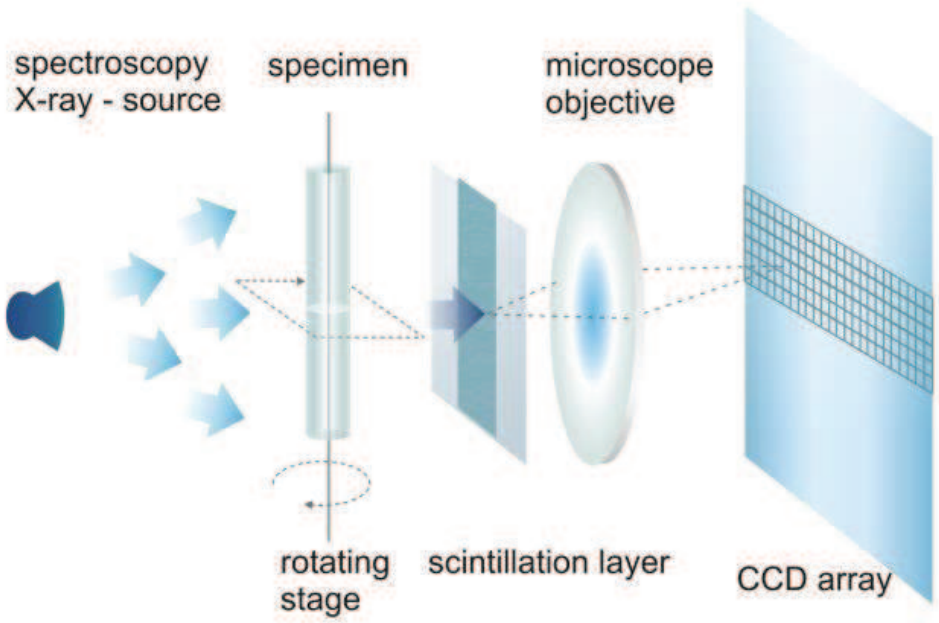

Figure 19: Basic principle of X-Ray microCT. Taken from [104].

The microCT measurement resolution is closely related to the optimal settings of the micro-CT scanning. The source spot size (SS) is a parameter of the X-ray tube and is strongly dependent on the power used. The desired pixel size (PS) can be achieved by proper combination of SS and the source distance (SD) and detector distance (DD) from the sample according to [104]:

$$PS \geq SS\frac{DD}{SD} \qquad (24)$$

The resulting resolution also depends on the sample size and on the desired magnification. Generally speaking, the smaller the scanned samples are the lower the pixel size and the better the resolution achieved. However, for low absorbing samples the need for high resolution also prolongs the scanning time. Low energy X-rays are required to improve the absorption to at least 20 % in the case of small polymer samples (below 1 mm in diameter). For comparison, higher absorbing materials are scanned with optimal settings around 75 – 85 % of X-rays absorbed by the sample [106].

X-Ray measurements were performed by Dr Svoboda (New Technologies Research Center, UWB Plzeň, Czech Republic) using the Xradia XCT 400 with a 90 kV X-Ray source tube and a (2000x2000) px detector. This device is able to achieve a voxel size of 0.2 µm for samples with a size smaller than 400 µm. The focal spot size (FSS) of the X-Ray emitter is in the range of 4 – 10 µm and thus the X-ray source is also stable during long term measurements.

The presented samples were scanned using an X-ray source set to 20 kV and 2 W. The pixel size of the presented tomography images is in the range 0.5 – 1.5 µm depending on particle size and microCT setting. In order to reduce the noise and artefacts most samples were scanned overnight at 1800 to 2000 angles during step-wise sample rotation about 360° [107, 108].

3.2.12 Mechanical Properties

3.2.12.1 Flexural properties - Modulus of Elasticity in Flexure

Measurements were done using the Instron 3366 device (Instron, USA).

Pressing took place in a Fontijne press (Netherland) applying pressure of 5 MPa at a temperature of 210 °C using an open mould according to the ISO 1873 standard followed by cooling at a rate of 15 °C/min. The thickness of the moulded plate was 4 mm.

The flexural modulus was measured on specimens with dimensions of 50x10x4 mm according to ISO 178. The flexural modulus was measured in a three-point arrangement with support spacing of 40 mm and speed of displacement of the mandrel of 1 mm/min.

3.2.12.2 Tensile Properties

Measurements were performed on an Instron 3366 instrument (Instron, USA). Test specimens of type 5 reduced in the ratio 1:2, were prepared from hot-pressed plates according to ISO 1873 with a cooling rate of 15 °C/min. The tensile test was carried out at 23°C according to ISO 527 with a gripping distance of 40 mm and a speed of jaw displacement of 50 mm/min.

3.2.12.3 Notch Impact Strength – Charpy

A CEAST 6545 Charpy impact pendulum instrument was used for fracture toughness evaluation (J^{ST}_{Id}- integral). Measurements were performed with a speed of 1.0 m/s. Test specimens of 50×10×4 mm dimensions with a notch depth a_0 = 5 mm (3.5 mm of the notch depth was cut by saw, 1.5 mm of notch depth was cut by a razor blade) were used.

Fracture toughness was evaluated according to the ISO 180 standard at -20 °C. Force versus deformation dependencies were obtained. The fracture surface of each test specimen was evaluated after measurement by an optical microscope.

3.3 POLYMERIZATION APPARATUS

Within the scope of this thesis a high-pressure stopped-flow polymerization apparatus for the homopolymerization of propylene and synthesis of polypropylene-*block*-poly(propylene-*co*-ethylene) was constructed.

The schema of constructed stopped-flow apparatus is shown in Figure 20. The main parts of the apparatus are as follows:

- 6-litre stainless steel pressure vessel equipped with a mechanical stirrer and water jacket for temperature control. This vessel was used as a storage vessel for catalyst slurry in liquid propylene. The catalyst concentration in propylene used in the experiments was in the range 0.1 - 0.5 mg/ml. The maximum amount of liquid propylene inside the vessel was 2 500 g.
- 8-litre stainless steel pressure vessel also equipped with a mechanical stirrer and water jacket for temperature control. This vessel was used as a storage

vessel for ethylene, which was dissolved in isopentane. The ethylene concentration in isopentane was ca. 12 wt. %. The maximum amount of isopentane inside the vessel was 3 500 g.

- Special set-up for dosing TEA diluted with *n*-hexane based on 12m long 6mm tubing.
- 100-litre stainless steel pressure vessel equipped with inlets surrounded by a water jacket for temperature control. The vessel was operated without a stirrer for accurate pressure control on the apparatus outlet.

As is obvious from Figure 20, the key part of the stopped-flow apparatus is the 100-litre pressure vessel, where the polymerization tubes and terminating agent are placed. The vessel had a maximum operating pressure and temperature of 2.2 MPa and 100 °C, resp. Pressure inside the vessel was monitored by a PM4 digital manometer (PMA, Germany) and temperature by an E-type thermocouple (Omega, USA). Another high-precision pressure difference meter PDM70 (Endress+Hauser, Germany) with a measuring range from -500 to 500 mbar was used also for pressure difference measurement between the 6-litre vessel containing the catalyst slurry and the 100-litre vessel in which the tubing of stopped-flow apparatus. The 6-litre stirred pressure vessel used for storage of catalyst slurry in liquid propylene had the maximum operating pressure and temperature 4.0 MPa and 100 °C, resp. The vessel stirrer was driven by an electric motor via a magnetic clutch. Pressure and temperature inside the 6-litre vessel were monitored by the same digital manometer and thermocouple as in the case of 100-litre vessel.

Finally, the 8-litre stirred vessel used for storage of ethylene solution in isopentane had the maximum operating pressure and temperature also 4.0 MPa and 100 °C, resp. Pressure and temperature inside the 8-litre vessel were monitored in the same way as in the case of 100-litre and 6-litre vessels. A system of two containers was used for co-catalyst (TEA) dosage. Prior to the polymerization experiment, 150 mL of TEA diluted in *n*-hexane was filled into the 12 m long stainless steel tube (diameter 6 mm) from a 1-litre storage vessel. Inside the storage vessel a permanent slight nitrogen overpressure (ca. 0.1 MPa) was maintained, measured with a gauge manometer.

The tubing for catalyst slurry in liquid propylene, TEA n-hexane and ethylene in isopentane was constructed of stainless steel seamless tubes (diameter 6 mm) and stainless steel capillaries (Grace, diameter 1/8 inch). All the valves and compression junctions were purchased from Swagelok.

Stopped-flow experiments were operated by an APT 1000G industrial computer (AMIT, Czech Republic) and controlled by special software programmed in ControlWeb 6.1 by ControlSoft s.r.o. (Czech Republic). The controlling procedures were developed within the scope of this thesis and implemented into the custom-made software. This software ensured good control and safe running of the apparatus and effectively eliminated potential plugging of the tube reactor and the manifold by the growing polymer.

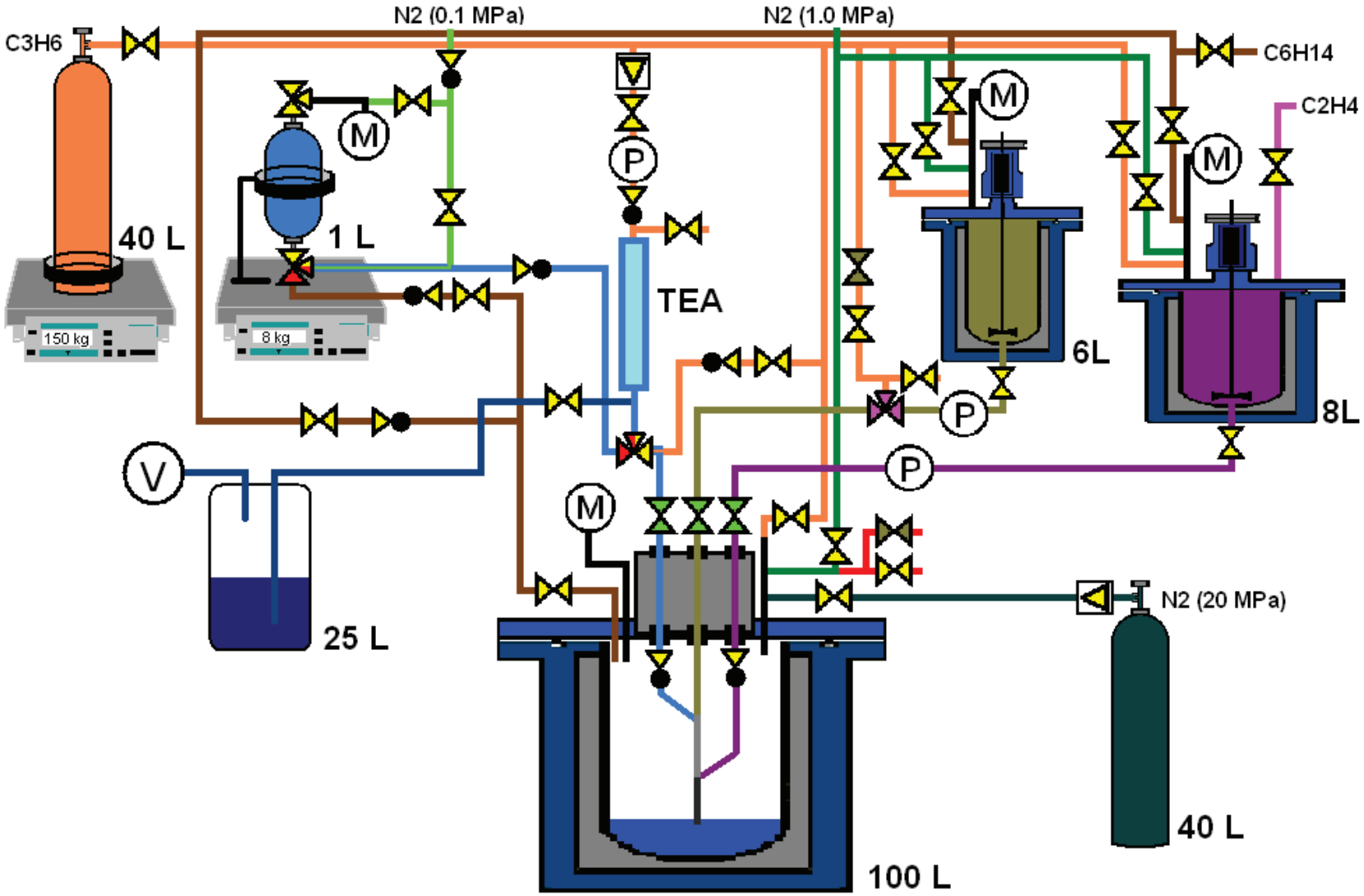

Figure 20: Schematic illustration of the high pressure stopped-flow polymerization apparatus for homopolymerization and block copolymerization.

3.3.1 Development of Mass Flowmeter for Catalyst Slurry

The flow rate of catalyst slurry was set by the pressure difference between the 6 L and the 100 L vessels. As commercially available flowmeters for liquids are not constructed for the measurement of heterogeneous slurry flow, a special mass flowmeter for slurry was designed within the scope of this thesis. The measurement was based on the exact determination of catalyst slurry temperature change after passing through a small cooler with a constant cooling efficiency. Calibration was then necessary for the evaluation of the corresponding slurry flow. Figure 21 shows that the value of slurry flow was evaluated from the three-dimensional dependence of flow rate (dC3/dt) on the difference between the inlet and outlet temperature of slurry (dTin-flow) and the cooling intensity (dTin-ch). The cooling intensity (dTin-ch) was defined by the difference between the temperature of the cooling water and the temperature of the catalyst slurry entering the flowmeter. The thermocouples utilized for the measurement of inlet temperature and cooling water were the 1 mm thick E type. The outlet temperature of the slurry was measured also by the E type thermocouple, but 0.5 mm thick only, and welded onto the outer surface of a 1/8 inch capillary. This very thin thermocouple enabled measurement of instant changes in slurry temperature with a rapid response. After the calibration, this mass flowmeter allowed the measurement of flow of liquid propylene with catalyst in the range of 200 – 7 000 g/h with an accuracy of about ± 2 % of the reading.

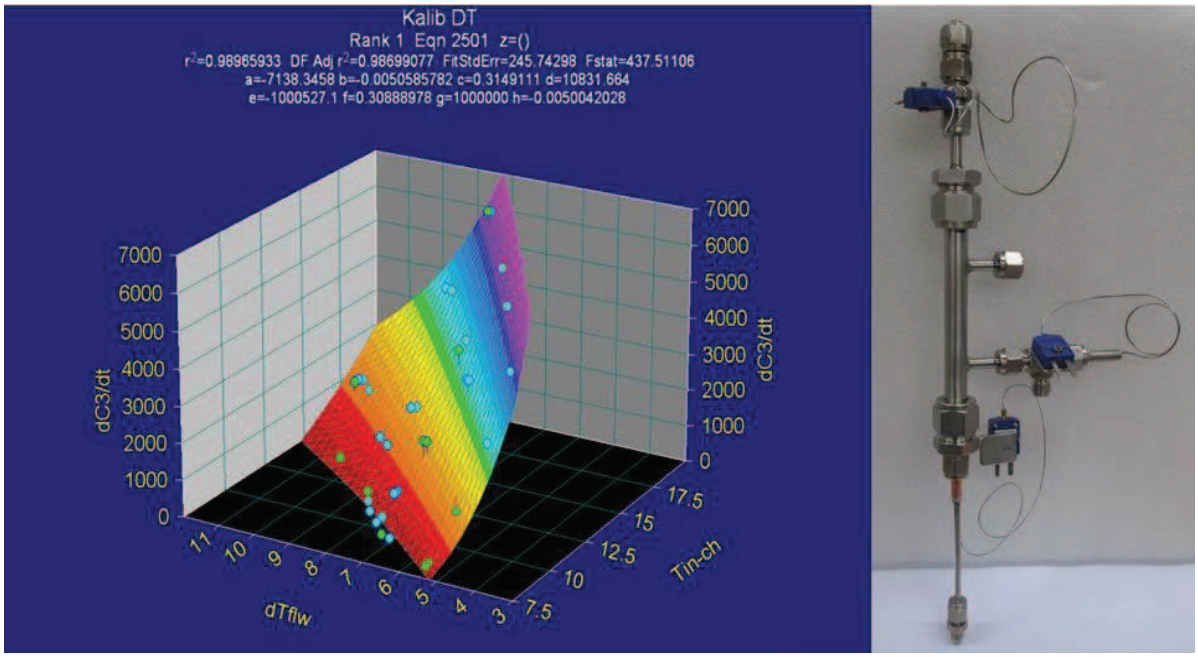

Figure 21: The self-made mass-flow meter and 3D calibration dependence of flow rate (dC3/dt) on the difference between the inlet and outlet slurry temperature (dTin-flow) and the cooling intensity (dTin-ch).

3.3.2 Polymerization Reactor

Within the scope of this thesis capillaries made from different materials were tested as possible capillary reactors for the stopped-flow apparatus. The stopped-flow capillary reactor was placed in a 100 L vessel. Finally, it was found that the most suitable material is glass, because in the case of metal capillaries (stainless steel or copper) the polymerizing catalyst was retained on the walls and caused plugging of the capillary reactor.

Originally, a stainless steel needle, placed in the centre of a polymerization capillary, was used for TEA dosage into the reactor. However, this configuration did not provide sufficient mixing of catalyst with co-catalyst, thus the catalyst was not completely activated and exhibited low polymerization activity.

The scheme of the developed system for catalyst, co-catalyst and co-monomer dosage into the capillary reactor is depicted in the right side of Figure 22. The final solution for catalyst, co-catalyst and co-monomer dosage into the capillary reactor utilized in the majority of stopped-flow experiments performed within this thesis is shown in scheme B in Figure 22. This system, based on four equivalent inlets of co-catalyst, allowed homogeneous catalyst activation throughout the whole diameter of the polymerization capillary.

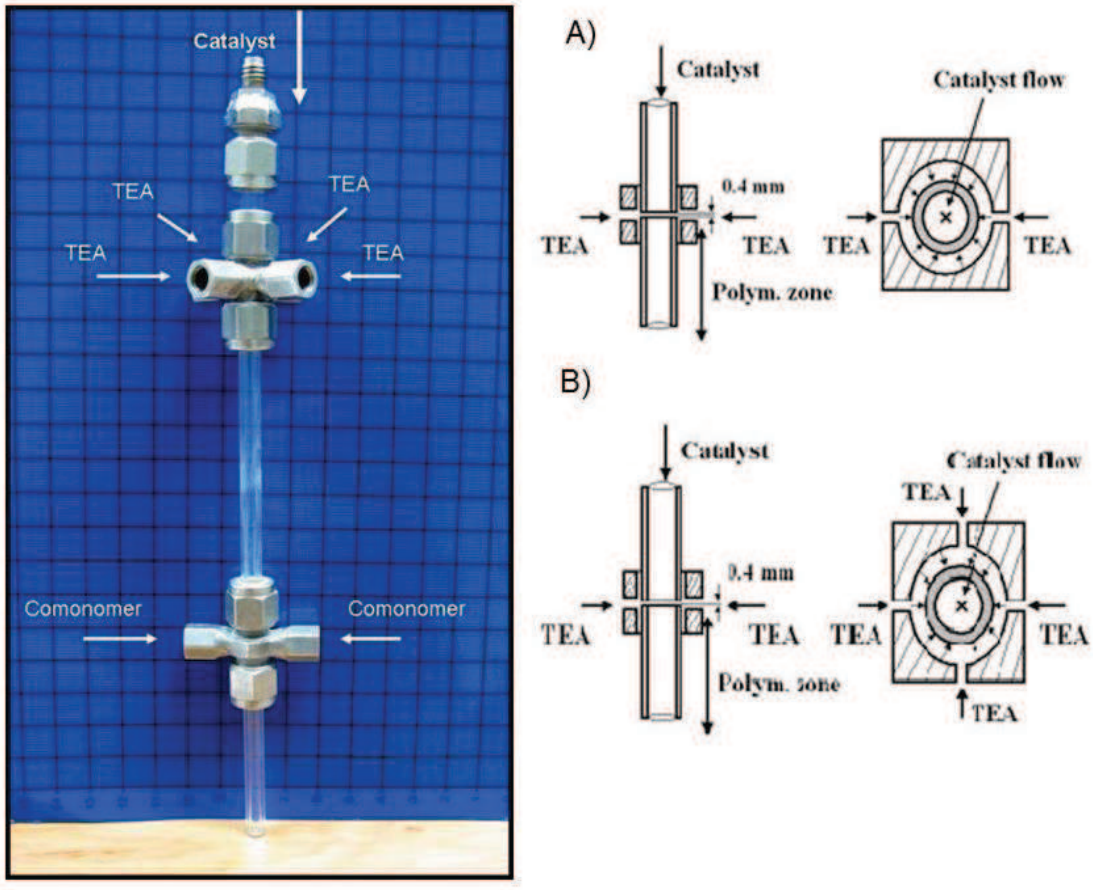

Figure 22: Picture of glass capillary polymerization reactor (on the left) and different designs of co-catalyst injection system (on the right).

The influence of design of the co-catalyst injection system on catalyst activity is shown in Table 2. The table clearly shows that co-catalyst (TEA) introduction through the needle did not provide sufficient mixing of the catalyst and TEA. The use of two inlets showed two times higher catalyst activity in comparison with the needle construction. It is obvious that the highest polymerization activity and the best catalyst activation were achieved with a four co-catalyst inlet system. In comparison with the two inlet system the activity increased almost four times. Therefore this design was used in all the stopped-flow experiments performed within this thesis.

Table 2: Dependence of catalyst activity on design of co-catalyst injection system (capillary diameter 3.5 mm).

Mixing point design	Activity [kg/(mmol-Ti*h)]
Needle	1.6
Circular jet (2 port)	3.2
Circular jet (4 port)	12.6

Besides this six of polymerization experiments with various capillary diameters were also performed. It was found that a capillary with a 3.5 mm diameter is optimal and allows the smooth course of the polymerization experiment with the tested catalyst (the diameter might be not suitable for a catalyst containing bigger particles).

The length of the capillary was modified to achieve different polymerization times, which varied from 0.1 s (length 20 mm) to 0.5 s (length 200 mm). A longer total polymerization time (sum of homopolymerization and copolymerization time) could not be achieved due to increased plugging of the longer capillaries. The plugging also limited the maximum concentration of the catalyst slurry to 0.3 mg/ml. With such conditions about 200 mg of the polypropylene homopolymer yield was typically obtained during each experiment.

3.4 POLYMERIZATION PROCEDURE

All the stopped-flow polymerizations performed within this thesis were carried out in liquid propylene. The polymerization procedure developed is described below.

3.4.1 Filling Catalyst Slurry into a 6-Litre Vessel

Before the stopped-flow polymerization run the 6-litre vessel was purified by nitrogen flow at 95 °C for ca. 60 min. Subsequently, the reactor was cooled to 15 °C still under the continuous nitrogen flushing. Then 25 µL of surface active agent (Atmer 163) was introduced by a Microman micropipette (Gilson, France). The pipette allowed dosing of viscous Atmer 163 with a high accuracy (± 3 %). Subsequently, 2 300 g of propylene was introduced from a 40-litre pressure cylinder, which was heated and placed on balances.

The defined amount of catalyst slurry in n-heptane was sampled from a storage vessel by a PE syringe with a metal needle and introduced into the catalyst charging

device under a protective flow of nitrogen. Then the catalyst slurry was flushed into the 6-litre vessel with ca. 200 g of liquid propylene. After catalyst introduction the total propylene amount in the vessel was 2 500 g.

To prevent penetration of the catalyst powder to the magnetic coupling (for the protection of the bearings), the cover of the 6L vessel was cooled with cold water. This procedure causes the condensation of propylene in the coupling of the stirrer and prevents the penetration of the catalyst into the bearings of the stirrer.

3.4.2 Filling Ethylene Comonomer into an 8-Litre Vessel

As ethylene is gaseous under the applied conditions, isopentane was chosen as a suitable solvent and carrier for ethylene. A known amount of isopentane (maximum 3 000 g) was transferred into the 8-litre vessel from a 20-litre pressure cylinder placed on balances. Subsequently, the isopentane was saturated with ethylene supplied from another 20-litre pressure cylinder. The amount of ethylene introduced into the 8-litre vessel was set to cause an increase in the pressure to ca. 0.1 MPa above the pressure in the 100-litre vessel. Besides this, the temperature of the 8-litre vessel was also set to a value ca. 10 °C higher than the temperature inside the pre-heating chamber for all the capillary inlets leading into the 100-litre vessel where the stopped-flow capillary reactor was placed. It was found that this configuration was optimal for preventing formation of ethylene bubbles in isopentane during the stopped-flow polymerization in the capillary reactor.

3.4.3 Filling of TEA into the Dosing Tube

The TEA diluted in n-hexane (concentration 20 wt. %) was filled into the 12 m long stainless steel tube (6 mm diameter) from a 1-litre storage vessel placed on balances. Before filling, the dosing tube was evacuated, then after the switching of a three-way valve the TEA solution was sucked from the 1-litre storage vessel into the tube by the under-pressure present inside the tube after evacuation. With this procedure the dosing tube was filled with ca. 150 mL of TEA solution.

3.4.4 Elimination of Catalyst Fouling on the Walls of the 6-Litre Vessel

It was observed that catalyst powder and liquid propylene have a limited miscibility. This low miscibility caused that in the presence of liquid propylene the catalyst powder tended to deposit on the walls of the 6-litre vessel (see Figure 23). The analysis of titanium and magnesium content in the termination solution after the polymerization revealed that more than one third of the charged catalyst amount remained in the 6-litre vessel as deposits on the walls. The formation of catalyst deposits significantly reduced polymer yield and adversely influenced the reproducibility of stopped-flow experiments.

Thus the introduction of surface active agent N,N-bis(2-hydroxyethyl)-$C_{13\text{-}15}$ alkyl amine (commercial name Atmer 163) was proposed into the 6-litre vessel for the elimination of catalyst powder depositing on vessel walls. However, it was observed

that Atmer 163 mixed directly with the catalyst before its introduction into the 6-litre vessel decreased subsequent catalyst activity in stopped-flow polymerization. To eliminate this disadvantage, in a similar way Atmer 163 modified by TEA was tested. Modification of Atmer 163 by reaction with TEA decreased the poisoning effect on the catalyst, however it also decreased the anti-fouling efficiency of Atmer 163 and a noticeably higher amount had to be applied to achieve satisfactory elimination of catalyst deposits on the 6-litre vessel walls. Unfortunately, the higher amount of Atmer 163 modified by TEA also resulted in low catalyst activity, probably due to the formation of a barrier around the catalyst particle, which retarded the penetration of the co-catalyst into the catalyst particle and activation of catalyst.

Finally, a procedure based on the dilution of Atmer 163 with liquid propylene before the catalyst introduction into the 6-litre vessel was utilized as described in Chapter 3.4.1.

Figure 23: Catalyst depositing in the 6 L vessel (left section) and its elimination by Atmer 163 surface active agent (right section).

3.4.5 Optimized Procedure of the Stopped-flow Experiment

Prior to the experiment, the 6-litre vessel with catalyst suspension in liquid propylene was heated to 50.0 °C (the cover was cooled to under 30 °C). At this temperature a pressure of ca. 1.85 MPa (g) was established inside the vessel.

A common plastic 10L bucket with terminating agent (2.5 L of isopropanol) was placed on the bottom of the 100-litre pressure vessel. The catalyst suspension feeding capillary and TEA feeding capillary, placed inside the terminating 100-litre vessel, were assembled with the mixing block. Before closing the 100-litre vessel, the polymerization capillary was permanently covered by a constant gaseous propylene

flow from a pneumatically switched 3-way TEA valve. Then the 100-litre vessel with a bucket filled with terminating solution was closed so that the outlet of the SF capillary was approximately 30 mm immersed into the terminating solution. Then the vessel was filled with nitrogen to reach a pressure close to the level previously equilibrated inside the 6-litre vessel with suspended catalyst in liquid propylene. The pressure difference between the 6-litre and the 100-litre vessels defined the flow rate of catalyst suspension from the 6-litre to the 100-litre vessel during the stopped-flow polymerization. As the 6-litre vessel was placed approximately 2.5 m above the 100-litre vessel, the pressure gradient between these two vessels has to include also the “hydrostatic” pressure of liquid propylene. Finally the pressure inside the lower 100-litre vessel had to be kept ca. 0.004 MPa above the pressure established inside the 6-litre vessel. The pressure difference of 0.004 MPa was experimentally determined and corresponded to a liquid propylene flow of ca. 3 500 g/h. The pressure gradient between 6-litre and 100-litre vessels was maintained during the whole polymerization with a high accuracy (± 0.001 MPa) this ensured steady flow of catalyst suspension during the whole experiment (3 500 ± 150 g/h) (see Figure 24). The pre-defined pressure gradient was maintained by a PID regulator, which automatically opened or closed the pneumatic needle valve which regulated rate of degassing of the 100-litre vessel. In the case of the 6-litre vessel the pressure inside was adjusted by accurate control of heating intensity (0 - 100 W).

When the defined pressure gradient between the 6-litre and 100-litre vessels was stabilized, the catalyst feeding capillary was filled with liquid propylene and the pneumatic valve placed under the 6-litre vessel was opened. When the flow of catalyst suspension was stabilized the electronically controlled three-way valve located at the end of 12 m long spiral tube filled with TEA was opened. Then the pre-defined flow of liquid propylene, controlled by a mass flow controller (Bronkhorst SA, the Netherlands), started to push out TEA from the tube into the flow of the catalyst suspension. In the mixing zone, described in Chapter 3.3.2, TEA flow was mixed with the flow of catalyst suspension in liquid propylene. This was considered as the start of polymerization. The polymerization took place in the glass capillary and the duration of the polymerization reaction was defined by its length. The end of the glass capillary was placed below the surface of a terminating agent of higher density (isopropanol), and thus after the active catalyst particle slurry in liquid propylene passed through the glass capillary, their polymerization reaction was immediately terminated by isopropanol. The termination reaction was facilitated by accessional flows of the slurry due to the high density difference between isopropanol and liquid propylene.

A special procedure for ending stopped-flow polymerization was developed, which prevented forming of undefined polymer during closing of the component flows into the capillary reactor. The ending procedure was as follows: First of all, the pneumatic valve for flushing of the catalyst line with liquid propylene was opened and the pneumatic valve located below the 6-litre vessel was closed 0.1 s later (this prevented potential overfilling of the 6-litre vessel with liquid propylene). This

procedure removed all the residual catalyst from the catalyst distribution system. Subsequently, the electronically controlled three-way valve closed the flow of TEA and TEA residuals were removed from the tube by flushing with liquid propylene. Only after the flushing of the catalyst and TEA tubing by liquid propylene was it possible to slowly decrease the pressure inside the 100-litre vessel to atmospheric level. Slow depressurising of the 100-litre vessel (lasting 2-3 hours) was necessary for moderation of propylene boiling from isopropanol. After reaching atmospheric pressure it was possible to carefully open the 100-litre vessel and remove the bucket with polymer and catalyst residues. The catalyst and TEA residues were stabilized in solution against precipitation by addition of 35 mL of hydrochloric acid. The polymer obtained was isolated from the isopropanol by filtration through the stainless steel sieve with an 18 μm mesh size. The prepared polymer samples were dried under vacuum and stored in a freezer at -18 °C.

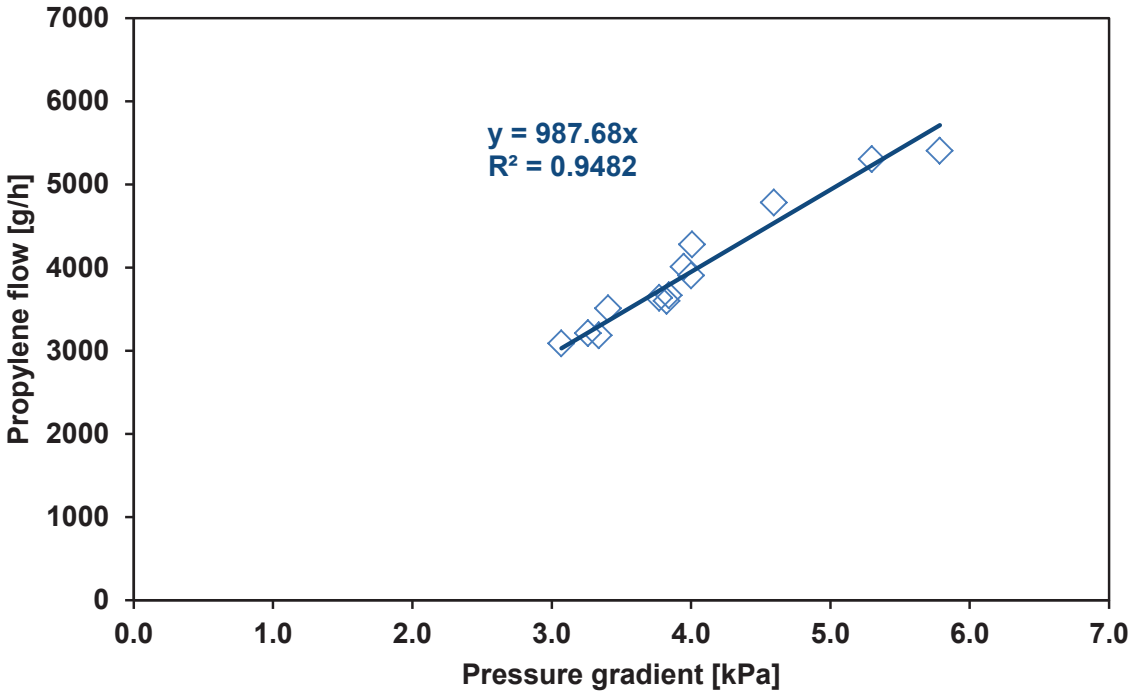

Figure 24: Dependence of catalyst suspension in liquid propylene flow on the pressure gradient between the 6-litre and 100-litre vessels.

3.4.6 Evaluation of Catalyst Ageing in Liquid Propylene

During the Stopped-Flow polymerization procedure development, the catalyst was stirred in liquid propylene in a 6-litre vessel for several hours, and sometimes also stored for days before the start of the stopped-flow experiment. Thus it was necessary to evaluate the effect of liquid propylene on the stability of catalyst polymerization performance in time. For this purpose several experiments in a 2-litre stainless steel reactor designed for catalyst testing were carried out. At model conditions in stopped-flow experiments, the polymerization runs were carried out without hydrogen and external donor.

The procedure was as follows: a 2-Litre reactor was purified by flushing with nitrogen at 95 °C for ca. 20 min. Subsequently the reactor was cooled to 25 °C. 400 g of propylene were introduced for the establishing of suitable starting conditions, then 200 mg of catalyst-oil slurry corresponding to 40 mg of the dry catalyst was introduced into the reactor, flushed with 50 g of liquid propylene via the catalyst charging device. The catalyst in liquid propylene was stirred for a defined time. When the pre-defined time of catalyst stirring in liquid propylene elapsed, the temperature inside the reactor was increased to 40 °C. The polymerization was initiated by addition of TEA in a molar ratio of Al / Ti = 150 / 1. The TEA co-catalyst (9.7 mmol) was introduced into the reactor also via the catalyst charging device, flushed with 50 g of liquid propylene. Introduction of TEA was considered as he start of polymerization, then after the elapsing of the defined polymerization time (120 s), the polymerization was terminated by the introduction 10 mL of methanol.

As is obvious from Table 3 and Figure 25, the catalyst activity decreased by 22 % after 3 hours of stirring in liquid propylene and by 25 % after 16 hours and after four days the catalyst exhibited half of the original activity.

To evaluate the effect of water, which is plausibly able to penetrate into the reactor through the seals during long-term storage of propylene in the reactor, a polymerization test with propylene aged in the reactor without a catalyst was performed.

Table 3 and Figure 25 show that the fresh catalyst introduced into the propylene stored for 16.5 hours in the reactor exhibited a catalyst activity lower by ca. 10 % only. This is apparently less than in the case when the catalyst was aged together with propylene. These experiments revealed that the catalyst is noticeably deactivated in the presence of liquid propylene, thus it is necessary to avoid storage of the catalyst in liquid propylene in 6-litre vessel for periods longer than several hours.

To investigate how much influence on catalyst performance the residual content of water and oxygen in the 2L polymerization facility had, reference polymerization was performed under the same polymerization conditions but with a different order of charged polymerization components: The co-catalyst (TEA) was introduced to the reactor at first, just after the 2L reactor’s purification. Subsequently, propylene was introduced and polymerization was started by spraying the catalyst into the reactor. After the elapsing of the defined polymerization time, the polymerization was terminated by the introduction of methanol (10 mL). Comparison of the reference experiment with the runs performed with pure propylene storage defined the level of residual impurities reactive with TEA (water, oxygen, etc.). The difference between the reference polymerization and polymerization without aging was small (3 %).

Table 3: Influence of liquid propylene on catalyst activity. Experimental conditions: polymerization time 120 s, temperature 40 °C, pressure 1.6 MPa, propylene 500 g, catalyst amount 64.7 µmol-Ti, TEA 9.7 mmol, Al/Ti 150 mol/mol.

	Aging [hour]	Activity [kg-PP/(mmol-Ti*h)]	Activity level [%]
reference	0.00	7.2	103
Propylene + Catalyst	0.00	7.0	100
	0.02	6.8	97
	0.03	6.8	97
	3.17	5.4	78
	15.50	5.2	75
	16.25	5.3	76
	17.33	5.1	73
	65.50	4.0	57
	94.00	3.7	53
Propylene	3.33	6.7	96
	16.67	6.3	90
	16.67	6.2	88

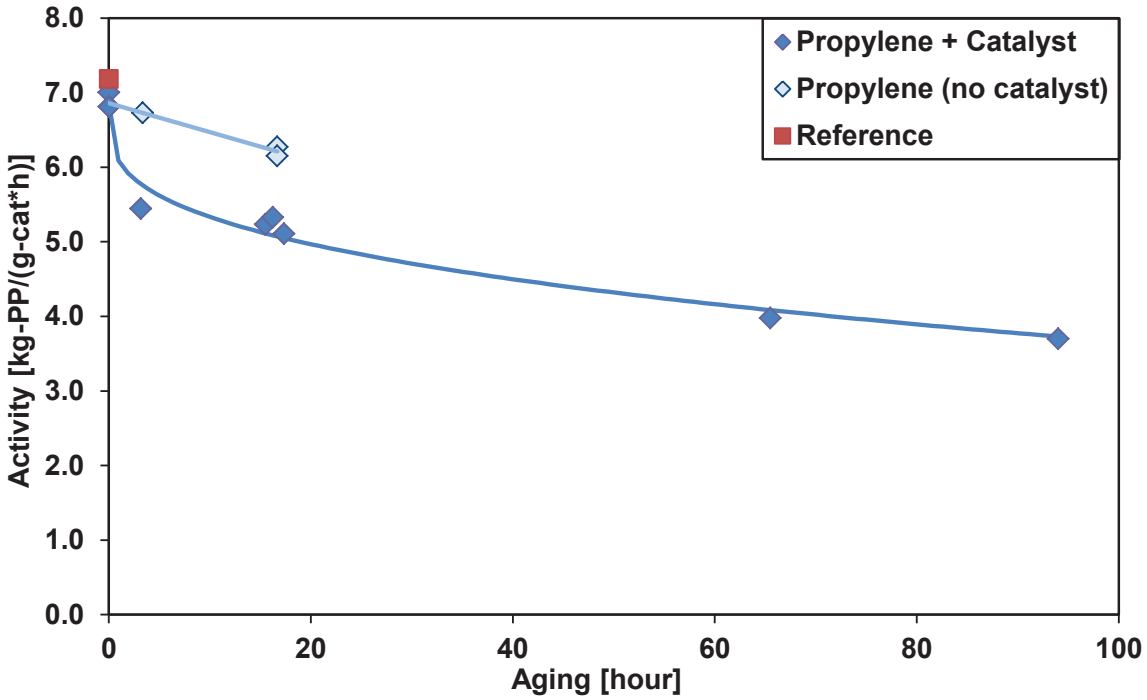

Figure 25: Dependence of catalyst activity on catalyst aging in liquid propylene.

3.4.7 TEA Co-catalyst Influence on the Catalyst

The influence of TEA on Ziegler-Natta catalyst performance has been well investigated [38, 112]. The dependence of polymerization rate on TEA concentration exhibits a sharp increase of the polymerization rate with increasing TEA

concentration to a certain maximum depending on the type of catalyst and applied experimental conditions. Further increasing of the TEA amount in polymerization leads to a decreasing polymerization rate due to active sites over-reduction by the excess of TEA.

Development of the stopped Flow polymerization procedure performed within this thesis also required investigation of TEA co-catalyst influence on the catalyst activity at low temperature (35 °C) and high pressure (1.6 MPa). Thus, a set of 120 s polymerization runs with different initial TEA concentrations was performed in a 2-litre polymerization reactor similar to that described in chapter 3.4.7. Subsequently polymerizations with similar concentrations of TEA co-catalyst and polymerization conditions were performed with a polymerization time of 0.2 s in the stopped-flow apparatus.

Table 4 summarizes the results of TEA concentration dependence on polymerization activity. In both polymerization reactors (2-litre and stopped-flow) the catalyst activity increases with the concentration of TEA. The results in Table 4 also show an increase in the xylene soluble fraction (X.S.) with increasing concentration of TEA. This was an expected effect, probably related to the extraction of an internal electron donor from the catalyst and transformation of isospecific active sites into low stereospecifity types.

Figure 26 shows a comparison of TEA concentration influence on the catalyst activity in the 2-litre and stopped-flow reactors. The catalyst activity in the stopped-flow apparatus is apparently higher than the activity in the 2-litre reactor and apparently approaches a plateau at levels of TEA higher than 15 mmol/L. The higher catalyst activity observed in stopped-flow polymerizations can be attributed to the significantly shorter polymerization time (0.2 s versus 120 s in the case of the 2-litre reactor). As it is described in Chapter 1.2, in very short polymerization times (less than 1.0 s) the TEA co-catalyst only activates the catalyst by reduction of Ti^{4+} to Ti^{3+}. Then in polymerizations longer than 1.0 s a decrease of catalyst activity occurs by further reduction of Ti^{3+} to the inactive Ti^{2+} form. Other possibilities of deactivation or dormant active sites as described in Chapter 1.2 are low probability due to the low polymerization temperature and very short polymerization time.

Table 4: Influence of TEA concentration on the catalyst activity and the amount of PP soluble in cold xylene (X.S.). Experimental conditions in the 2-litre reactor: polymerization time 120 s, temperature 30 °C, pressure 1.6 MPa (g), propylene 500 g, catalyst amount 64.7 µmol-Ti. Experimental conditions in the stopped-flow apparatus (SF): polymerization time 0.2 s, temperature 30 °C, pressure 1.6 MPa (g), propylene flow 3 000 g/h, catalyst flow 0.4 mmol-Ti/h.

	[TEA] [mmol/L]	Activity [kg-PP/(mmol-Ti*h)]	X.S. [%]
2-liter reactor	5.3	2.3	-
	10.8	4.8	4.4
	21.3	8.2	5.3
	31.1	11.1	7.0
Stopped-flow reactor	0.7	2.6	-
	1.1	6.0	-
	6.2	13.2	-
	15.3	19.2	-
	25.5	20.3	-

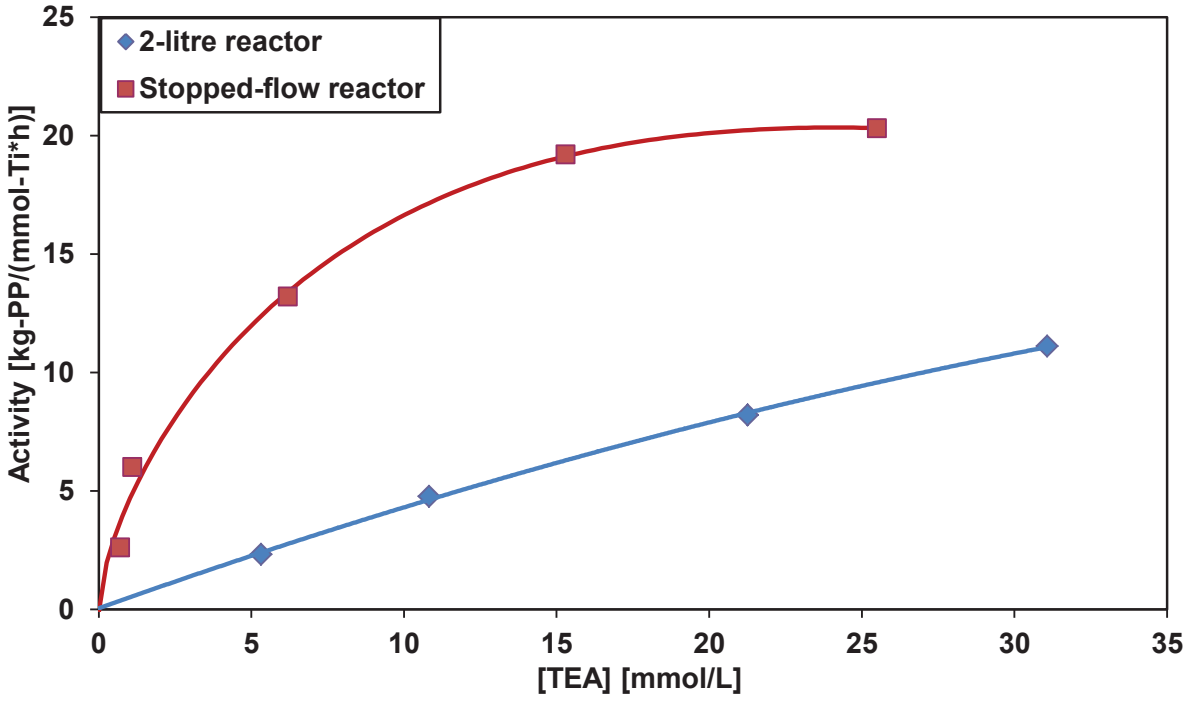

Figure 26: Dependence of catalyst activity on TEA concentration in reactor. Graph shows a comparison between the catalyst activity observed in 2-litre reactor (polymerization time 120 s) and the catalyst activity observed in the stopped-flow apparatus (polymerization time 0.2 s).

3.5 BLENDING OF COMMERCIAL ICP WITH PP-*BLOCK*-EPR COPOLYMER

Good blends of ICP with PP-*block*-EPR copolymer could be prepared in the kneader [111]. The main advantage of the kneader was the possibility of processing relatively small amounts of material. This is an important feature, because the amount of PP-*block*-EPR copolymer prepared in the stopped-flow apparatus was limited. The Brabender Plasti-Corder double-rotor kneader with an oil heated kneading chamber (50 cm^3) was used for the preparation of model ICP blends with the PP-block-EPR copolymers produced in stopped-flow polymerization. The mixtures of ICP with PP-*block*-EPR copolymers as well as the original ICP sample were kneaded for 5 min at 220 °C. Before kneading, blends were stabilized by 0.3 wt. % of Irganox B225 antioxidant.

Buráň [111] empirically determined that the most suitable kneading speed of ICP/PP-*block*-EPR blends in a Brabender kneader is 50 rpm. Under these conditions the ICP material shows a good dispersion of EPR domains in the PP homopolymer matrix, which is demonstrated by high fracture toughness. At a higher speed (70 rpm) the EPR dispersion in the matrix is not that good, because the fracture toughness of the material is significantly lower.

4 RESULTS AND DISCUSSION

4.1 STOPPED-FLOW HOMOPOLYMERIZATION

Finally, after completion of the stopped-flow apparatus and optimization of the stopped-flow polymerization procedure, the initial basic study focused on the evaluation of the relationship between polymerization time and polymer yield was performed. The results shown in Figure 27 indicate, that a lot of experiments trace the relatively long period within which the polymerization rate is increasing. In reality, it almost looks like the polymerization reaction started after ca. 0.10 s after the catalyst and TEA co-catalyst flows mixing. As Mori et al. [4] determined that the formation of active sites (i.e. reaction of the catalyst with the co-catalyst) occurs within a very short period (ca. 0.01 s), it is obvious that some physical phenomena caused a retardation of the activation reaction of the catalyst with the co-catalyst and the formation of active sites in our stopped flow experiments. We assume that the diffusion limitation in liquid propylene around catalyst particles is the main reason that slows the catalyst activation in the stopped-flow capillary reactor.

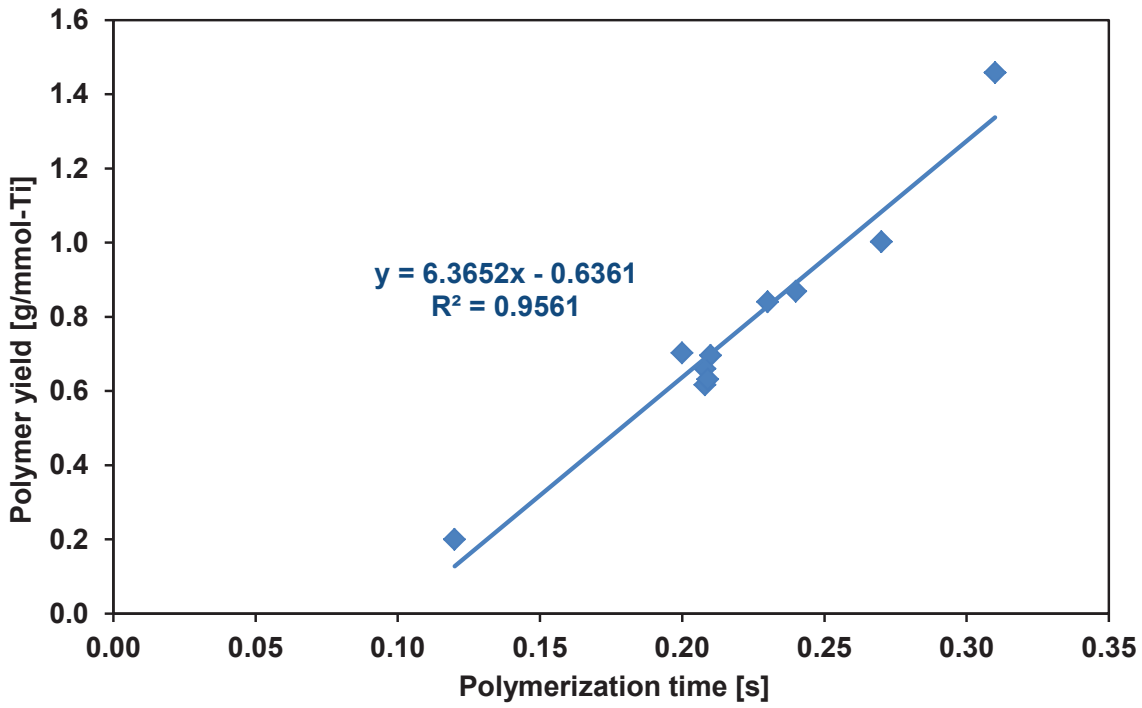

Figure 27: Dependence of homopolymer yield on polymerization time in the capillary reactor of the stopped-flow apparatus. Experimental conditions: Capillary diameter 3.5 mm, polymerization temperature 30 °C, pressure 1.6 MPa (g), catalyst flow 0.3 mmol-Ti/h, Al/Ti molar ratio 450 mol/mol.

4.1.1 Catalyst Activation study

For deeper understanding of catalyst activation consequences, several catalyst pre-activation experiments with TEA were performed to accelerate the slow initial polymerization start-up described in Chapter 4.1. For the study of the pre-activation

effect the standard stopped-flow homopolymerization procedure had to be modified. The 6-litre vessel was purified according to the standard procedure described in Chapter 3.4.1. However, after it was cooled, the appropriate co-catalyst (TEA) amount and a surface active agent (Atmer 163) were introduced with a Microman micropipette. Then, instead of propylene, 2 300 g of propane were introduced into the 6-litre vessel. The catalyst slurry was charged with a PE syringe into the catalyst charging device and flushed into the reactor with ca. 200 g liquid propane against the propane pressure. After the catalyst introduction, the total propane amount in the 6-litre reactor was 2 500 g. Before commencing the stopped-flow polymerization, the catalyst was kept in contact with TEA for ca. 20 min. Subsequently, the polymerization was initiated by mixing the activated catalyst flow with flow of liquid propylene with additional TEA.

The results presented in Table 5 and Figure 28 show the apparent increase of catalyst activity after the activation. It is obvious that catalyst activation at an Al/Ti molar ratio of 43 mol/mol led to more than three times higher catalyst activity in comparison with the experiment performed without catalyst activation. A further Al/Ti ratio increase to ca. 140 mol/mol did not cause any significant change in catalyst activity. This indicates that an Al/Ti molar ratio of 43 mol/mol is already sufficient for full catalyst activation.

However, as further shown in Table 5 and Figure 28, the results obtained by DSC revealed that catalyst activation with TEA caused an apparent decrease of polymer crystallinity and melting temperature. After catalyst activation at an Al/Ti molar ratio of 85 mol/mol, the crystallinity of the produced polymer was lower by ca. 40 % in comparison with the polymer produced on the catalyst, which was not activated before the introduction of the propylene.

The crystallinity decrease is probably caused by the TEA induced extraction of an internal electron donor from the catalyst. This causes a significant decrease in the stereospecifity of the active sites. The solution would lie in reducing the pre-activation time or adding an external electron donor. Shortening the pre-activation time is not possible in the current configuration of the stopped-flow apparatus because of the need to set accurately the pressure difference between the 6-litre and the 100-litre vessels. Adding an external electron donor during the activation process has not been investigated yet.

Table 5: Influence of the pre-activation Al/Ti molar ratio on catalyst activity and the properties of the produced polymer (melting temperature and crystallinity). Experimental conditions: pre-activation time 20 min, polymerization time 0.27 s, temperature 35 °C, pressure 1.8 MPa (g), catalyst flow 0.5 mmol-Ti/h, Al/Ti molar ratio during polymerization 850 mol/mol.

		DSC		
Pre-activation Al/Ti molar ratio	**Activity**	**Tm**	**ΔHm**	**Crystallinity by DSC**
	[kg-PP/(mmol-Ti*h)]	**[°C]**	**[J/g]**	**[%]**
0	13.4	160.7	91.6	44.2
43	46.4	159.7	63.3	30.6
85	52.7	158.2	53.8	26.0
140	55.0	158.7	53.1	25.6

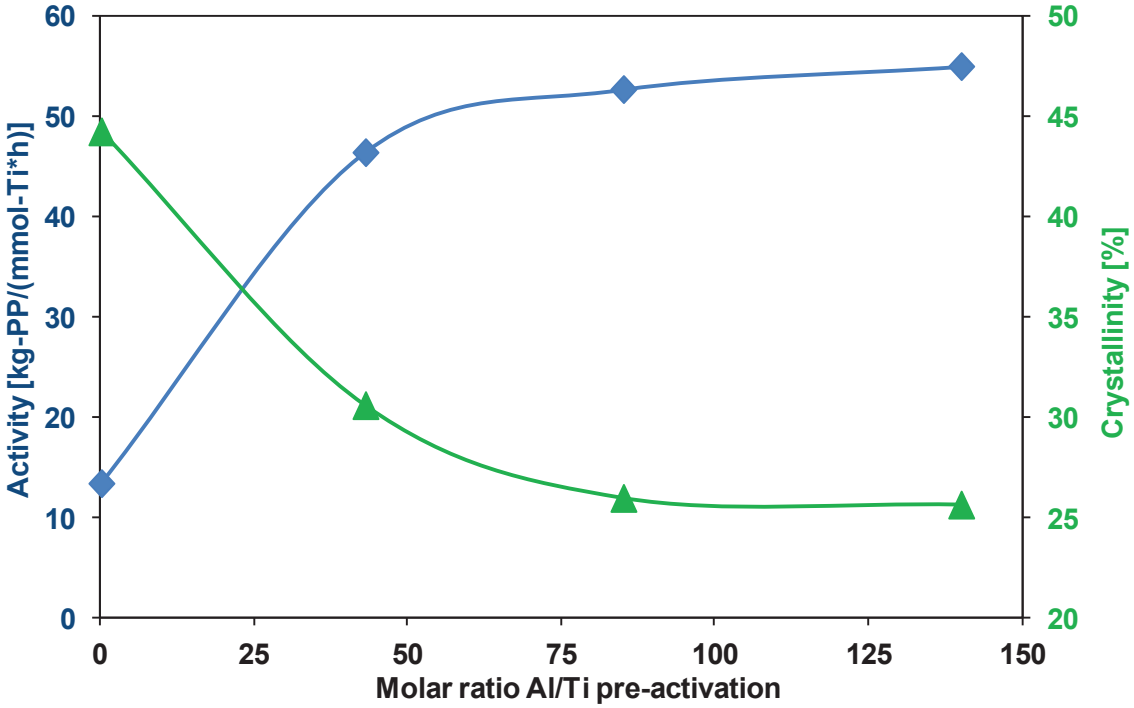

Figure 28: Dependence of catalyst activity and polymer crystallinity on the Al/Ti molar ratio applied in pre-activation.

Figure 29 shows SEM pictures of polymer particles produced with activated catalyst in dependence on the applied Al/Ti activation molar ratio. It is obvious that polymer particle morphology apparently changes with the increasing Al/Ti ratio. This change is related to the increasing amount of amorphous polymer material produced in polymerization. The particles with a higher content of amorphous polymer have an apparently smooth surface in comparison with particles where the content of amorphous polymer is low (see Figure 29).

Computer micro-tomography (μ-CT) was used to study the morphology of polymer prepared by stopped-flow technique. Figure 30 shows computer micro-tomography scans of homopolymer without pre-activation and homopolymer with pre-activation at an Al/Ti molar ratio of 140 mol/mol. Samples contain polymer particles of size 20 to 50 μm. Samples without pre-activation (Figure 30a) consists of porous particles, suggesting that the polymerization is carried out mainly on the surface and the particles are hollow inside, because inactivated catalyst residues were removed during the polymer isolation procedure by dissolving in acidified isopropanol without leaving anything inside the polymer particles. On the other hand, the sample with pre-activation (Figure 30b) is formed by polymer particles which are filled by polymer. It shows that the pre-activation process facilitates activation of the active site precursors also inside the catalyst particles. The contrast of the tomography images of the particles in the case of these particles are lower which can be explained by the lower crystallinity of the polymer produced on fully activated inner active site precursors. The polymer also easily penetrated into the particle pores surrounding the inner active species.

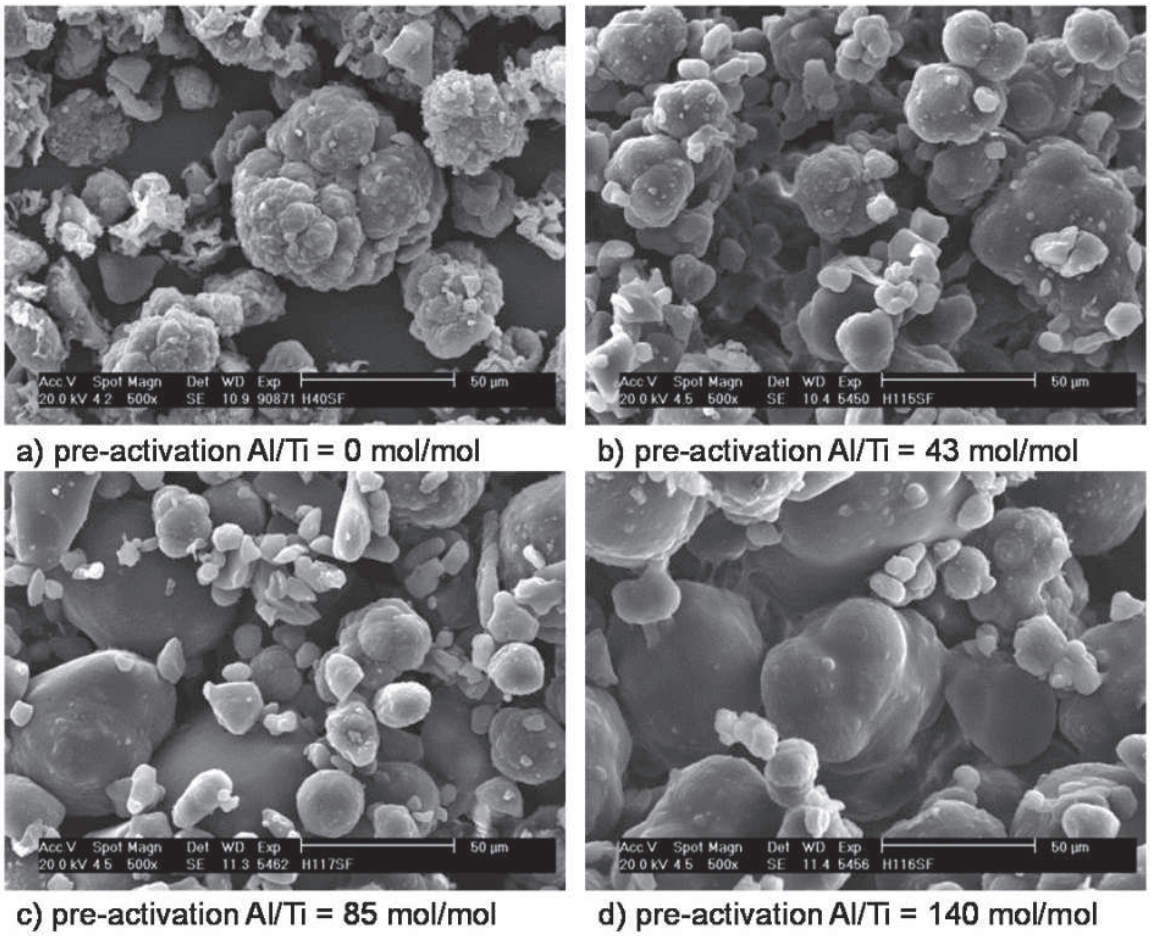

Figure 29: Morphology of polymer particles in dependence on applied activation molar ratio observed by SEM.

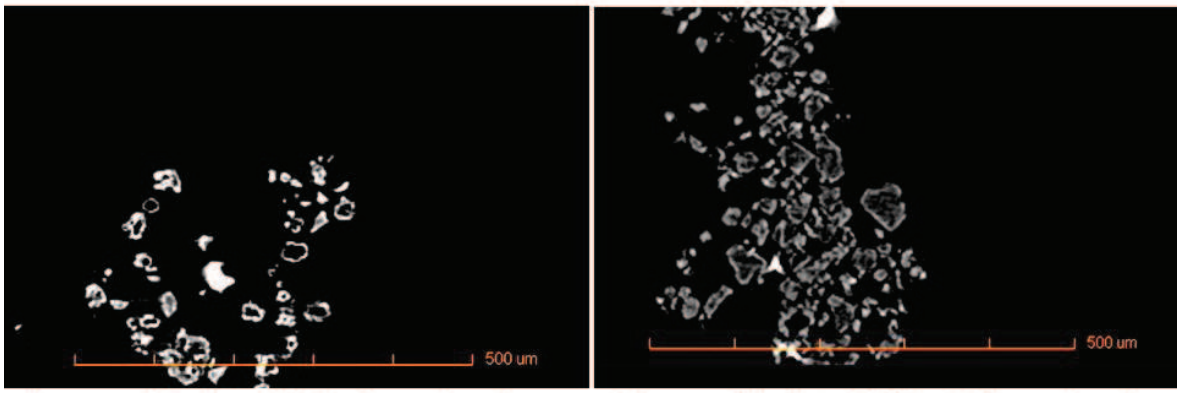

a) pre-activation Al/Ti = 0 mol/mol b) pre-activation Al/Ti = 140 mol/mol

Figure 30: Morphology of polymer particles of polypropylene homopolymer without pre-activation (a) and with pre-activation Al/Ti molar ratio = 140 mol/mol (b) observed by micro - computer tomography. Bright areas on the figures are probably inorganic parts (impurities).

4.2 STOPPED-FLOW BLOCK COPOLYMERIZATION

The main focus of this work was targeted at block copolymer synthesis because the obtained products were subsequently further utilized for blending with commercial ICP.

When preparing the block copolymer in the stopped-flow apparatus, homopolymerization takes place in the first part of the capillary reactor. The catalyst in liquid propylene is activated in the mixing zone as described in Chapter 3.3.2. After activation of the catalyst in the first mixing zone with TEA solution, homopolymerization of propylene took place in the first capillary reactor. It is limited to a short time to avoid transferring the polymer chain out from the active sites. The comonomer is added to the polymerizing propylene chains on the active catalyst in the second mixing zone, and thus in the second part of the capillary copolymerization occurs. The polymerization is then terminated by the quenching agent isopropanol as described in Chapter 3.4.5.

The block copolymerization was performed mainly with an ethylene comonomer. Besides this, several runs with 1-butene were also performed for comparison. Figure 31 shows the influence of the applied comonomer on polymer yield produced in stopped-flow capillary reactors with different polymerization times set by the lengths of the capillaries.

It was found that the copolymerization of propylene with ethylene and 1-butene apparently differs in activity. Experiments with ethylene and 1-butene were performed under similar conditions, and thus it is possible to directly compare polymerization activity and comonomer incorporation. Figure 31 indicates that catalyst activity in the copolymerization of ethylene is ca. 4.3 times higher than in the copolymerization of 1-butene. It is a well-known fact that the 1-butene molecule is apparently less reactive than the ethylene molecule; therefore 1-butene incorporation into the polymer chain is noticeably slower.

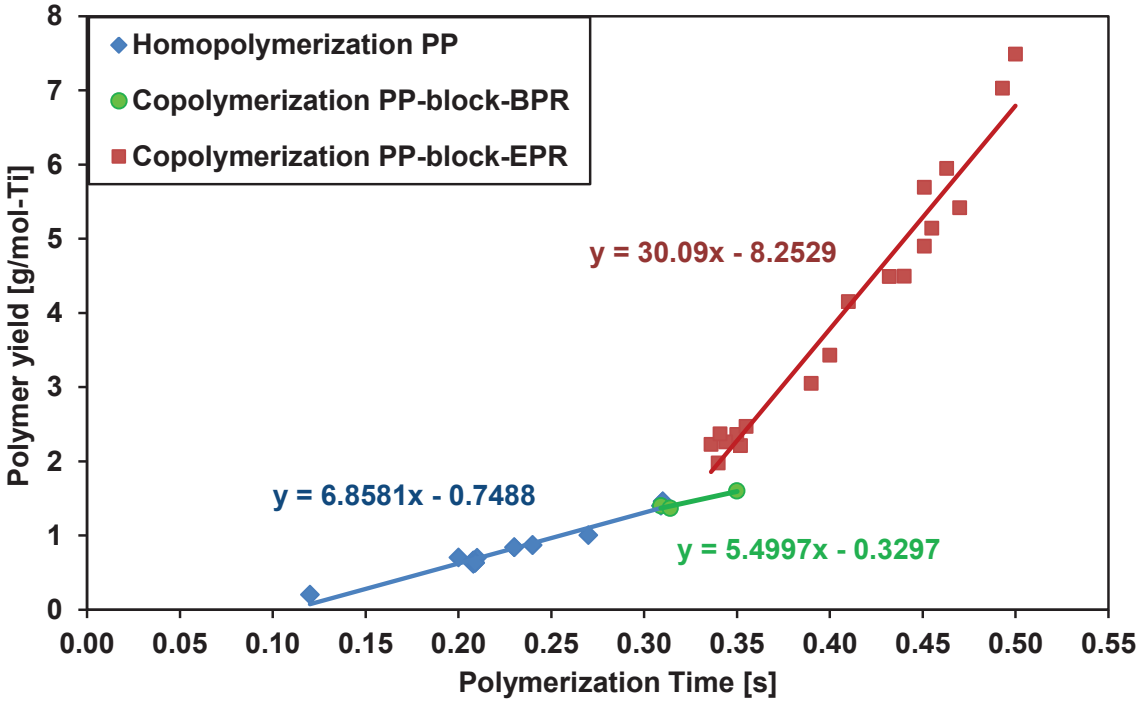

Figure 31: Dependence of polymer yield produced in homo- and copolymerization in the stopped-flow capillary reactor on polymerization time. BPR – butene-propylene rubber, EPR – ethylene-propylene rubber.

Table 6 show amount of comonomer incorporated into the polymer during stopped-flow copolymerization. The amount of comonomer in the polymer was determined by FTIR analysis. Figure 32 shows the FTIR spectra obtained of PP homopolymer and copolymers of propylene with ethylene and 1-butene prepared by stopped-flow apparatus. In the FTIR spectrum of the PP-BPR copolymer 1-butene comonomer was defined by the peak at 767 cm^{-1}. 1-Butene content in this sample was calculated to be only 1.5 wt. %. In the spectrum of PP-EPR, copolymer peaks at 729 and 720 cm^{-1} were identified. These peaks correspond to longer ethylene sequences. It was determined that ethylene content in the sample was ca. 28.0 wt. % and the EPR copolymer was constituted of ethylene and propylene in a weight ratio of 40:60.

Table 6: Influence of a comonomer type on catalyst activity and its incorporation in the polymer chain. Experimental conditions: polymerization temperature 35 °C, pressure 1.6 MPa (g), catalyst flow 0.3 mmol-Ti/h, Al/Ti 760 mol/mol, without Atmer 163.

	Homo time [s]	Copo time [s]	Total time [s]	Comonomer flow [g/h]	Activity [kg/(mmol-Ti*h)]	Comonomer content in polymer [wt%]
Homopolymerization PP	0.20	-	0.20	-	12.6	-
Copolymerization PP-BPR	0.20	0.15	0.35	200	16.4	1.5
Copolymerization PP-EPR	0.20	0.15	0.35	200	22.6	28.0

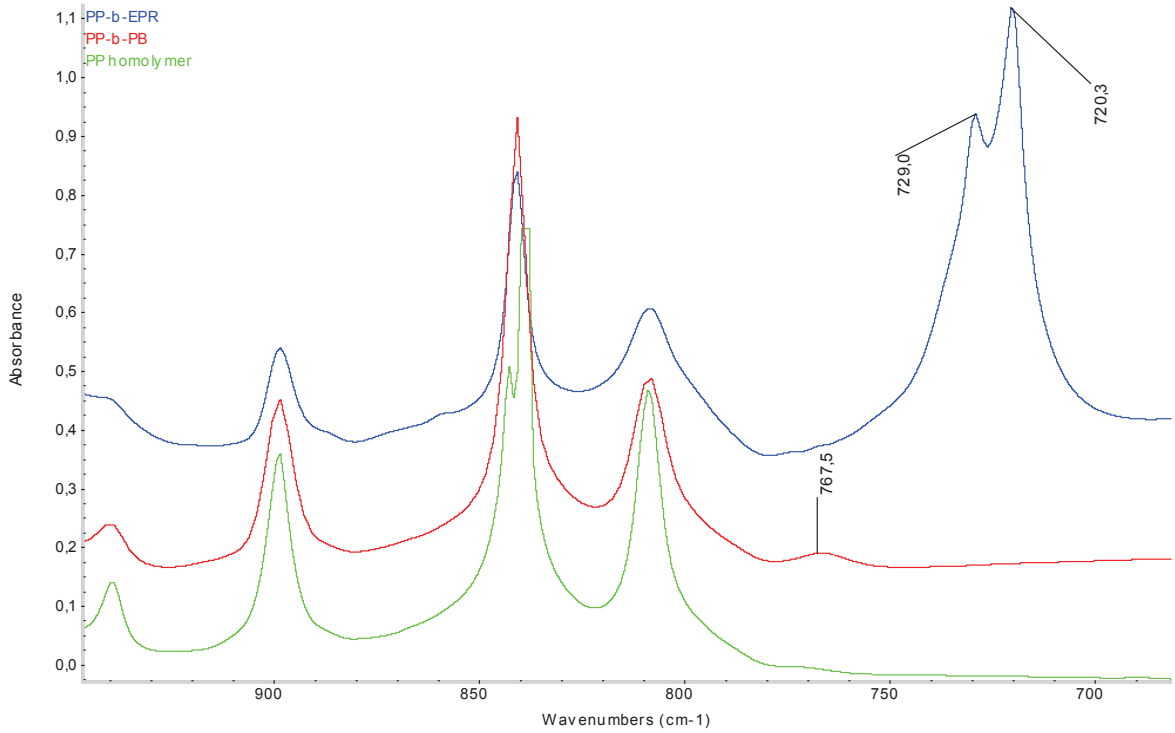

Figure 32: FTIR spectra of polypropylene homopolymer, PP-block-BPR and PP-block-EPR copolymers.

The polymer particle morphology of the prepared samples is shown in Figure 33. The observed pictures are in congruence with the results of FTIR analysis. The PP-*block*-BPR polymer particles have a similar morphology to the particles of PP homopolymer. This corresponds to very low incorporation of 1-butene comonomer in polypropylene chains. Conversely, in the case of polymer particles of PP-*block*-EPR copolymer (Figure 33c) a typical morphology of copolymer particles with a significant content of random ethylene-propylene copolymer was observed.

Figure 34 show the computer micro-tomography scans of polypropylene homopolymer (Figure 34a) and PP-*block*-EPR copolymer (Figure 34b) with homopolymerization time 0.30 s and propylene-ethylene copolymerization time 0.15 s. The copolymer particles are also filled by amorphous phase of the random ethylene-propylene copolymer. They also exhibits broader distribution of sizes (units to tens of micrometres). The broad distribution might indicate inhomogeneity in the copolymerization zone caused by scatter of comonomer concentration in the second zone of the capillary reactor and/or distribution of copolymerization time across the capillary diameter.

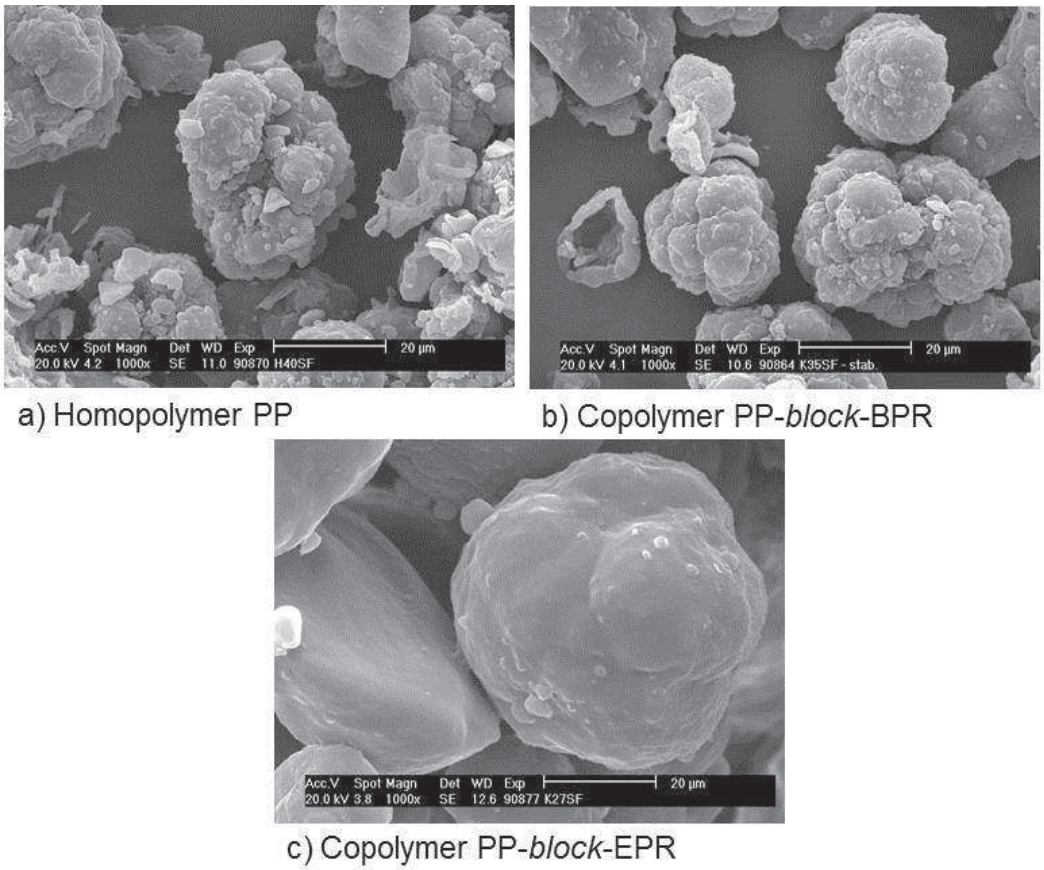

Figure 33: SEM pictures of polymer particles produced in a stopped-flow capillary reactor. a) polypropylene homopolymer, b) copolymer prepared by homopolymerization of propylene in the first zone followed with propylene-1-butene copolymerization in the second zone, c) copolymer prepared by homopolymerization of propylene in the first zone and propylene-ethylene copolymerization in the second zone.

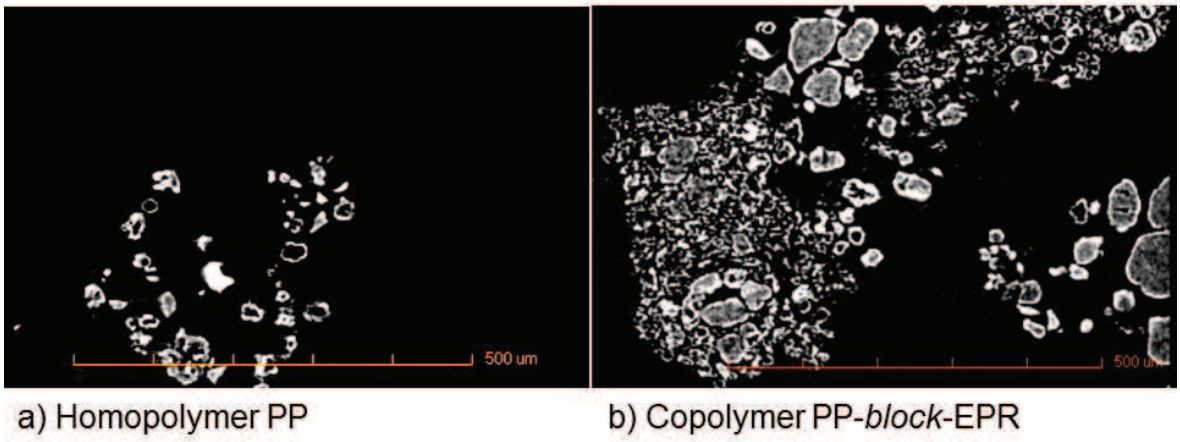

Figure 34: Morphology of polymer particles of polypropylene homopolymer (a) and copolymer prepared by homopolymerization of propylene in the first zone and propylene-ethylene copolymerization in the second zone. (b) observed by micro - computer tomography. Bright areas on the figures are probably inorganic parts (impurities).

Figure 35 shows a comparison of molecular weight distribution and M_w of the block copolymer prepared in stopped-flow apparatus (M_w = 589 500) and a homopolymer which has been synthesized under similar conditions as the homopolymer block of this block copolymerization (M_w = 314 550). It is highly probable that in the second zone of the reactor already chain transfer occurs because the homopolymerization time is prolonged by the copolymerization time to eliminate the transfer in copolymerization, while the length of the capillary for EPR block preparation was shorter. Furthermore, the diffusion rate of comonomer solution to polymerizing active centres is also limited, so that some active centres continue in homopolymerization even in the copolymerization zone (homopolymerization time may be in some active centres longer than in the case of homopolymerization). The molar mass comparison indicates that the copolymerization reactor produced a polymer with higher M_w which gives a basic idea of weight ratios between iPP and EPR blocks in the whole block copolymer.

Table 7: Comparison of molecular weight (M_n, M_w and M_z) and molecular weight distribution of the homopolymer and block copolymer. Polymerization conditions: temperature 35 °C, pressure 1.8 MPa, catalyst flow 0.5 mmol-Ti/h, Al/Ti molar ratio: 1200 mol/mol, [Atmer 163] = 0.03 mmol/L

	Homopolym. time [s]	**Copolym. time [s]**	**GPC**			
			M_n [kg/mol]	**M_w [kg/mol]**	**M_z [kg/mol]**	**M_w/M_n**
Homopolymerization	0.40	0.00	46	315	950	6.9
Copolymerization PP-EPR	0.40	0.10	68	590	1921	8.7

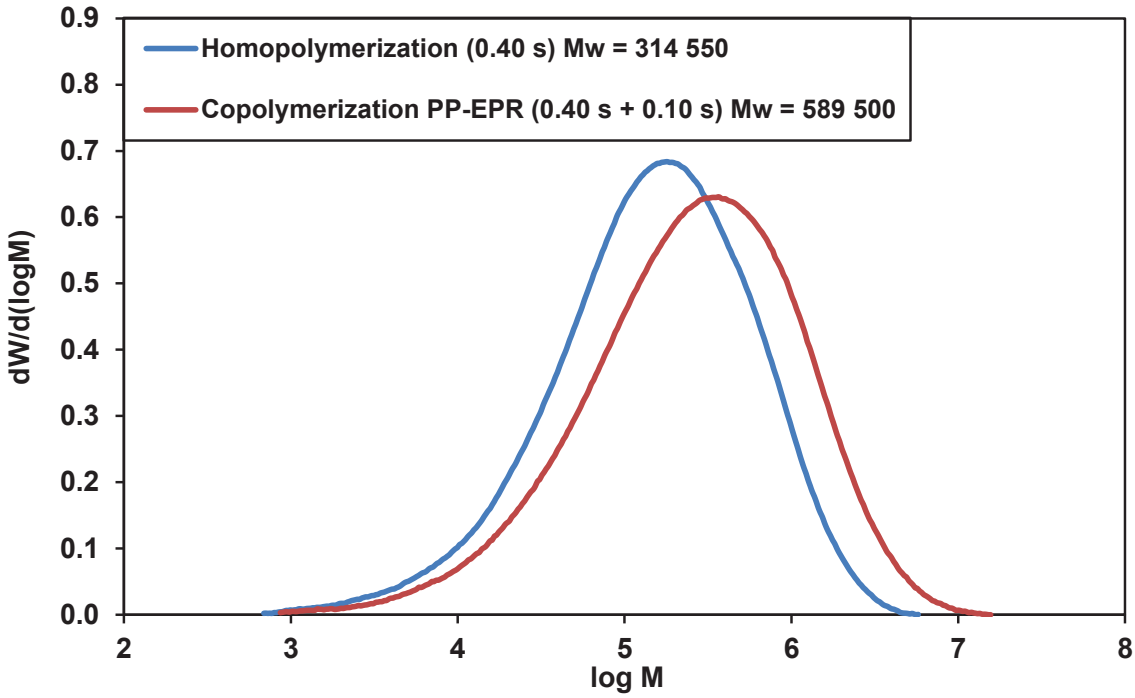

Figure 35: Comparison of the molecular weight distribution of the block copolymer (Mw = 589 500) and a homopolymer which corresponds to the homopolymer parialt conditions of this block copolymer (Mw = 314 550).

4.2.1 Characterization of Block Copolymer via TREF Fractionation

Three samples of block copolymers prepared with different ratios between the blocks of isotactic polypropylene homopolymer and ethylene-propylene rubber were selected for the next detailed analysis. After TREF analysis (Figure 36), the samples were divided into three fractions (F40, F100 and F140 °C) using the preparative TREF method. This method allows the separation of the polymer on the basis of its ability to crystallize at different temperatures as described in Chapter 3.2.6. The ratios of individual fractions obtained by preparative TREF are shown in Table 8.

TREF analysis revealed that the sample K79SF had the highest proportion of amorphous polymer (defined by fraction F40), while on the other hand the sample K104SF had a significant portion of the crystalline fraction F140 (see Table 8 and Figure 37). Finally, the K70SF sample had comparable contents of amorphous and crystalline components.

Table 8: Results of the preparative TREF records of three block copolymers produced in the stopped-flow apparatus under different conditions. Polymerization conditions: temperature 35 °C, pressure 1.8 MPa, catalyst flow 0.5 mmol-Ti/h, Al/Ti molar ratio: 1200 mol/mol, [Atmer 163] = 0.03 mmol/L

	Homopolym. time [s]	Copolym. time [s]	Ethylene flow [g/h]	Ethylene concentration [mg/L]	TREF fraction F40 (20-40 °C) [wt. %]	F100 (41-100 °C) [wt. %]	F140 (101-140 °C) [wt. %]
K79SF	0.40	0.15	66	18	41.8	24.6	33.7
K70SF	0.32	0.10	77	21	36.0	26.1	37.9
K104SF	0.38	0.11	44	12	14.4	18.7	66.9

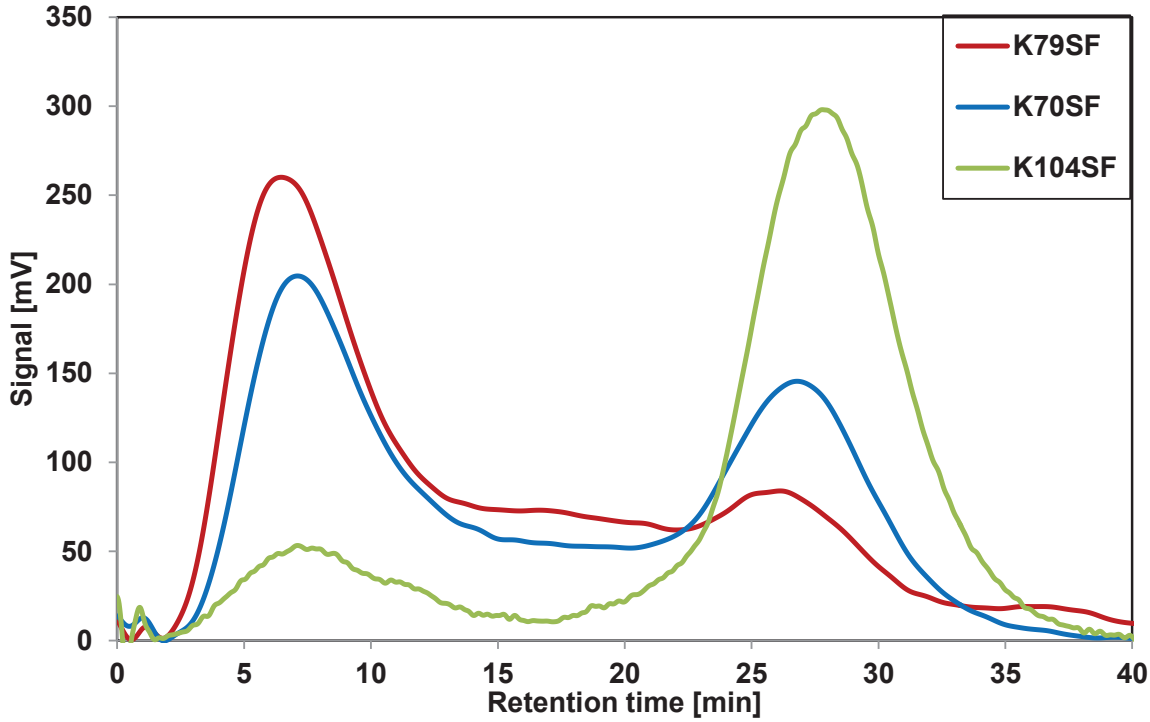

Figure 36: Analytical TREF of block copolymers produced in the stopped-flow apparatus under different polymerization conditions.

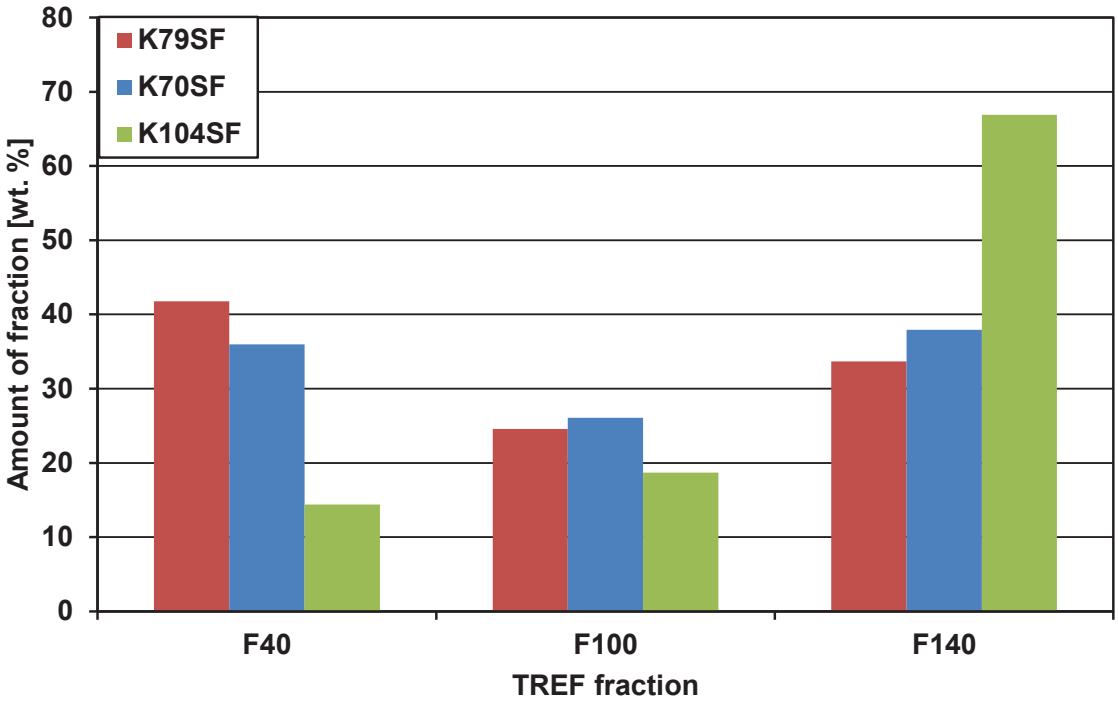

Figure 37: Comparison of the amounts of fractions obtained by preparative TREF from samples of copolymers prepared by using stopped-flow apparatus.

For the evaluation of the separation efficiency of preparative TREF, selected individual fractions from preparative TREF were further characterized by using of the analytical TREF method to verify the quality of the fractions obtained by the TREF preparative method. Figure 38 shows that the individual fractions of the sample K79SF obtained by preparative TREF are well separated, eluograms from analytical TREF of each fractions obtained by preparative TREF can be assembled together into a curve similar to the overall fraction curve from preparative TREF.

Also, to confirm the presence of real block copolymers PP-*block*-EPR in the samples produced in the stopped-flow apparatus, it was important to thoroughly separate the F140 fraction from fractions containing amorphous EPR chains (mainly F40). Then the random EPR copolymer found in the fraction F140 should be the EPR copolymer, which is directly bounded by a covalent bond to the block of crystalline PP homopolymer.

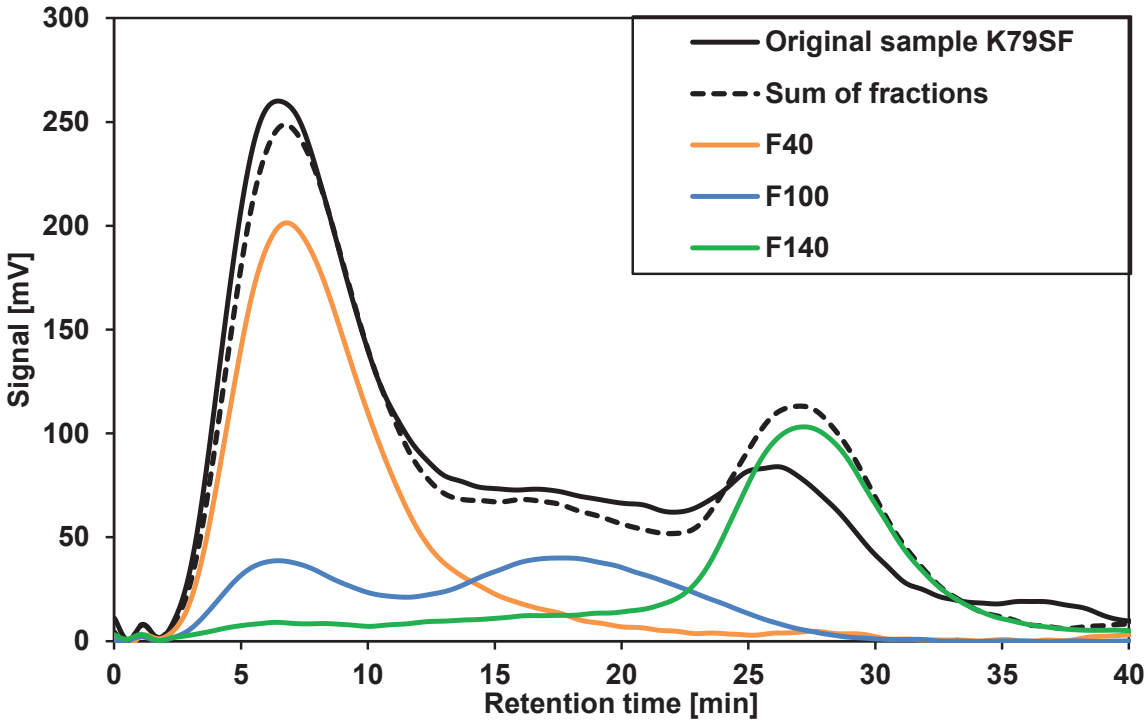

Figure 38: Analytical TREF of the original sample K79SF and fractions obtained from a preparative TREF. The dashed line corresponds to the sum of fractions based on the amount of each fraction in the original sample.

Table 9 summarizes the composition and properties of the original materials prepared by stopped-flow polymerization and their fractions obtained by preparative TREF fractionation. The composition of the samples was analysed by ^{13}C-NMR and melting temperature and crystallinity was determined by DSC. Molecular weight and molecular weight distribution was evaluated by GPC.

In the case of samples K79SF and K104SF the amount of incorporated ethylene decreases with increasing the elution temperature as shown in Figure 39. Sample K70SF exhibits the maximum incorporated ethylene in fraction F100. This sample contains the highest amount of ethylene in all fractions. The highest amount of ethylene in the crystalline fractions F100 and F140 indicate that the polymerization conditions applied in the stopped-flow apparatus during the synthesis of the K70SF sample were suitable for producing a significant amount of the real PP-*block*-EPR copolymers.

As shown in Figure 40, the fraction F40 consisted mainly of an amorphous random EPR copolymer of a low crystallinity (ca. 4 wt. %). The fraction F100 consisted of a mixture of polymer chains, which have a partial ability to crystallize. The last fraction F140 presumably contained mainly polypropylene homopolymer chains, chains with longer polyethylene sequences and chains of block copolymers PP-*block*-EPR with a long block of PP homopolymer. ^{13}C-NMR analysis revealed that this fraction contained from 2.5 to 15.6 mol. % of ethylene. As it is obvious from Table 9, the amount of ethylene in this fraction directly depends on polymerization conditions. The analyses indicated that polymer materials produced in the stopped-flow apparatus

contain significantly more ethylene in the F140 fraction than commercial sequential (ICP) copolymers, where only ca. 0.4 mol. % was determined (see Table 10). This indicates that the samples prepared in the stopped-flow apparatus probably contain a significant quantity of PP-block-EPR copolymers.

Table 9: Characterization of original copolymer samples and their TREF fractions by ^{13}C-NMR, DSC and GPC methods.

		Amount of fraction	^{13}C-NMR		DSC - 2nd melting			GPC			
			Ethylene	Propylene	ΔHm	Tm	Crystallinity	M_n	M_w	M_z	M_w/M_n
		[wt. %]	[mol. %]	[mol. %]	[J/g]	[°C]	[%]	[kg/mol]	[kg/mol]	[kg/mol]	
K79SF	original	100.0	21.0	79.0	13.2	162.1	6.4	36	325	1123	9.0
	F40	41.8	35.2	64.8	8.7	67.1	4.2	22	157	512	7.3
	F100	24.6	21.5	78.5	59.9	121.2	29.0	60	267	624	4.5
	F140	33.7	2.9	97.1	83.9	164.1	40.5	110	331	688	3.0
K70SF	original	100.0	33.4	66.6	33.0	162.7	15.9	48	228	924	4.7
	F40	36.0	43.0	57.0	10.0	60.4	4.8	-	-	-	-
	F100	26.1	51.2	48.8	25.2	151.4	12.1	-	-	-	-
	F140	37.9	15.6	84.5	72.3	164.8	34.9	-	-	-	-
K104SF	original	100.0	9.0	91.0	82.6	160.2	39.9	68	590	1921	8.7
	F40	14.4	23.8	76.2	-	-	-	-	-	-	-
	F100	18.7	20.3	79.7	47.1	124.2	22.7	21	222	876	10.7
	F140	66.9	2.4	97.6	97.2	160.3	47.0	95	305	640	3.2

Table 10: Characterization of commercial ICP sample and their TREF fractions by ^{13}C-NMR.

		Amount of fraction	^{13}C-NMR	
			Ethylene	Propylene
		[wt. %]	[mol. %]	[mol. %]
ICP	original	100	25.8	74.2
	F40	25.9	59.2	40.8
	F100	10.6	48.8	51.2
	F140	63.5	99.6	0.4

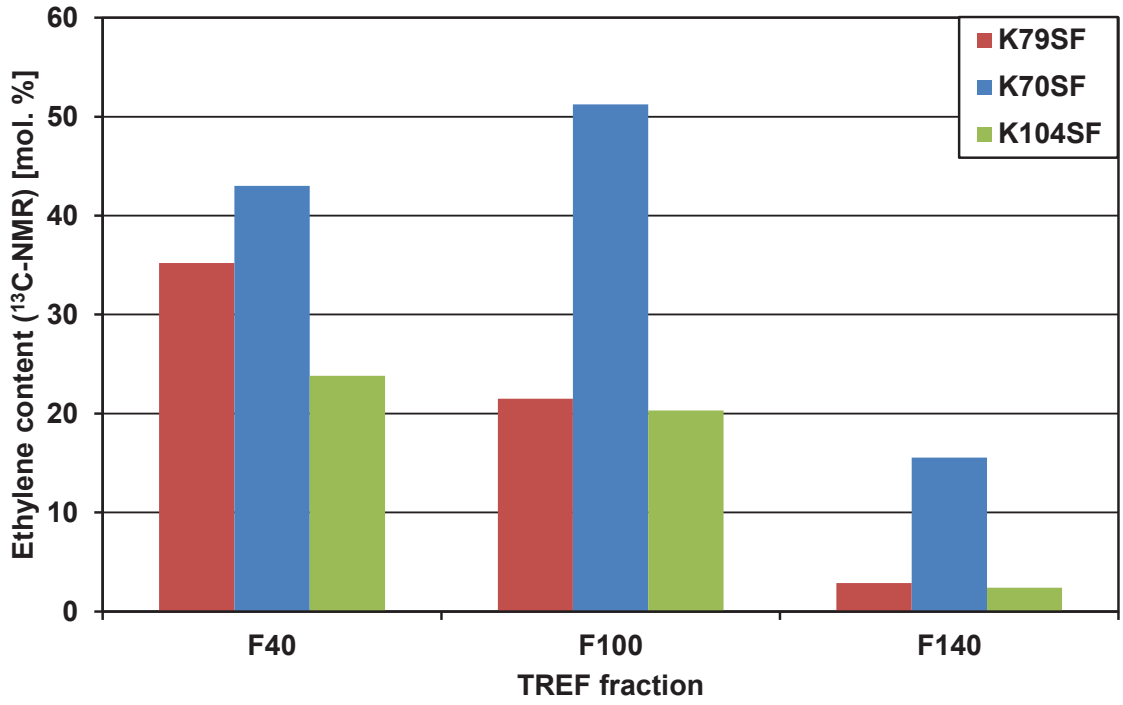

Figure 39: Content of ethylene determined in TREF fractions by ^{13}C-NMR.

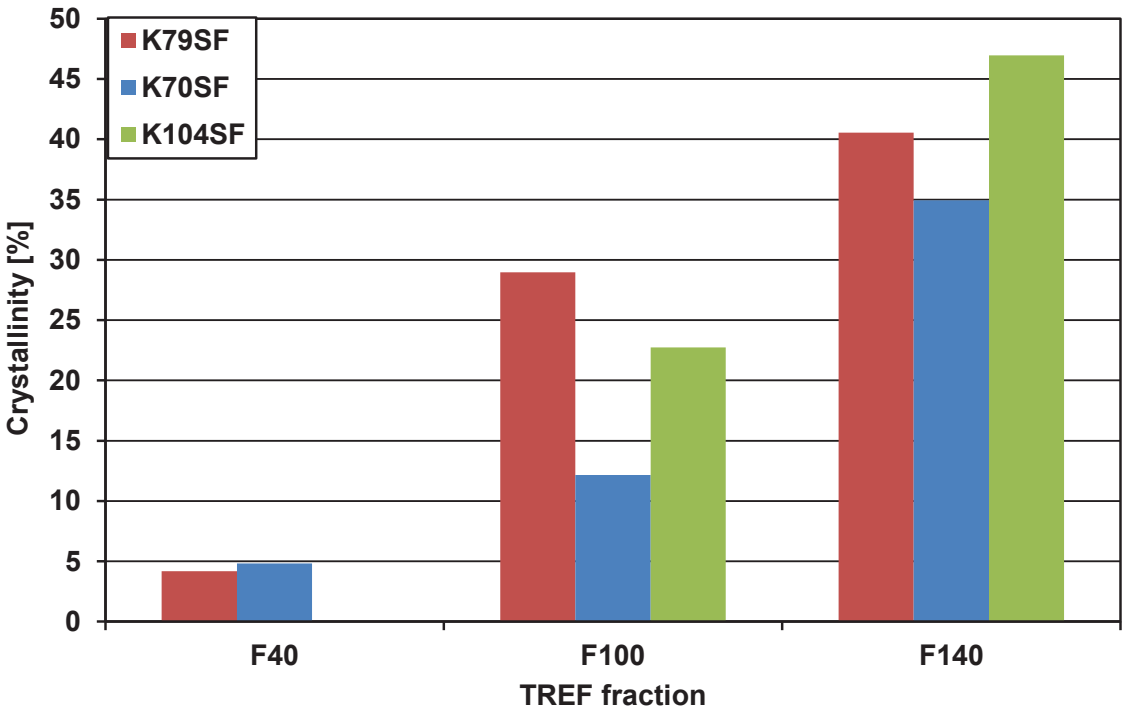

Figure 40: Crystallinity of TREF fractions determined by DSC. There was a rather low amount of fraction F40 of the sample K104SF, not enabling perform of the DSC assessment.

The polydispersity index (M_w/M_n) of the TREF fractions was determined by GPC analysis, see Figure 41. The polymer fraction F40, which contains mainly amorphous EPR polymer, has a broad molecular weight distribution (M_w/M_n = 7.3). The high

polydispersity observed in the case of the F40 fraction could be explained on the basis of a simple assumption: The EPR is produced during the copolymerization period, which follows homopolymerization, and thus the probability of chain transfer reactions increases with the prolonging of the time of polymerization. It is probable that the transfer reactions occur mainly during copolymerization (due to the longer total polymerization time and the possibility of transferring with the comonomer), which results in a broader MWD of the amorphous F40 fraction. Conversely, as was mentioned above, during the homopolymerization period transfer reactions virtually do not occur, hence, as shown in Figure 41 the crystalline fraction F140 has a significantly lower polydispersity index (M_w/M_n = 3.0).

Figure 42 shows that the crystallinity of the F140 fraction directly depends on ethylene comonomer flow. As was also mentioned above, ^{13}C-NMR analysis revealed that the fraction F140 comprises mainly of isotactic PP chains, chains with longer polyethylene sequences and chains of block copolymers with a long block of PP homopolymer. At higher concentrations of ethylene comonomer the incorporation of ethylene into the EPR block increases, which results in a decrease in the crystallinity of the whole block copolymer.

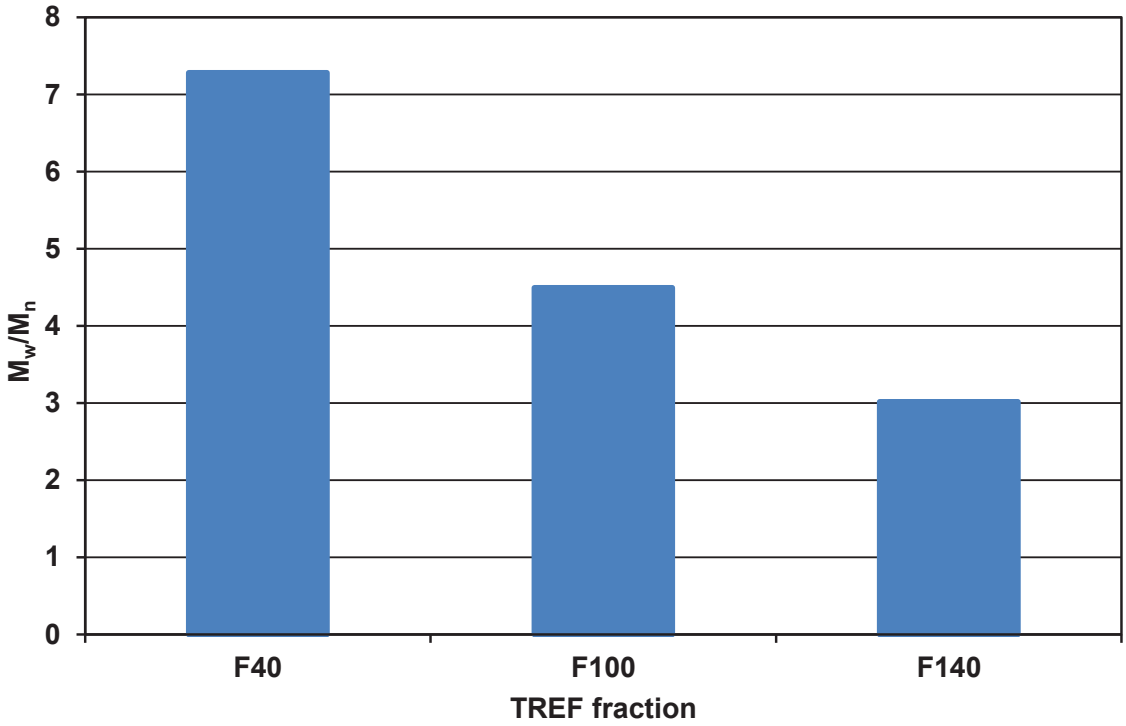

Figure 41: Polydispersity index M_w/M_n of TREF fractions of sample K79SF.

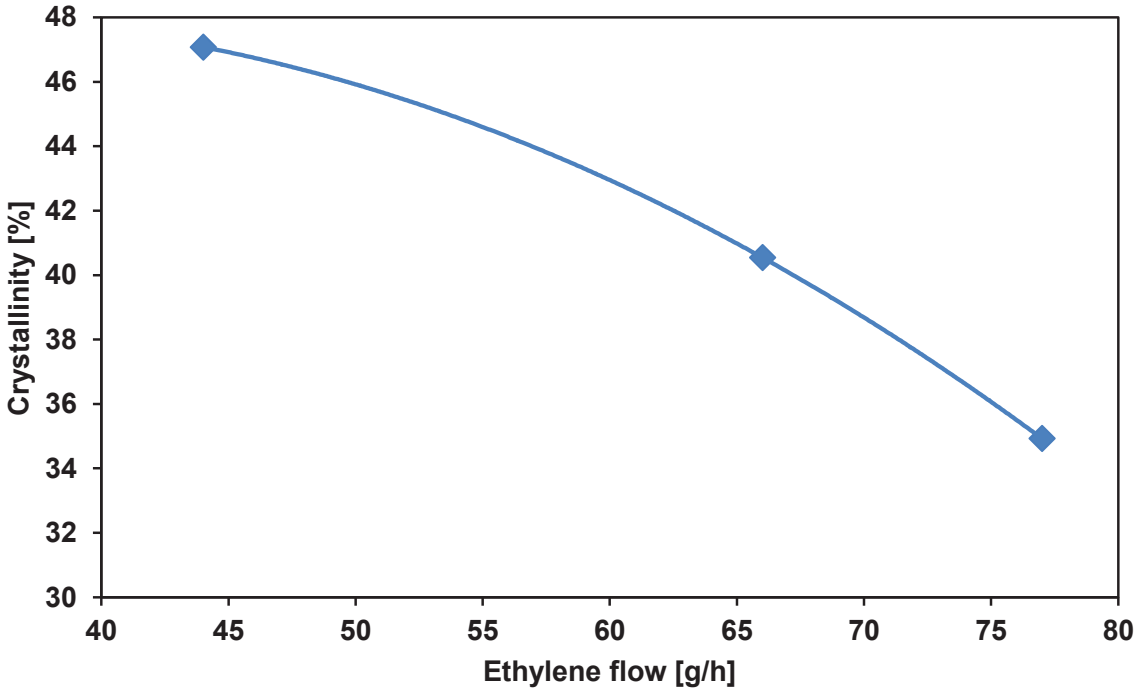

Figure 42: Dependence of polymer crystallinity determined by DSC in the fraction F140 on ethylene flow applied in stopped-flow polymerization.

4.3 BLENDS OF COMMERCIAL ICP WITH PP-*BLOCK*-EPR COPOLYMER

Three mixed samples with comparable portions of PP-*block*-EPR copolymers were synthesized in the stopped-flow apparatus and subsequently used for the preparation of model mixtures with ICP. For the testing it was necessary to produce ca. 5 g of each PP-*block*-EPR copolymer sample by mixing of 3-5 separated runs in the stopped-flow apparatus, then 3 g were used for kneading with ICP and the rest of the sample was used for the TREF fractionation and characterization. Table 11 shows the conditions applied during stopped-flow experiments and the subsequent amount of amorphous F40 (20 – 40 °C) and the crystalline fraction F100 + F140 (41 – 140 °C), determined by preparative TREF. The fractions containing chains that could crystallize (fraction 41 – 140 °C) were analysed by ^{13}C-NMR in order to determine the composition and content of total incorporated ethylene (see Table 12).

As shown in Figure 43 and Figure 44, the samples K9x and K10x were prepared with a short copolymerization time resulting in production of a minimal amount of amorphous EPR (fraction F40). The low content of free EPR chains (i.e. without covalently bonded PP homopolymer) was important in order to be able to evaluate the effect of PP-*block*-EPR copolymers on the properties of ICP. For comparison, the K8x sample with a higher content of amorphous EPR was also selected for blending with ICP.

Table 12 summarizes the composition and properties of original materials prepared by stopped-flow polymerization and their crystalline fractions (fraction 41 – 140 °C) obtained by preparative TREF fractionation. The composition of the samples

was determined by ^{13}C-NMR. Furthermore, melting temperature, melting enthalpy and crystallinity was determined by DSC.

As shown in Table 12, the K8x sample contains the most of ethylene in the crystalline fraction obtained by preparative TREF. It is possible that this sample contains the highest amount of the block copolymer PP-*block*-EPR. Samples K9x and K10x contain a significantly lower amount of ethylene in the crystalline phase, and probably a smaller amount of block copolymer.

Although the crystallinity of the crystalline part of samples K8x and K9x is almost the same, sample K9x contains less than half of the ethylene in the crystalline portion compared to K8x. This fact indicates that the composition of the EPR block (primarily the ratio between the ethylene and propylene in EPR) is dependent on the conditions of the synthesis of the polymer in the stop-flow apparatus. However, it is evident that the ratio between incorporated ethylene and propylene in the EPR block does not have to effect the crystallinity of the crystalline fraction of the block copolymer. The K10x sample probably contains shorter EPR blocks and longer blocks of isotactic polypropylene, which increases its crystallinity. This sample also has the lowest amount of incorporated ethylene in the crystalline fraction.

Table 11: Polymerization conditions in stopped-flow experiments and contents of F40 (amorphous) and F100+140 (crystalline) fractions determined by preparative TREF. Experimental conditions: temperature 35 °C, pressure 1.8 MPa (g), catalyst flow 0.5 mmol-Ti/h, Al/Ti molar ratio: 1200 mol/mol, [Atmer 163] 0.03 mmol/L.

	Homopolym. time [s]	Copolym. time [s]	Ethylene flow [g/h]	TREF fraction F40 (20-40 °C) [wt. %]	TREF fraction F100 + F140 (41-140 °C) [wt. %]
K8xSF	0.30	0.15	44	26.2	73.8
K9xSF	0.35	0.10	44	15.6	84.4
K10xSF	0.40	0.10	44	14.4	85.6

Table 12: Characterization of the original samples and theirs crystalline TREF fractions (F100+140, range of elution temperature 41 – 140 °C) by ^{13}C-NMR and DSC.

		Amount of fraction [wt. %]	^{13}C-NMR Ethylene [mol. %]	^{13}C-NMR Propylene [mol. %]	DSC - 2nd melting ΔHm [J/g]	DSC - 2nd melting Tm [°C]	DSC - 2nd melting Crystallinity [%]
K8xSF	original sample	100.0	22.7	77.3	53.8	158.9	26.0
	F100 + F140	73.8	19.6	80.4	71.0	160.7	34.3
K9xSF	original sample	100.0	17.0	83.0	64.5	159.6	31.1
	F100 + F140	84.4	9.6	90.4	70.3	159.8	34.0
K10xSF	original sample	100.0	9.0	91.0	82.6	160.2	39.9
	F100 + F140	85.6	6.1	93.9	97.2	160.3	47.0

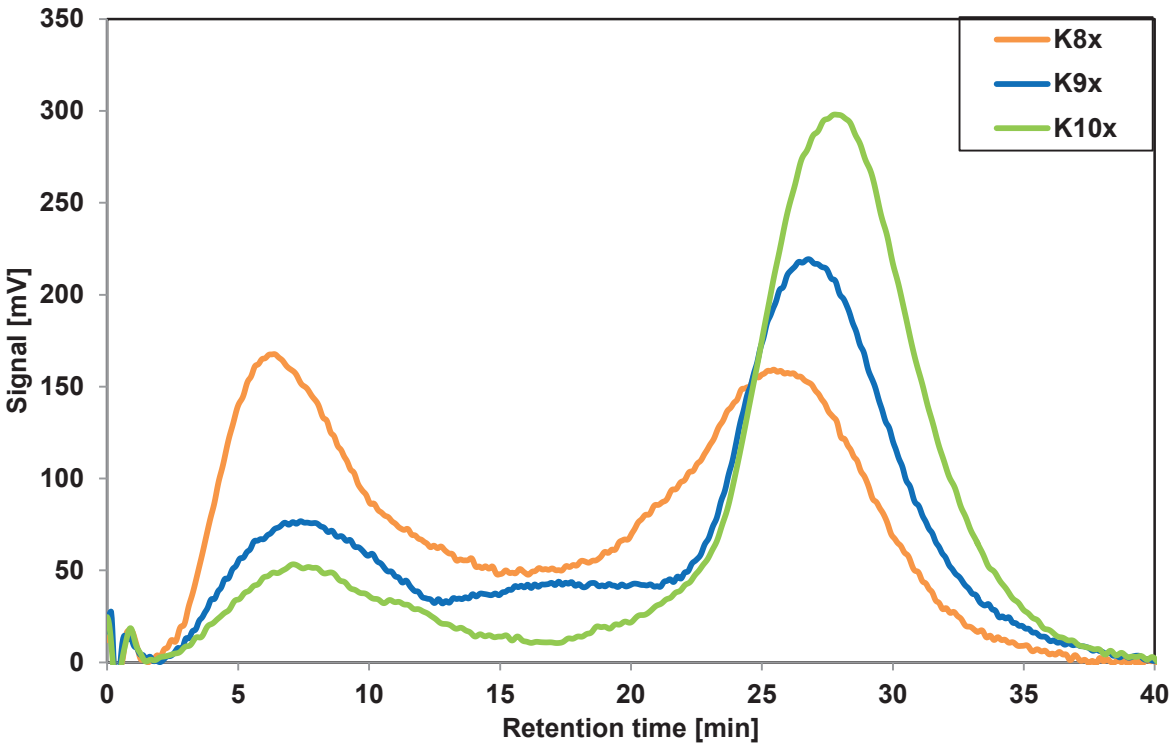

Figure 43: Fractionation of prepared samples by analytical TREF.

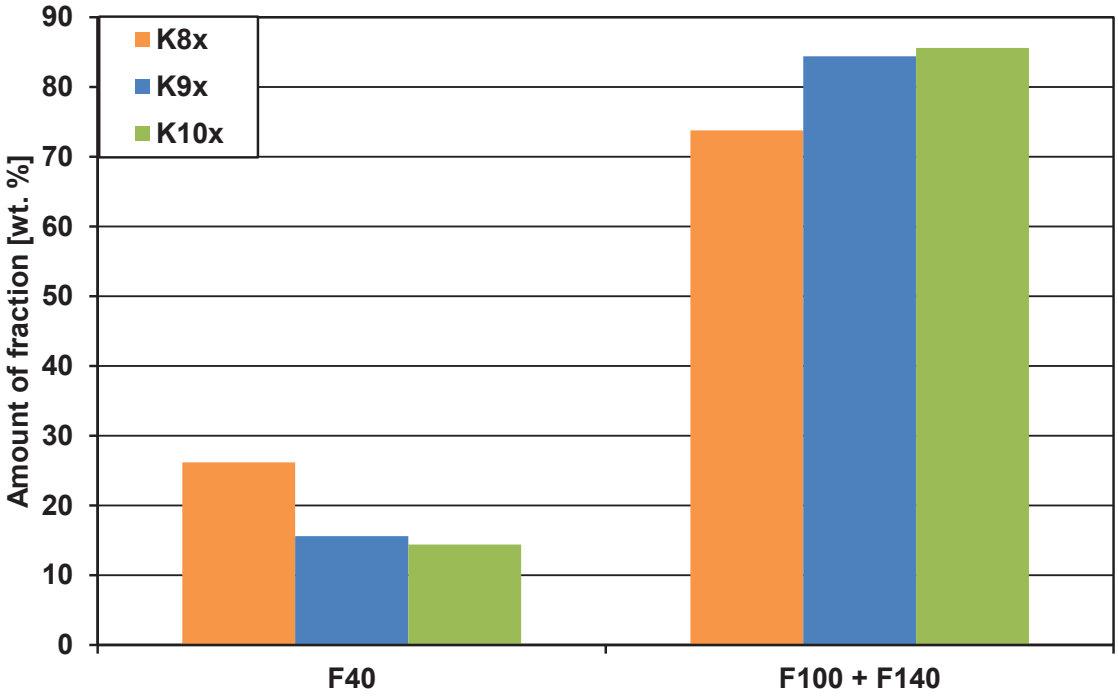

Figure 44: Comparison of amounts of amorphous and crystalline fractions obtained by preparative TREF from samples of copolymers prepared by using stopped-flow apparatus.

4.3.1 SSA

Figure 45 shows SSA profiles of the original copolymer as it was prepared in the stopped-flow polymerization and its crystalline fraction (F100 + F140) obtained after sample fractionation by the TREF method. This comparison confirmed that the preparative TREF method is convenient for the separation of crystallizable material from amorphous, especially in the case of real PP-*block*-EPR copolymers. On the SSA profile real PP-*block*-EPR copolymers could be found in the range of short segments of length 5 – 11 nm. As shown in Figure 46, in this range the SSA profile of the original copolymer sample matches well with the SSA profile of the crystalline fraction F100+F140 from the preparative TREF. Missing long segments in the range 50 – 70 nm in the case of crystalline fraction F100+F140 might be attributed to partial elimination of long iPP chains by filtration before sample fractionation by the preparative TREF method.

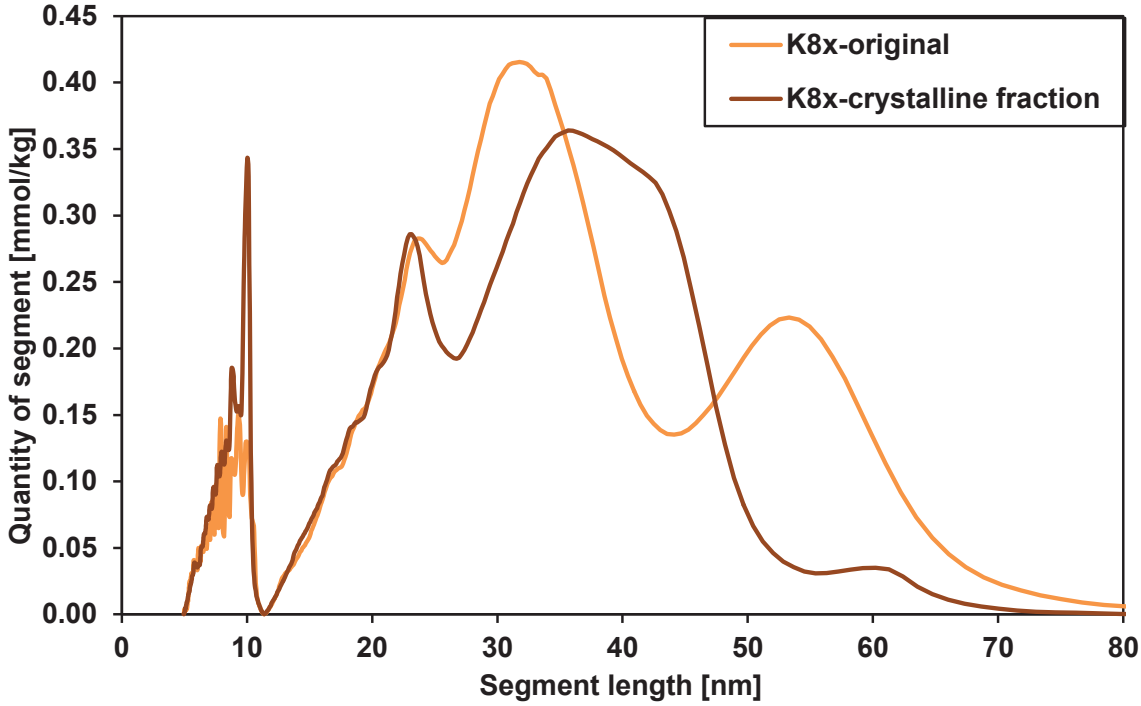

Figure 45: SSA profiles of the original copolymer sample K8x and its crystalline fraction (F100 + F140).

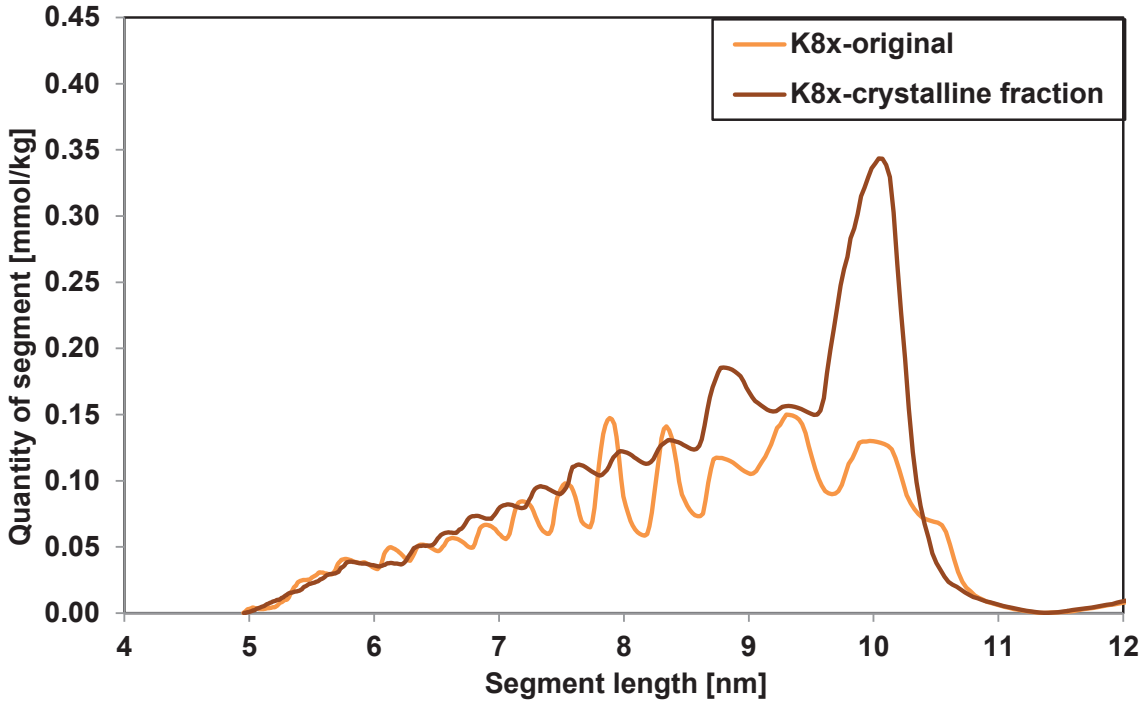

Figure 46: Detailed view of SSA profiles between 5 and 12 nm of the original sample K8x and its crystalline fraction (F100 + F140). This area corresponds to the segment lengths of real PP-block-EPR copolymers.

Figure 47 shows SSA profiles of the crystalline fractions F100+F140 of two different copolymer samples prepared in the stopped-flow apparatus. Sample K8x contains more amorphous fraction than sample K10x. This corresponds to a shorter time of homopolymerization) and a longer time of copolymerization for the sample K8x as shown in Table 11.

From the SSA profiles it is obvious that the K10x sample contains more crystalline chains than sample K8x. This matches the DSC analysis indicated in Table 12, where a noticeably higher crystallinity was determined (43.4 % versus 34.3 %) for the K10x sample. Table 11 further shows that the higher content of crystalline iPP in the sample K10x is also confirmed by ^{13}C-NMR analysis, where in the crystalline fraction F100+F140 ca. 91 wt. % of iPP was determined. In the case of the crystalline fraction of the K8x sample it was only ca. 74 wt. %.

From the SSA profiles in Figure 47 it is obvious that iPP chains form long segment lengths in the range 20 – 70 nm.

The content of segments that could correspond to block copolymers (i.e. range 5 – 11 nm), is similar for both the samples (see Figure 48).

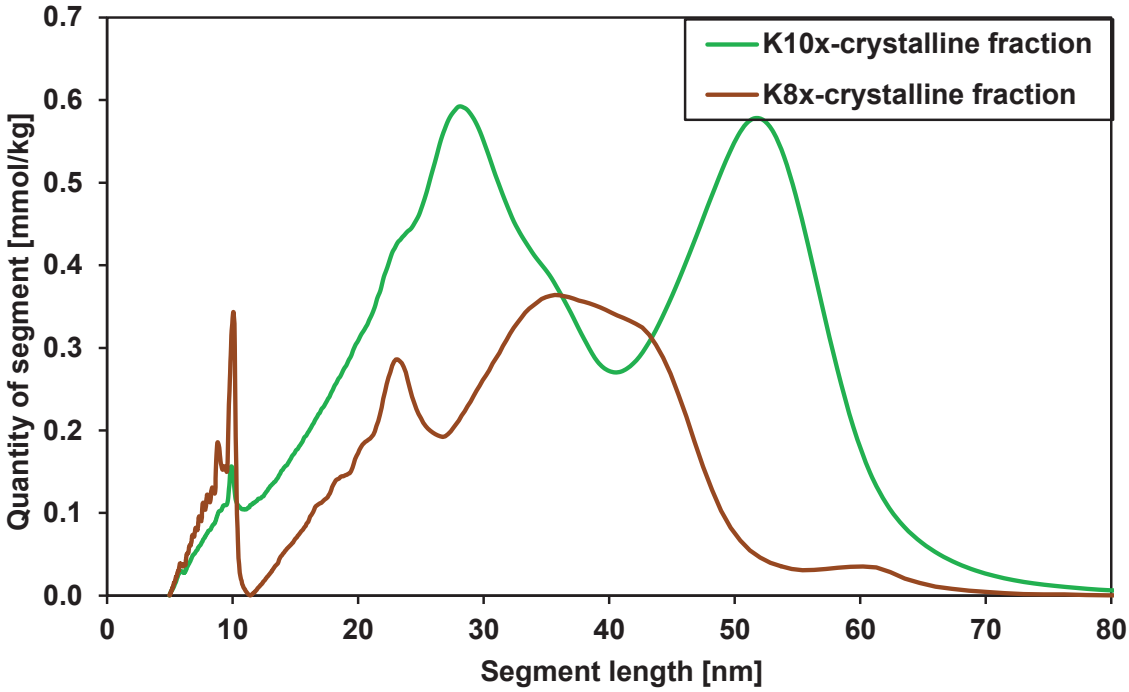

Figure 47: Comparison of SSA profiles of crystalline fractions (F100 + F140) of the samples K8x and K10x.

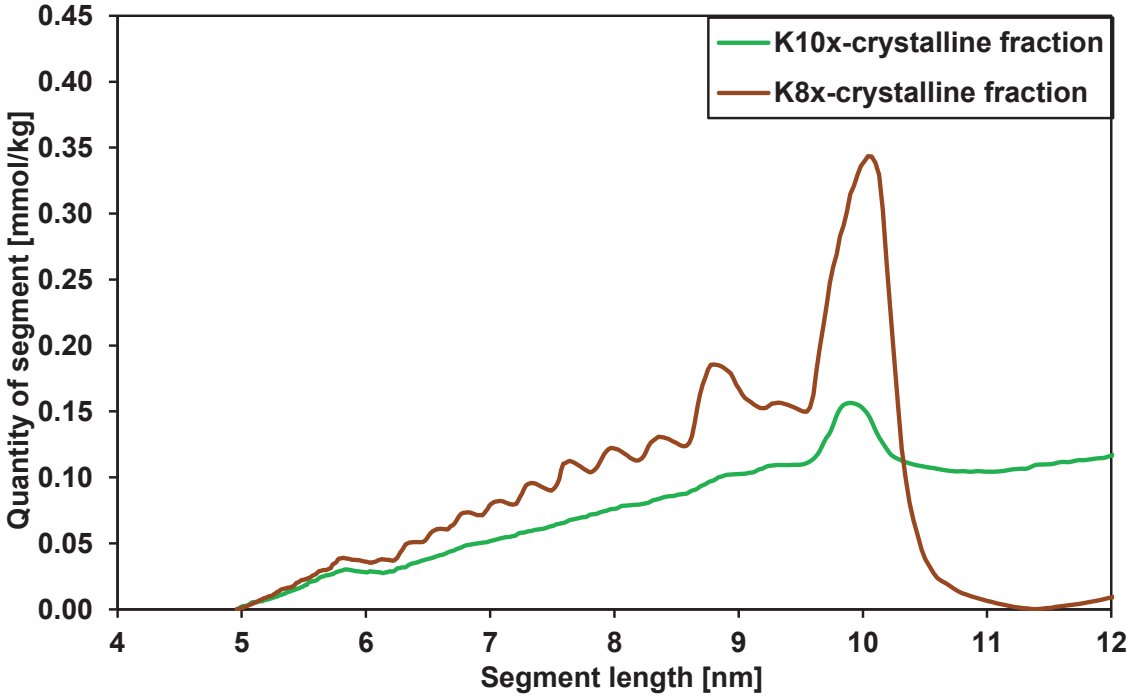

Figure 48: Detailed view of SSA profiles between 5 and 12 nm in the case of crystalline fractions (F100 + F140) of the samples K8x and K10x. This area corresponds to the segment length of real PP-block-EPR copolymers.

4.3.2 EPR Domain Size Distribution via SEM

In this chapter, the influence of block copolymer composition on the dispersion and size of EPR domains in a commercial ICP was studied by SEM. The procedure of specimen cutting and subsequent etching of the amorphous EPR phase is described in Chapter 3.2.10.

The SEM pictures of etched fracture surfaces obtained are shown in Figure 49. After the picture processing and calculation of EPR domain sizes the EPR domain size distribution profiles were computed and can be seen in Figure 50. It is obvious that the original ICP sample (i.e. without addition of any block copolymer) contains a significant portion of EPR domains smaller than 0.5 µm. Conversely in the case of ICP samples blended with PP-*block*-EPR copolymers mainly EPR domains with sizes bigger than 0.5 µm were observed in the samples. The average domain sizes (d50), shown in Table 13 and Figure 51, indicate that EPR domains d50 of all the ICP samples with added block copolymers have d50 ca. four times higher in comparison with original ICP. Such an obvious difference in EPR domains size distributions is an interesting observation, because Jang et al. [67] consider 0.5 µm to be the critical diameter for EPR domains in ICP. He assumes that only EPR domains with a diameter bigger than 0.5 µm could improve the fracture resistance of heterogeneous ICP materials.

Moreover, Chen et al. [89] published that the mechanically dispersed EPR phase in the PP matrix typically does not form domains bigger than 0.2 µm. Fan et al. [71] proposed that the main reason for the small EPR domains formed in mechanically prepared PP/EPR blends is the absence of the EbP component.

The results obtained within this study agree with the theory of Fan et al. [71]. It is evident that the amount of block copolymers in standard ICP materials is rather low, and thus small EPR domains are formed preferentially. Then the addition of an extra portion of block copolymer into the ICP sample caused significantly bigger EPR domains to be formed.

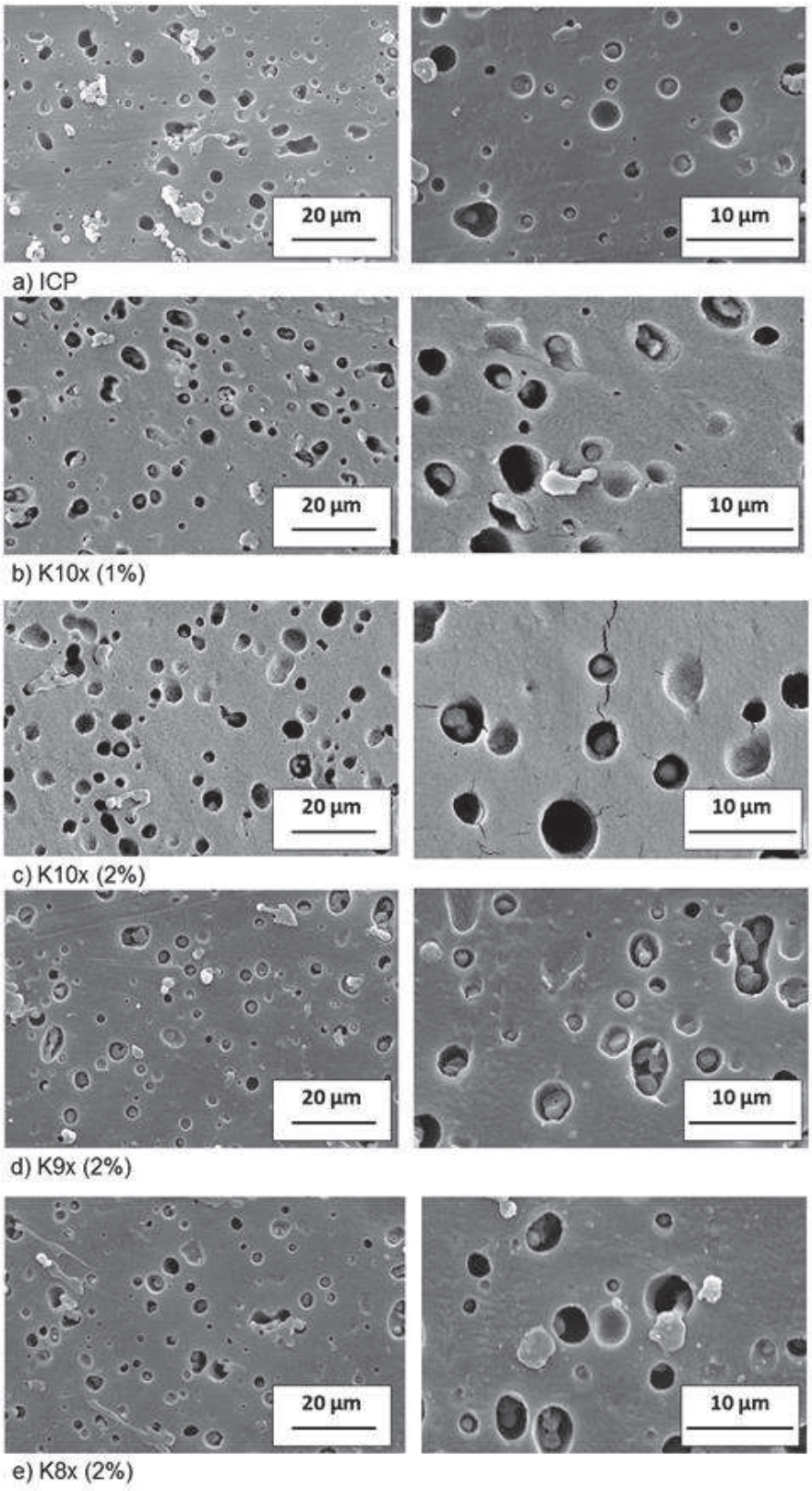

Figure 49: SEM pictures of etched fracture surfaces: a) original ICP, b) ICP with 1 wt. % of PP-block-EPR copolymer K10x, c) ICP with 2 wt. % of PP-block-EPR copolymer K10x, d) ICP with 2 wt. % of PP-block-EPR copolymer K9x, e) ICP with 2 wt. % of PP-block-EPR copolymer K8x.

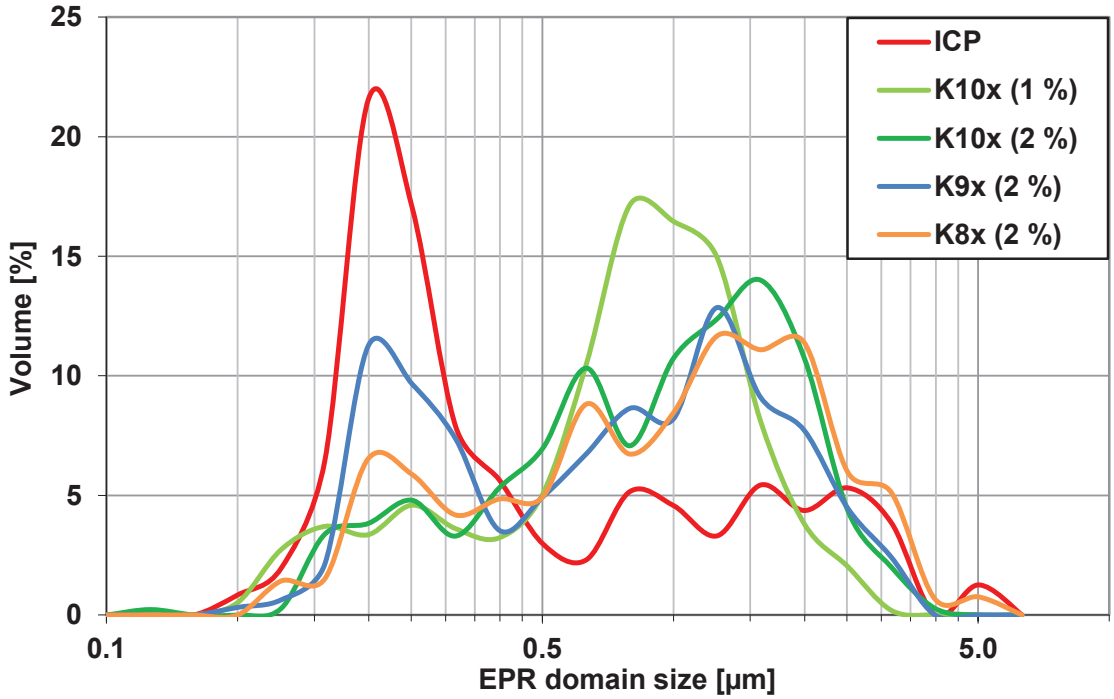

Figure 50: Profiles of EPR domain distributions for the original ICP and ICP with added PP-block-EPR copolymers.

Table 13: Average size of EPR domains (d50) evaluated from SEM pictures. The amount of ethylene in PP-block-EPR copolymer was determined by ^{13}C-NMR analysis in the crystalline fraction (41-140 °C) of samples prepared in the stopped-flow apparatus.

	E in EPR-block in ICP [wt. %]	Average EPR domain size (d50) [µm]
ICP	0.00	0.23 ± 0.05
K10x (1 %)	0.04	0.77 ± 0.05
K10x (2 %)	0.07	0.88 ± 0.05
K9x (2 %)	0.11	0.85 ± 0.03
K8x (2 %)	0.21	0.86 ± 0.02

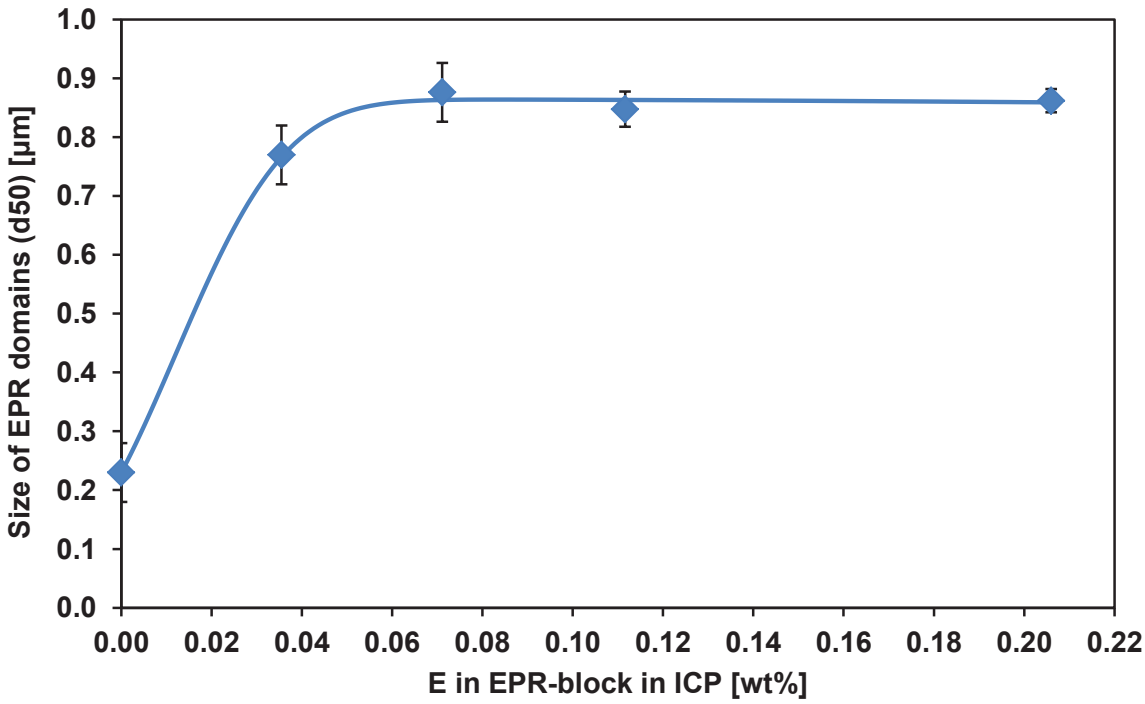

Figure 51: Correlation of average size of EPR domains (d50) with the amount of ethylene in PP-block-EPR copolymer added to the ICP.

4.3.3 Rheological Properties

Rheological properties measured by an oscillation rheometer are often used to describe the linear viscoelastic behaviour of immiscible polymer blends in the presence of an interfacial agent [109, 110]. Figure 52 shows the complex viscosities (η*) of the original ICP and the ICP containing added PP-*block*-EPR copolymer. At low frequencies the viscosity of the original ICP is lower than that of the ICP with added block copolymer prepared by the stopped-flow technique. The ICP sample with 1 wt. % of PP-*block*-EPR copolymer K10x is an exception. This can be explained by the fact that the ICP sample with 1 wt. % K10x contains a lower amount of the block copolymer and thus this sample has a composition comparable to the original ICP copolymer. Overlapping viscosity curves at high frequencies indicate that all these samples have a similar composition of low molecular weight fraction.

Higher complex viscosities of the samples containing PP-*block*-EPR copolymers in comparison with original ICP were ascribed to the presence of a higher content of iPP. This iPP constitutes a significant part of the PP-*block*-EPR copolymer, thus the viscosity of this copolymer should be higher than that of the pure EPR, where no iPP is present. Pursuant to this fact it is expected that the η* values of ICP with block copolymers labelled as K9x and K10x are higher than the viscosity of the sample comprising K8x block copolymer. As was previously described in Chapter 4.2.1, the EPR content in K9x and K10x is lower in comparison with K8x. However, the EPR content is not the only factor that controls the viscosity of the ICP, as the PP-*block*-EPR block copolymer content may also play a role. This is obvious, when comparing the η* of sample K10x with that of K8x, which has a significantly higher content of the

block copolymer (incorporated ethylene in crystalline fraction as shown in Table 12). In other words, the rheological behaviour of ICP can be different from classical PP/EPR binary blends, whose complex viscosity depends monotonically on the EPR content.

In our opinion these results further confirm the compatibilizing effect of the PP-*block*-EPR copolymer, the presence of which decreases the interfacial tension between the PP and EPR phases and enhances their mutual adhesion indicated by the change of the proportion of elastic/viscous behaviour and the shift of the complex viscosity curve (see Figure 52).

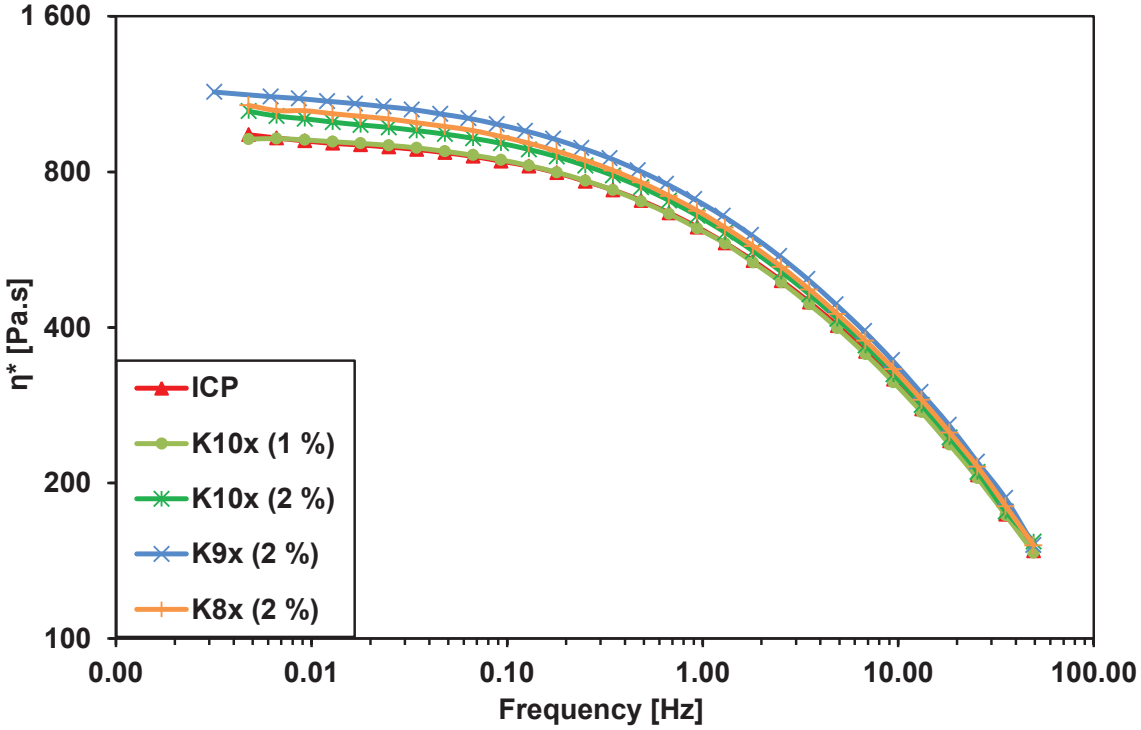

Figure 52: Complex dynamic viscosities of the original ICP and the ICP blends with PP-block-EPR copolymers as a function of angular frequency.

Figure 53 shows the change in the elastic modulus G' at low frequencies. The shift at low frequencies reflects changes in the composition of the high molecular weight fraction causing higher melt elasticity. This means that longer molecules and/or entanglement and/or new interactions between the individual phases are present in samples comprising of added PP-*block*-EPR copolymers. The higher concentration of block copolymer, which acts as a compatibilizer between the iPP and EPR phases, also increases the structural strength of the material determined by the differences in elastic modulus at the highest measured frequency (see Figure 54). Higher structural strength is achieved for samples with the addition of PP-*block*-EPR copolymers and the increase is proportional to the amount of the block copolymer in ICP.

However a small increase in the viscous moduli is observed with increasing content of the block copolymer prepared in the stopped-flow apparatus. Changes in the viscous modulus G" are smaller in comparison with elastic modulus, as shown in Figure 55 and Figure 56.

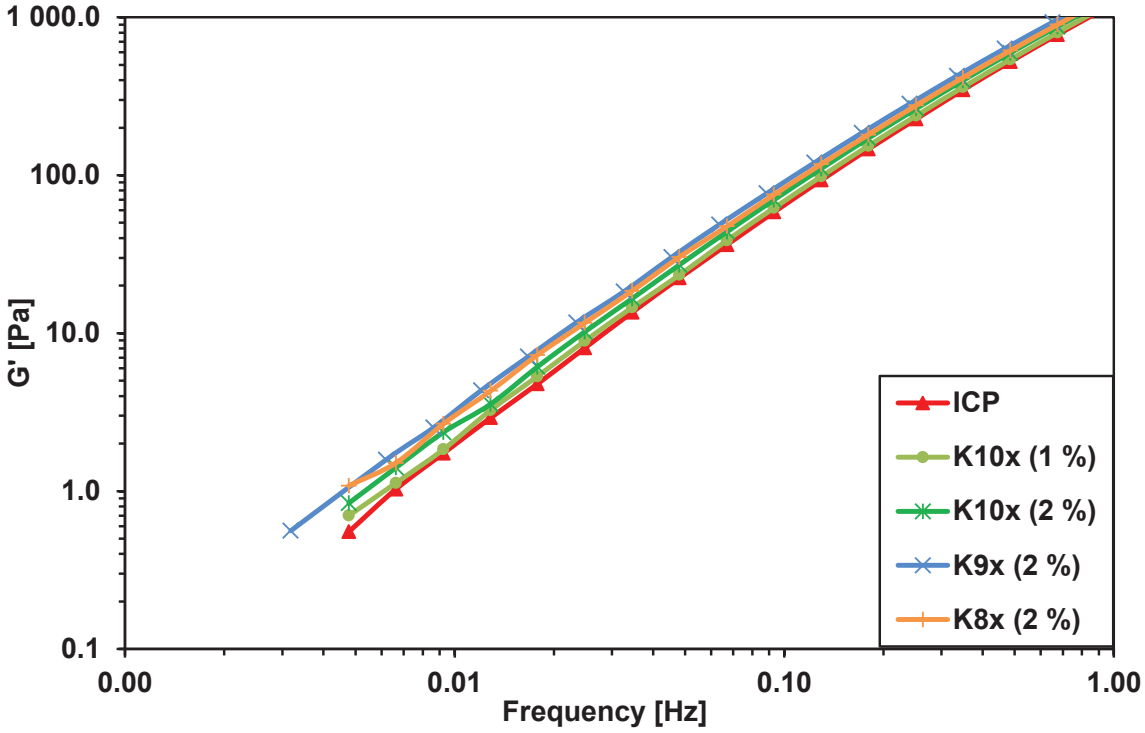

Figure 53: Dependence of the elastic modulus (G') on frequency at low frequencies.

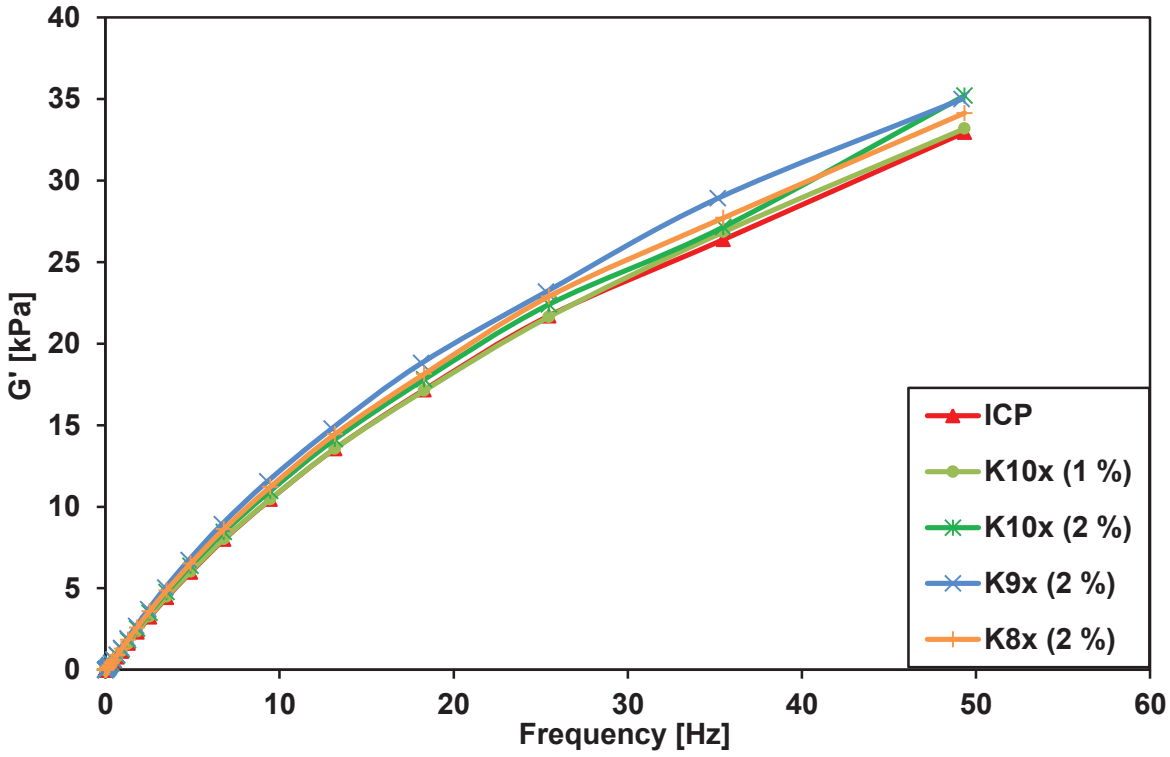

Figure 54: Dependence of the elastic modulus (G') on frequency.

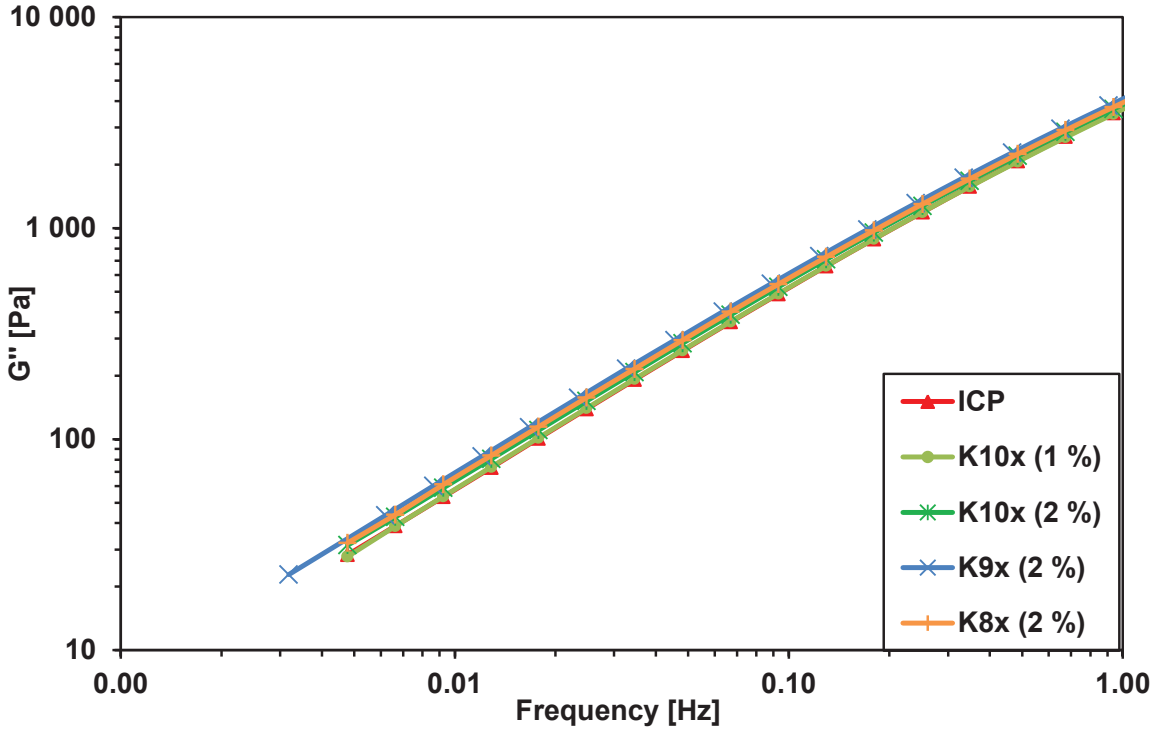

Figure 55: Dependence of the viscosity modulus (G") on frequency at low frequencies.

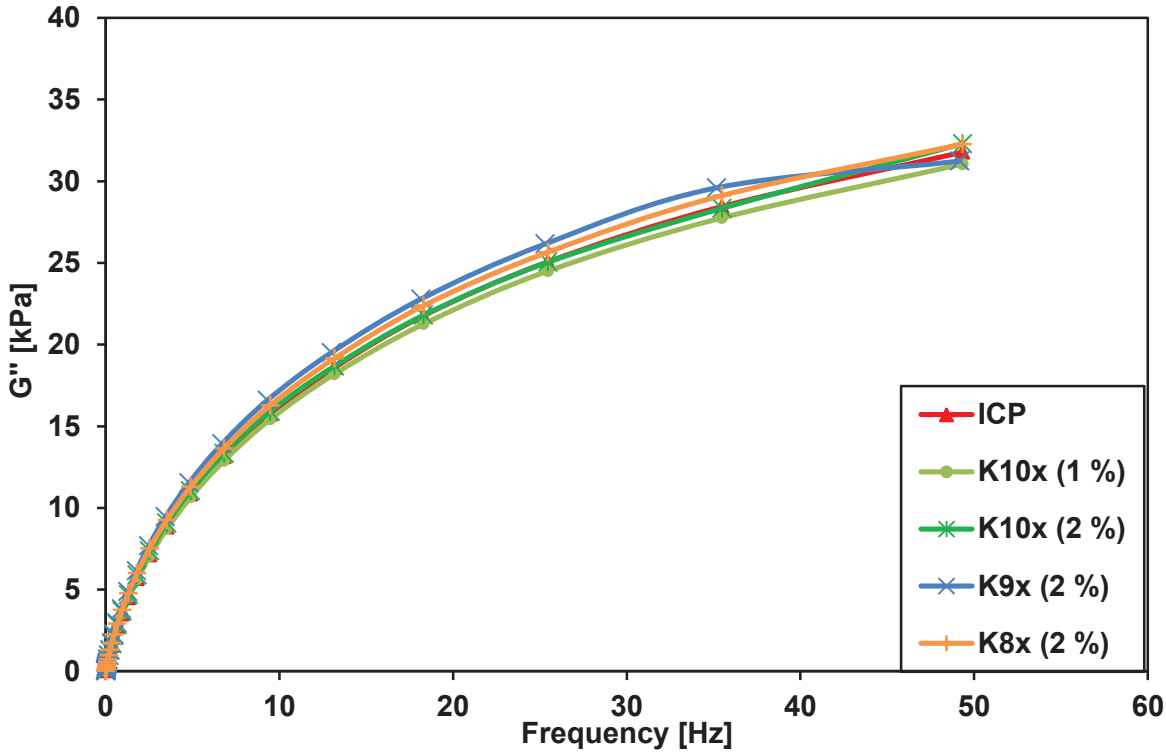

Figure 56: Dependence of the viscosity modulus (G") on frequency.

The crossing point of the elastic and viscous modulus (G'=G") can be used for comparison of the average molar mass and molar mass distribution as described in Chapter 3.2.7. Thus, in the case of the polymer blends studied within this thesis the positions of the crossing points on the y-axis would indicate that all the samples have a similar molecular weight distribution (i.e. polydispersity index). On the other hand positions on the x-axis would imply different average molecular weights. The main component of the mixtures – a commercial ICP sample without addition of the block copolymer exhibits a rheological performance attributable to the lowest average molecular weight, whereas the G'=G" point of the ICP samples with added PP-*block*-EPR copolymer is shifted to lower frequencies in comparison with the original ICP. Samples with the addition of 1 wt. % and 2 wt. % of the PP-*block*-EPR copolymer K10x exhibit a similar performance (like the same molecular weight), but higher than that of the sample with 2 wt. % of the PP-*block*-EPR copolymer K8x. The highest molecular weight would be assigned to the ICP sample with 2 wt. % of the PP-*block*-EPR copolymer K9x. Such performance of the blends cannot be simply assigned to increasing the average molecular weight of the samples with the addition of block copolymer because the MMs of the PP-*block*-EPR copolymers could not be expected outside the ranges presented in Table 9. Most likely, some long polymer branches of the added PP-*block*-EPR copolymer twined together with the original ICP sample and formed intermolecular structures of higher viscosity performance. This effect is desirable in order to increase compatibility between iPP and EPR in ICP.

Table 14: The polydispersity index evaluated from the crossing point of elastic and viscous modulus determination by rheology.

	E in EPR-block in ICP [wt. %]	**Polydispersity index**
ICP	0.00	3.28
K10x (1 %)	0.04	3.49
K10x (2 %)	0.07	3.51
K9x	0.11	3.45
K8x	0.21	3.32

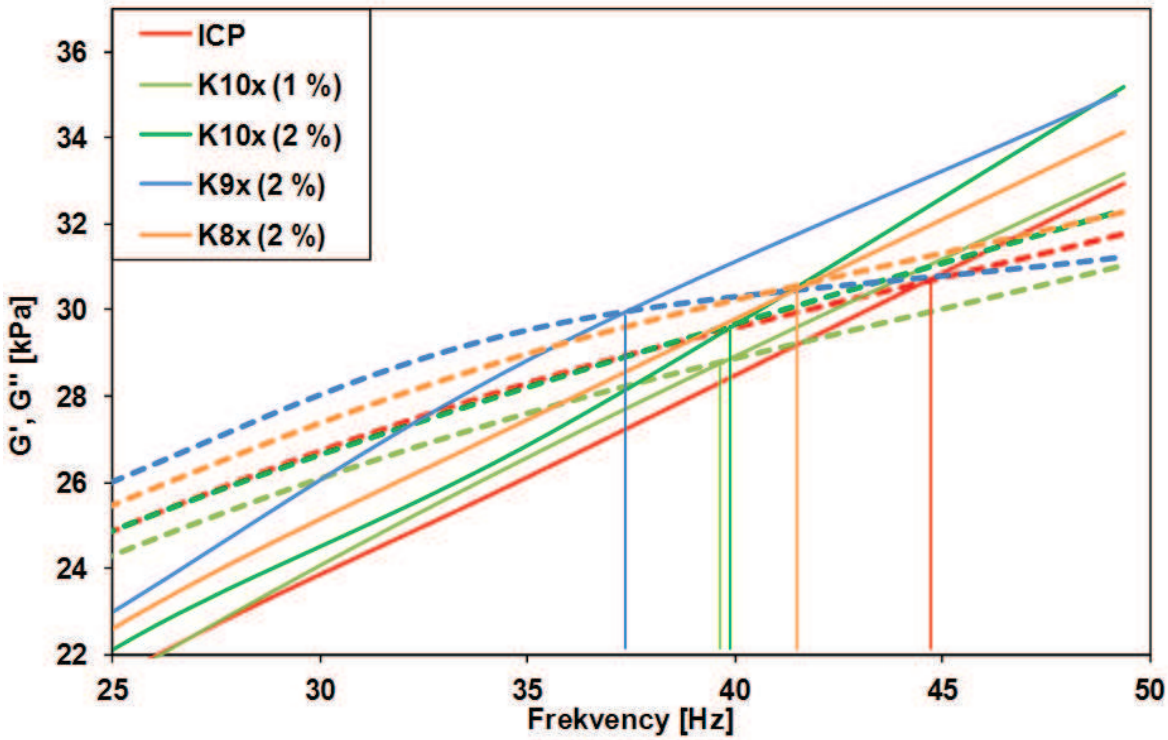

Figure 57: Comparison of elastic (solid line) and viscous moduli (dashed line) of the original ICP sample and the ICP samples with added PP-block-EPR copolymers. Comparison of the average molar mass and molar mass distribution can be determined from the crossing point of G'=G".

4.3.4 Dynamic Mechanical Properties

Dynamic-mechanical analysis (DMA) was performed under the conditions specified in Chapter 3.2.8. The complex modulus (E) dependence on temperature for the original ICP sample and the ICP samples with added PP-*block*-EPR copolymers is shown in Figure 58. The differences among all the studied samples are relatively small. However in Figure 59, where a detailed view of the temperature region -80 to -10 °C is shown, it is obvious that all the samples with added block copolymers have a noticeably higher complex elasticity modulus in comparison with the original ICP. The higher complex modulus observed in the case of ICP samples containing added PP-*block*-EPR copolymers could be related to the phenomena discussed in the context of "increasing" molar mass with block copolymer addition in chapter 4.3.3. – increasing the amount of "tangled" macromolecules upon real block addition or the presence of further iPP, which was added together with the PP-*block*-EPR copolymer and which caused a nucleation effect due to its very high molar mass.

However, no difference was observed between the samples with the addition of block copolymers K8x and K10x with different contents of iPP as shown in Table 12 (65 wt. % vs. 84 wt. %). Thus it can be assumed that the presence of the block copolymer PP-*block*-EPR also increases the modulus of the mixture at temperatures below T_g of iPP.

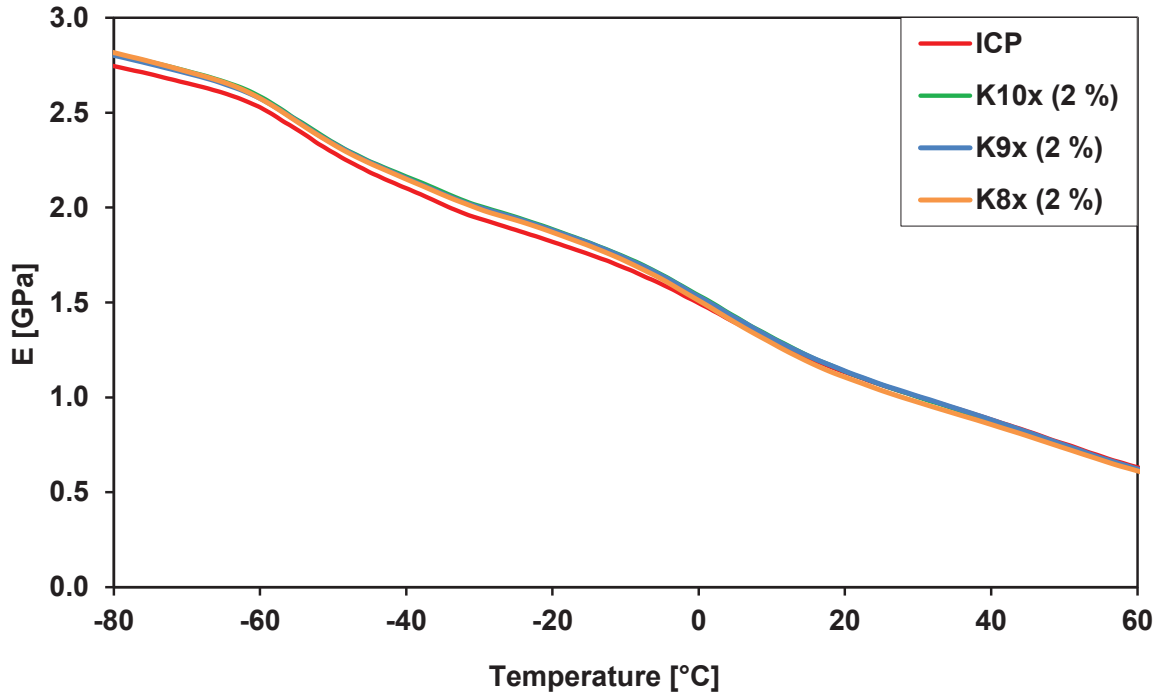

Figure 58: Dependence of complex elasticity modulus (E) on temperature for the original ICP sample and the ICP samples with added PP-block-EPR copolymers.

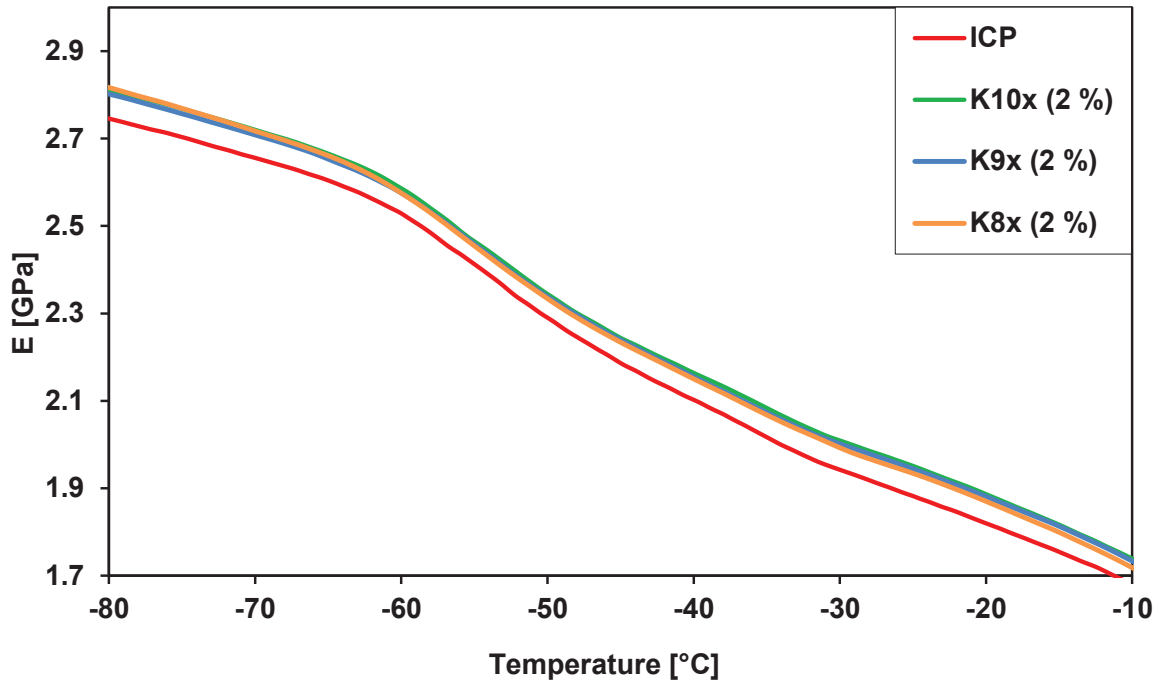

Figure 59: Detailed view of complex elasticity modulus dependence on temperature in the range from -80 to -10 °C.

Figure 60 shows the dependence of the loss modulus E" on temperature for the original the ICP sample and the ICP samples with added PP-*block*-EPR copolymers. An obvious difference in the values of the loss modulus E" was observed mainly in the area of the glass transition temperature of the PP-homopolymer T_g (PP) ~ 3 °C. In this area, all the samples with added PP-*block*-EPR copolymer exhibit a higher E" modulus in comparison with the original ICP sample. The highest E" modulus was observed in the case of the ICP sample containing 2 wt. % of the block copolymer K8x. In the case of the ICP samples which contained K9x and K10x block copolymers a similar E" modulus of PP homopolymer was determined as shown in Table 15 and Figure 61.

The ICP sample with the K8x block copolymer has the highest E" modulus in the area of the glass transition of ethylene/propylene copolymer T_g (EPR) ~ -50 °C. The ICP samples with the K9x and K10x block copolymers exhibit at T_g (EPR) a comparable or a slightly lower loss E" modulus to the original ICP. As determined by ^{13}C-NMR and DSC analyses, the K8x copolymer contains the highest portion of the amorphous EPR phase and most likely also the highest portion of real PP-*block*-EPR copolymers (see Table 12). The presence of the higher amount of the EPR phase could explain the observed higher E" modulus of the EPR phase. However, it was also observed that the K8x sample improved the loss modulus of the PP homopolymer phase of the ICP. It is assumed that the higher E" modulus in the case of the ICP with K8x is a result of better compatibility between the EPR and the iPP phases caused by the presence of a higher amount of real PP-*block*-EPR copolymers.

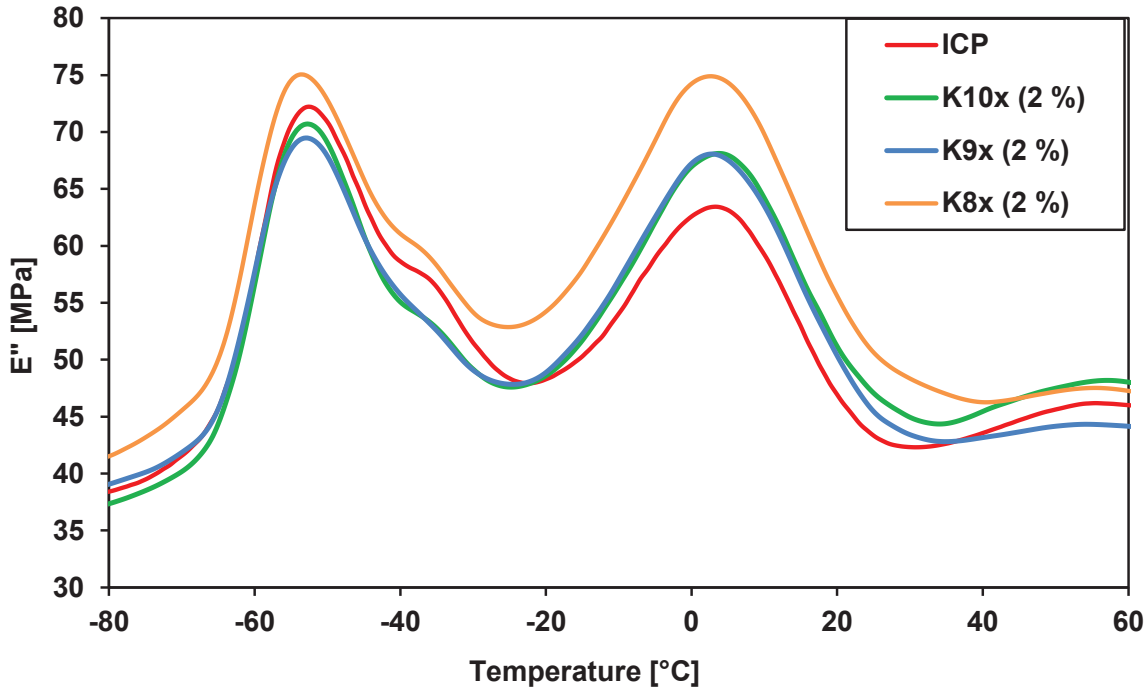

Figure 60: Dependence of loss modulus E" on temperature for the original ICP sample and the ICP samples with added PP-block-EPR copolymers.

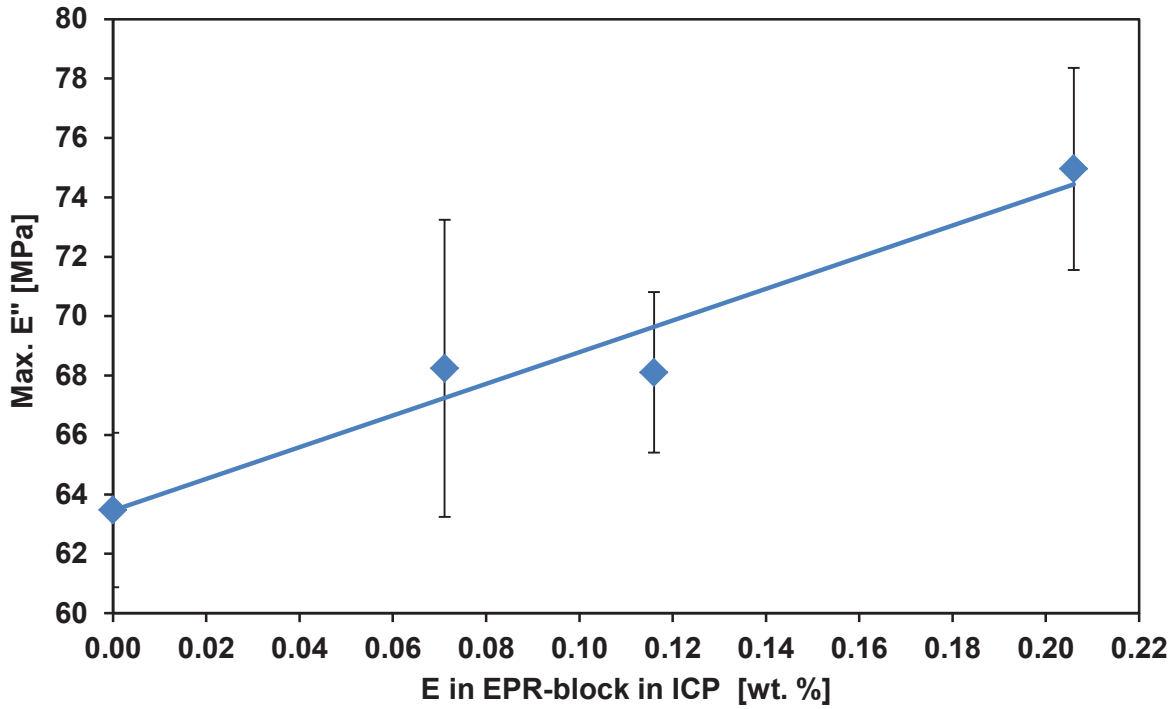

Figure 61: Dependence of maximum of loss modulus E" in the area of the glass transition temperature of PP-homopolymer T_g (PP) on the amount of ethylene in the PP-block-EPR copolymer added to the ICP.

The dependence of loss angle tan(δ) on temperature is shown in Figure 62. A difference between the original ICP sample and the ICP samples with added PP-*block*-EPR copolymers is obvious mainly in the area which corresponds to T_g of iPP (~ 3 °C). Dependence of the maxima of loss angle tan(δ) in the area of the glass transition temperature of the PP-homopolymer T_g (PP) on the amount of ethylene in the PP-block-EPR copolymer added to the ICP are shown in Figure 63. As in the case of the loss E" modulus, the highest increase was observed in the case of the ICP sample containing 2 wt. % of block copolymer K8x. The higher tan(δ) for all the ICP samples with added block copolymers in comparison with the original ICP could be explained by the better compatibility between the EPR phase and the iPP matrix due to the presence of real PP-*block*-EPR copolymers.

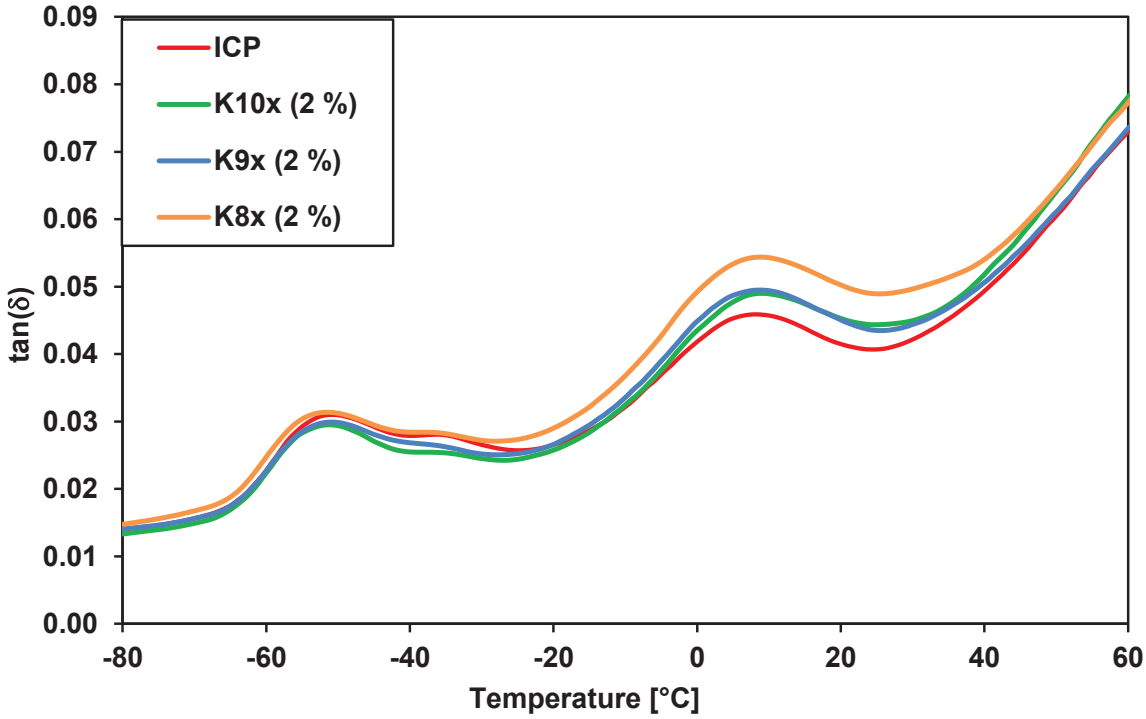

Figure 62: Dependence of loss angle tan(δ) on temperature for the original ICP sample and the ICP samples with added PP-block-EPR copolymers.

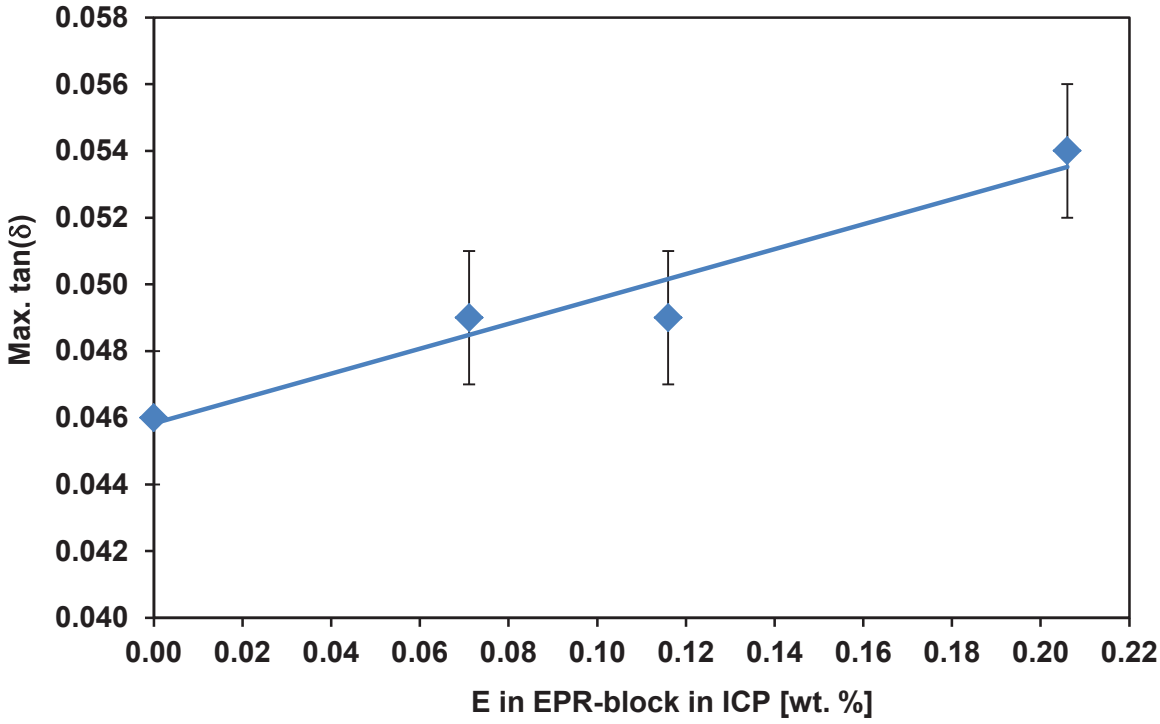

Figure 63: Dependence of the maximum of loss angle tan(δ) in the area of the glass transition temperature of the PP-homopolymer T_g (PP) on the amount of ethylene in the PP-block-EPR copolymer added to the ICP

Finally, Figure 64 shows the dependence of the glass transition temperature of iPP homopolymer and EPR phase on the amount of a block copolymer added to the ICP. The figure shows that for both the phases there is a decrease of T_g with increasing content of block copolymer. In the case of the iPP phase the T_g decrease is not significant as it is by only 0.5 °C at 0.21 wt. % of ethylene in the PP-*block*-EPR copolymer added to the ICP. In the case of the EPR phase the decrease of T_g is more obvious, being by ca. 1.0 °C with 0.21 wt. % of ethylene in the PP-*block*-EPR in ICP.

Table 15: Dependence of the glass transition temperature of the homopolymer T_g (PP) and the EPR phase T_g (EPR) and the maximum of loss modulus E" and loss angle tan(δ) in the area of the glass transition temperature of the PP-homopolymer T_g (PP) on the amount of ethylene in the PP-block-EPR copolymer added to the ICP.

	E in EPR-block in ICP	T_g (PP)	T_g (EPR)	max. E" in area of T_g (PP)	max. tan (δ) in area of T_g (PP)
	[wt. %]	[°C]	[°C]	[MPa]	[MPa]
ICP	0.00	-52.5 ± 0.1	3.1 ± 0.2	63.5 ± 2.6	0.046 ± 0.02
K10x (2 %)	0.07	-52.6 ± 0.4	3.7 ± 0.4	68.2 ± 5.0	0.049 ± 0.02
K9x (2 %)	0.12	-52.8 ± 0.2	2.9 ± 0.2	68.1 ± 2.7	0.049 ± 0.02
K8x (2 %)	0.21	-53.4 ± 0.2	2.6 ± 0.3	75.0 ± 3.4	0.054 ± 0.02

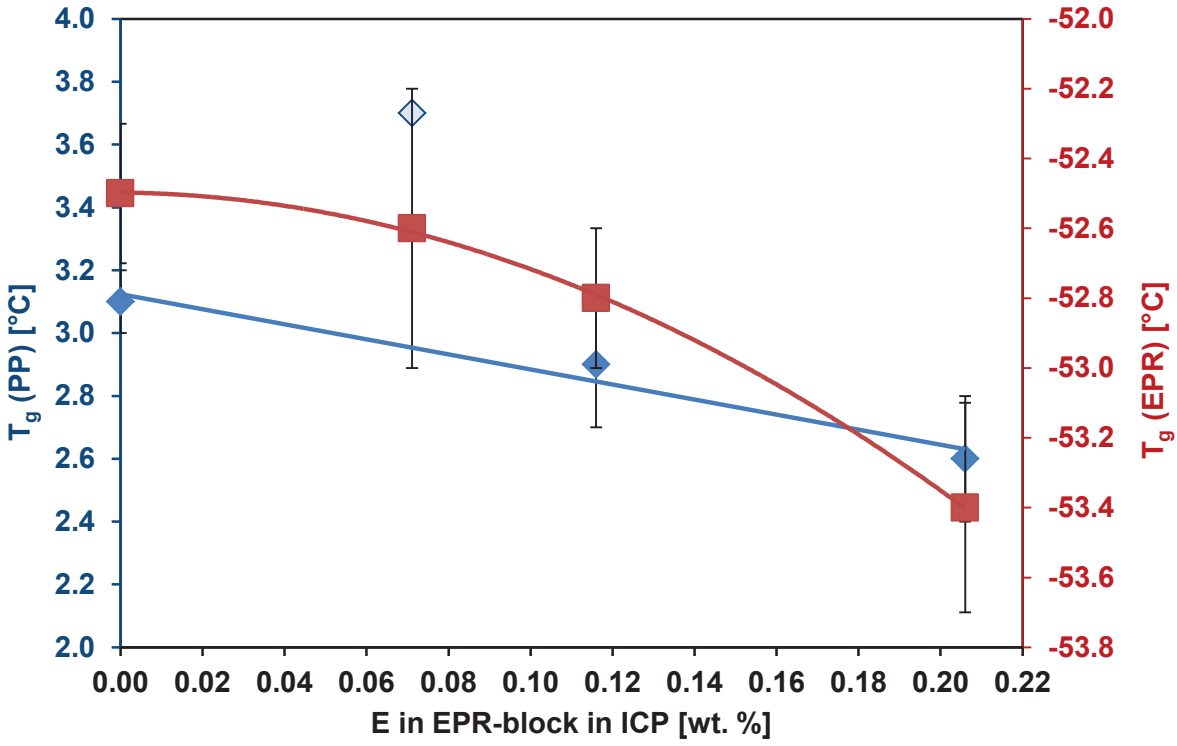

Figure 64: Dependence of the glass transition temperature of the homopolymer T_g (PP) and the EPR phase T_g (EPR) on the amount of ethylene in the PP-block-EPR copolymer added to the ICP. The remote diamond in the case of the T_g (PP) of the ICP sample containing 0.12 wt. % of EPR block was excluded from dependency.

4.3.5 Mechanical Properties

The reference ICP material and the ICP blends which contained defined amounts of PP-*block*-EPR copolymers prepared in stopped-flow polymerizations were used for the preparation of test specimens for determination of mechanical properties. Test specimens were cut from hot pressed plate as described in Chapter 3.2.12 and tested according to the ISO 178 standard.

The dependence of the flexural modulus on the amount of ethylene added to the ICP as a part of the PP-block-EPR copolymer is shown in Table 16 and Figure 65. As is obvious from Figure 65, the ICP samples with added PP-block-EPR copolymer exhibited a flexural modulus noticeably lower in comparison with the original ICP. It was found that addition of a small amount of the PP-*block*-EPR copolymer caused an obvious decrease in flexural modulus by ca. 120 MPa. A further increase of the PP-*block*-EPR copolymer in ICP did not cause any further decrease in the flexural modulus.

The Charpy notched impact strength was measured at -20 °C and the results are shown in Table 16. Figure 66 indicates its steep increase with the increasing content of the PP-*block*-EPR copolymer. Addition of a small amount of PP-*block*-EPR copolymer increased the Charpy notched impact strength by 0.5 kJ/m^2 to 2.7 kJ/m^2. A further addition of the block copolymer caused only a small increase to 2.9 kJ/m^2. The increase of the notched impact strength is in accordance with the decrease in the flexural modulus. The higher toughness of the ICP material with added PP-*block*-EPR copolymer was also confirmed by the elongation at break dependence shown in Table 16 and Figure 67. The elongation at break decreases by 43 % by adding a small amount of the PP-*block*-EPR copolymer. As in previous cases a further addition of block copolymer caused only a small change in the elongation at break value.

A lower elastic modulus and higher toughness is usually achieved by increasing the amount of the EPR fraction in the ICP material [113]. In order to examine whether the observed effect of the PP-*block*-EPR copolymer on mechanical properties is not only related to a simple increase in EPR content in the ICP caused by added PP-*block*-EPR copolymer, the data from the mathematical model were compared with the observed results. The model developed by Grůza [114] was based on the known PP matrix MFR, the MFR of the final ICP, the content of EPR in ICP and the EPR composition and is able to predict the corresponding mechanical properties. The effect of increasing the amount of EPR in the ICP on flexural modulus was evaluated by this model and compared with flexural moduli determined on ICP samples modified by added PP-*block*-EPR copolymer. Figure 68 shows a decrease in flexural modulus caused by the addition of PP-*block*-EPR copolymer that is significantly higher in comparison with the decrease in flexural modulus predicted by the model where only a simple increase in the EPR amount in ICP was taken into account. According to the model the addition of 0.5 wt. % of the EPR copolymer caused a decrease in the flexural modulus by only ca. 25 MPa. However the addition of the same amount of EPR, but as a part of a PP-*block*-EPR copolymer, caused a

decrease in the flexural modulus by ca. 70 MPa. This indicates that PP-*block*-EPR copolymer samples prepared in the stopped-flow polymerization are able to positively influence the mechanical properties of standard ICP materials. As described in Chapter 4.3.2, a detailed analysis of EPR domain size distribution in ICP revealed that the presence of PP-*block*-EPR copolymers caused a significant increase of the average (d50) size of EPR domains (Figure 51). In my opinion the change in EPR domain size distribution and the better adhesion of the EPR domains to the iPP matrix are the main factors behind the observed changes in mechanical properties.

Table 16: Dependence of mechanical properties and average EPR domain size on the amount of ethylene in the crystalline fraction (41-140 °C) of samples prepared in the stopped-flow apparatus and the total amount of EPR in ICP. The total amount of EPR in ICP was calculated from the triad distribution (^{13}C-NMR analysis) using 1st order Markovian statistics

	E in EPR-block in ICP	EPR total in ICP	Flexural modulus	Izod impact strength notched (-20°C)	Elongation at break	Tensile Stress at Yield	Average EPR domain size
	[wt. %]	[wt. %]	[MPa]	[kJ/m^2]	[%]	[MPa]	[µm]
ICP	0.00	12.50	1546 ± 32	2.1 ± 0.1	13.6 ± 3.1	25.0 ± 0.4	0.23 ± 0.05
K10x (1 %)	0.04	12.61	1428 ± 37	2.7 ± 0.2	7.8 ± 2.7	24.3 ± 0.1	0.77 ± 0.05
K10x (2 %)	0.07	12.72	1418 ± 42	2.9 ± 0.2	8.2 ± 2.3	24.1 ± 0.2	0.88 ± 0.05
K9x (2 %)	0.11	12.96	1469 ± 36	2.8 ± 0.1	7.8 ± 1.5	24.0 ± 0.2	0.85 ± 0.03
K8x (2 %)	0.21	13.04	1474 ± 50	2.9 ± 0.2	6.5 ± 2.4	24.7 ± 0.4	0.86 ± 0.02

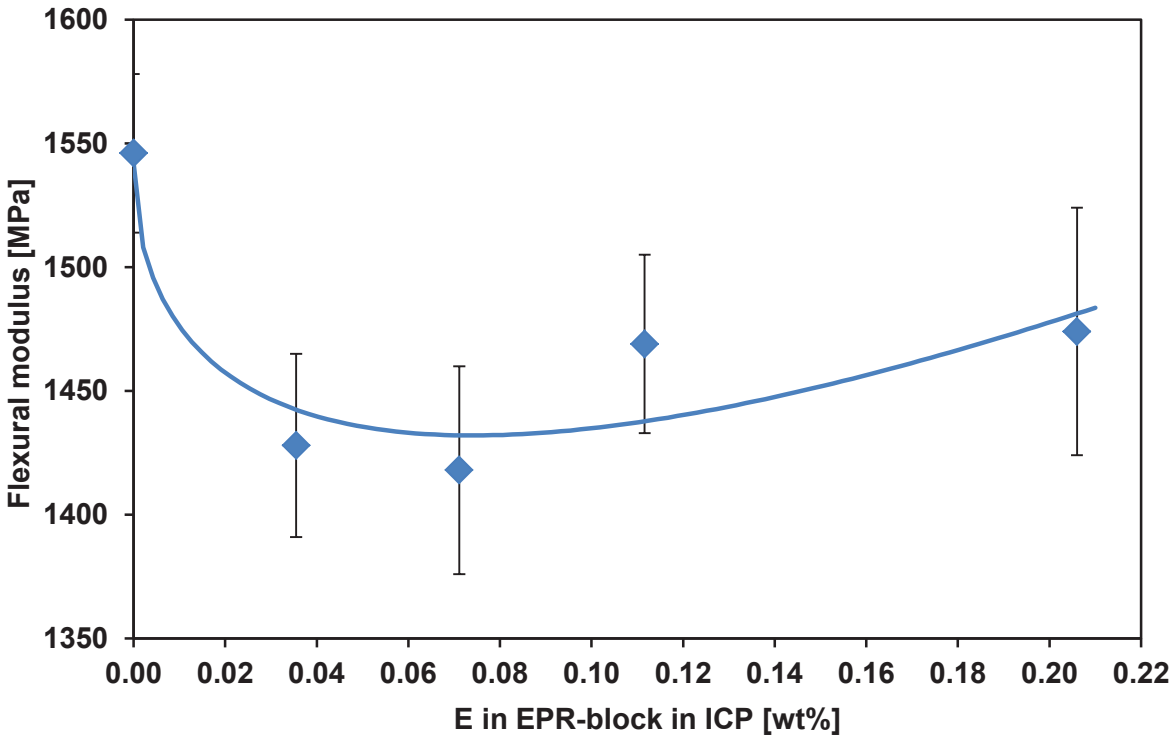

Figure 65: Dependence of flexural modulus on the amount of ethylene in the PP-block-EPR copolymer added to the ICP.

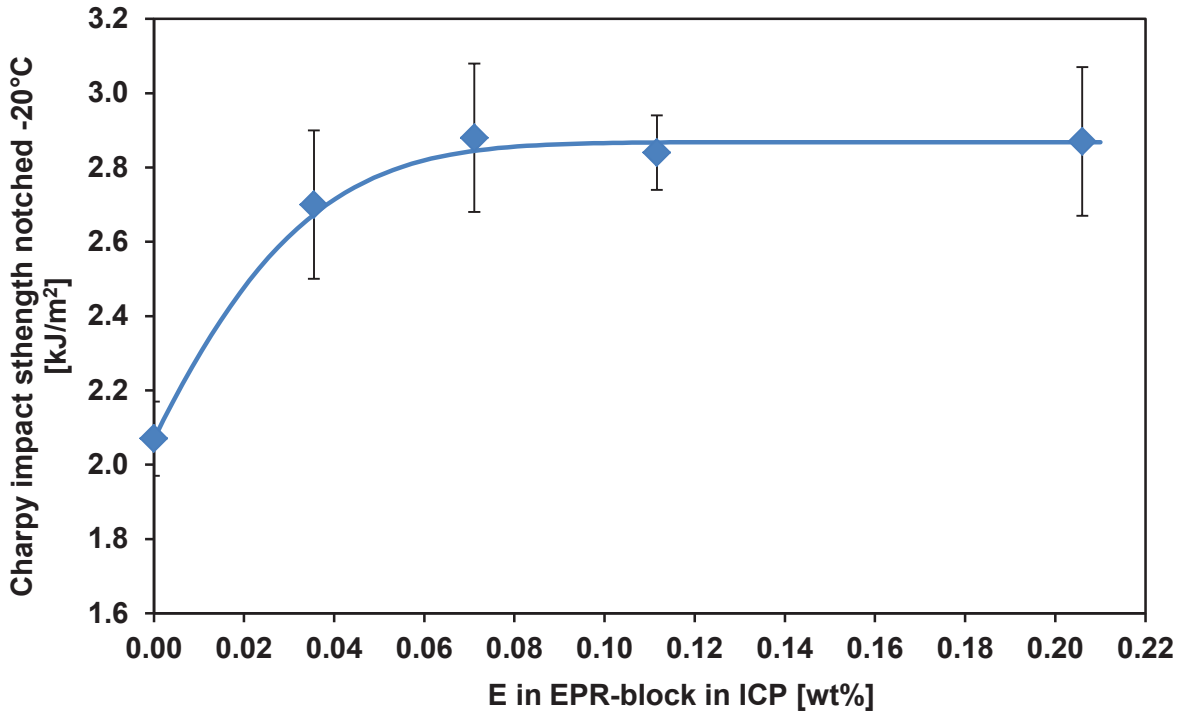

Figure 66: Dependence of the Charpy impact strength notched (measured at -20°C) on the amount of ethylene in the PP-block-EPR copolymer added to the ICP.

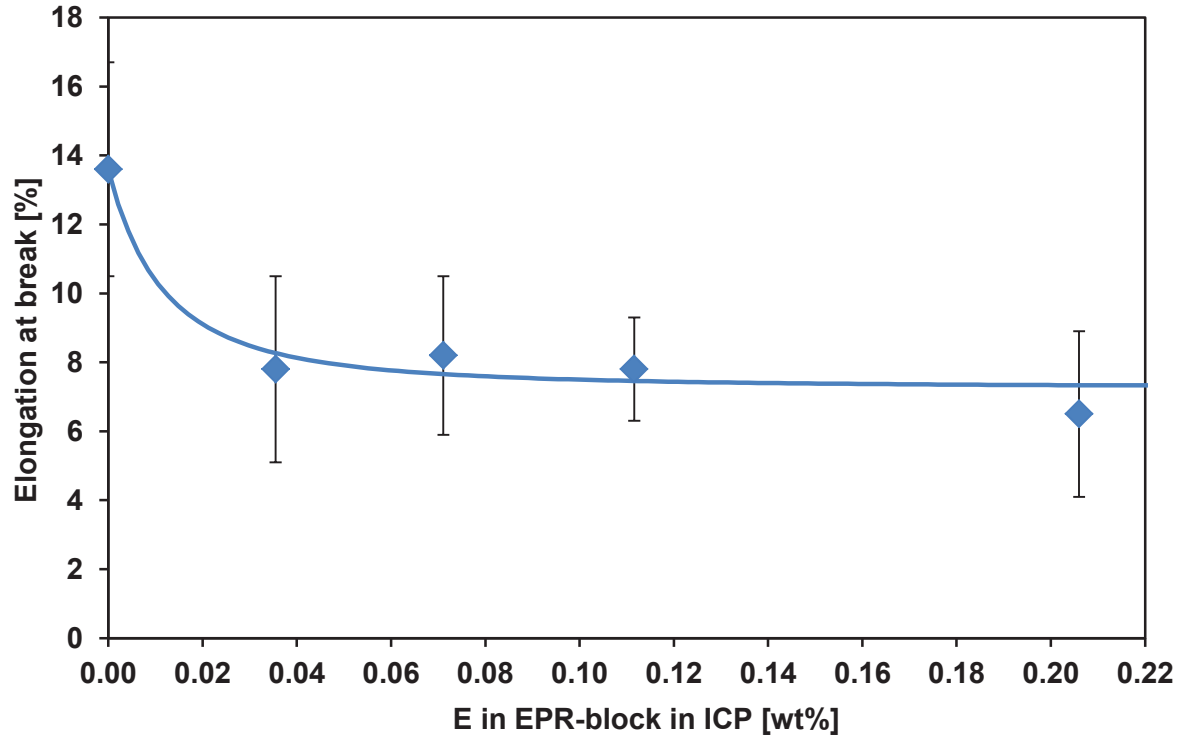

Figure 67: Dependence of elongation at break on the amount of ethylene in the PP-block-EPR copolymer added to the ICP.

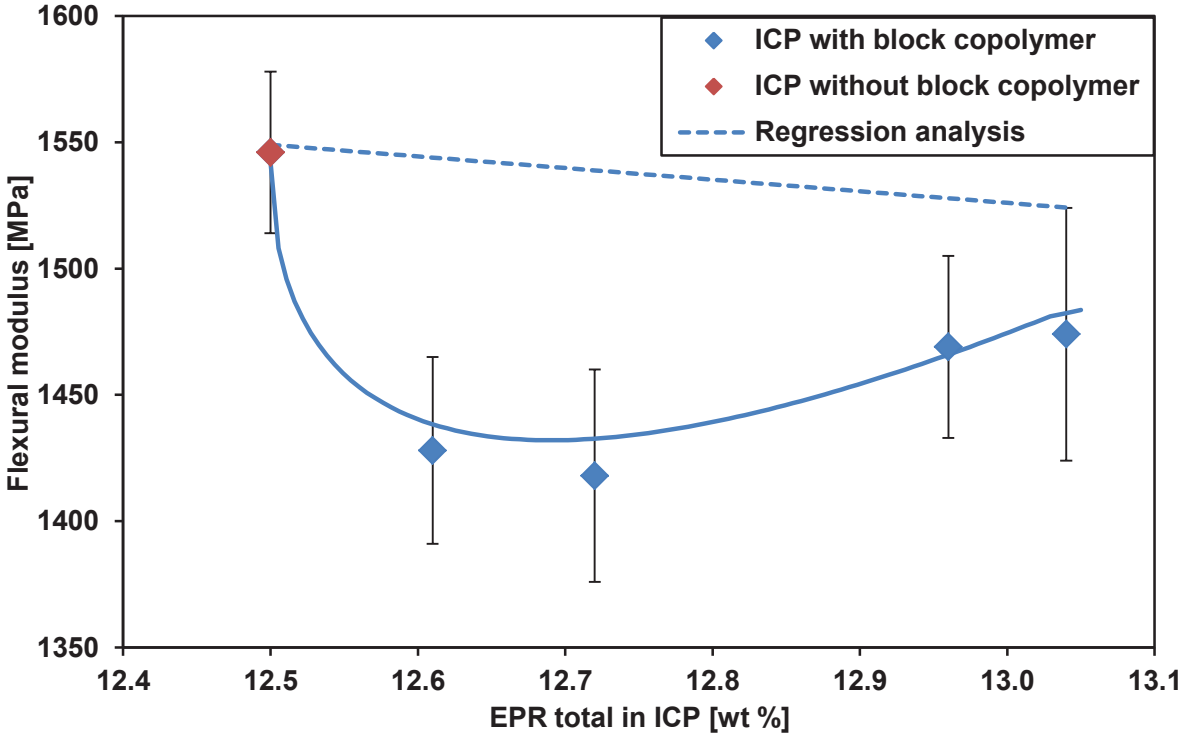

Figure 68: Dependence of flexural modulus on the total amount of EPR in the ICP including EPR added together with block copolymer. The dashed line indicates the profile of dependence for the standard type of ICP evaluated from the regression analysis.

5 CONCLUSION

The main objective of this work was to construct a unique high pressure stopped-flow apparatus enabling polymerization in very short polymerization times on a commercial $MgCl_2$/phthalate/$TiCl_4$ catalyst. The stopped-flow technique enables the performing of polymerization in a shorter time than the average lifetime of the growing polymer chain, which ensures that the states of active sites are not significantly influenced by time-dependent changes and chain-transfer reactions.

The first part of the experimental study was focused on the homopolymerization of propylene. It was found that polymerization time was in the range of 0.10 - 0.35 s and the polymerization exhibits “quasi-living” character.

This is important for the synthesis of well-defined PP-*block*-EPR copolymers. The apparatus also enabled the production of sufficient amounts of materials for characterizing and subsequent blending with ICP. The very short polymerization times applied in stopped-flow capillary reactors ensured that the active sites of a Ziegler-Natta catalyst produced polymer chains consisting of a block of semi-crystalline polypropylene homopolymer and a block of amorphous random copolymer. The block copolymerization was performed mainly with an ethylene comonomer, but polymerizations with 1-butene were also performed for comparison.

It was found that the copolymerization of propylene with ethylene and 1-butene apparently differs in activity. Catalyst activity in the copolymerization of ethylene is more than four times higher than in the copolymerization of 1-butene. It is a well-known fact that the 1-butene molecule is apparently less reactive than the ethylene molecule, and therefore 1-butene incorporation into the polymer chain is noticeably slower.

Copolymer materials synthesized in the stopped-flow apparatus with ethylene comonomer were fractionated by preparative TREF. The fractions obtained were subsequently analysed by the DSC, ^{13}C-NMR and GPC methods. These analyses revealed the presence of incorporated ethylene, also in the crystalline fraction (100 – 140 °C), presumably bonded to homopolymer crystalline chains which brought the macromolecules to the crystallizable fractions. This finding confirmed that a significant portion of polymer chains produced in the stopped-flow polymerization were real block copolymers consisting of semi-crystalline PP homopolymer and amorphous-to-partially crystalline EPR copolymer in one polymer chain.

The three samples with a known quantity and quality of composition were blended in a melt with a commercial ICP material.

The differences in EPR domain morphology and placement in the PP matrix were studied by SEM as shown **Chapter 4.3.2**. The obvious influence of the PP-*block*-EPR copolymer on ICP properties was observed mainly in the morphological changes of the EPR domains dispersed in the PP matrix. It was found that the original ICP sample contains a significant portion of EPR domains smaller than 0.5 μm. Conversely, in the case of ICP samples blended with PP-block-EPR copolymers, mainly EPR domains with sizes bigger than 0.5 μm were observed in the samples. The average domain size d50 of the EPR domains of all the ICP samples

with added block copolymers have a d50 ca. four times higher in comparison with the original ICP.

The results of oscillation rheology (**Chapter 4.3.3)** and Dynamic-mechanical analysis (**Chapter 4.3.4)** show relatively small differences among all the studied samples. The higher modulus observed in the case of ICP samples containing added PP-block-EPR copolymers could be related to “increasing” molar mass upon block copolymer addition and the subsequently increasing amount of “tangled” macromolecules upon real block addition or to presence of further iPP, which was added together with the PP-block-EPR copolymer and which caused some nucleation effect due to its very high molar mass.

However, no difference was observed between the samples with the addition of the block copolymers K8x and K10x with different contents of iPP as shown in Table 12 (65 wt. % vs. 84 wt. %). Thus, it can be assumed that the presence of the block copolymer PP-block-EPR increases the modulus of the mixture also at temperatures below Tg of iPP.

The reference ICP material and the ICP blends, which contained defined amounts of PP-*block*-EPR copolymers prepared in stopped-flow polymerization, were used for the preparation of test specimens for the determination of mechanical properties (**Chapter 4.3.5**). The ICP samples with added PP-block-EPR copolymer exhibited a flexural modulus noticeably lower in comparison with the original ICP. It was found that addition of a small amount of the PP-block-EPR copolymer caused an obvious decrease in flexural modulus by ca. 120 MPa. A further increase in the PP-block-EPR copolymer in ICP did not cause any further decrease in flexural modulus.

The Charpy notched impact strength was measured at -20 °C and the results indicate its steep increase with the increasing content of the PP-block-EPR copolymer. Addition of a small amount of the PP-block-EPR copolymer increased the Charpy notched impact strength more than five times. The increase of the notched impact strength is in accordance with the decrease of the flexural modulus. The greater toughness of the ICP material with added PP-block-EPR copolymer was also confirmed by the elongation at break dependence. The elongation at break decreases by 43 % by adding a small amount of PP-block-EPR copolymer. Based on the model, it was found that changes in mechanical properties were not caused simply by the addition of the amorphous phase of EPR to the sample of commercial ICP.

6 REFERENCES

1 Liu, B.; Matsuoka H.; Terano, M.: Stopped-Flow Techniques in Ziegler Catalysis. *Macromol. Rapid Commun*., 2001, vol. 22, pp. 1-24

2 Kissin, Y.V.: Multicenter Nature of Titanium-Based Ziegler-Natta Catalysts: Comparison of Etylene and Propylene Polymerization Reactions. *Journal of Polymer Science, Part A: Polym. Chem.*, 2003, vol. 41, pp. 1745-1758

3 Liu, B.; Matsouka, H.; Terano, M.: Kinetic Investigation of Propene Polymerization with Stopped-Flow Method. *Macromol. Symp*., 2001, vol. 165, pp. 3-10

4 Mori, H.; Yamahiro, M.; Terano, M.; Takahashi, M.; Matsukawa, T.: Lifetime of growing polymer chain in stopped-flow propene polymerization using pre-treated Ziegler catalysts. *Macromol. Chem. Phys*., 2000, vol. 201, pp. 289-295

5 McKenna, T. F. L.; Tioni, E.; Ranieri, M. M.; Alizadeh, A.; Boisson, Ch.; Monteli, V.: Catalytic olefin polymerisation at short times: Studies using specially adapted reactors. *The Canadian Journal of Chcemical Engeneering*, 2013, vol. 91, pp. 669-686

6 Lui, B.; Nitta, T.; Nakatani, H.; Terano, M.: Precise Arguments on the Distributuon of Stereospecific Active Sites on $MgCl_2$-Supported Ziegler-Natta Catalysts. *Macromol. Symp*., 2004, vol. 213, pp. 7-18

7 Keii, T.; Terano, M.; Kimura, K.; Ishii, K.: A kinetic argument for a quasi-living polymerization of propene with a $MgCl_2$-supported catalyst. *Makromol. Chem. Rapid Commun*., 1987, vol. 8, pp. 583

8 Chance, B: The accelerated flow method for rapid reactions. *J. Franklin Inst*., 1940, vol. 229. pp. 737–766

9 Yamahiro, M.; Mori, H.; Nitta, K.; Terano, M.: Synthesis and basic characteristics of polypropene-block-poly(ethene-co-propene) by modified stopped-flow polymerization with an $MgCl_2$-supported Ziegler catalyst. *Macromol. Chem. Phys*., 1999, vol. 200, pp. 134–141

10 Terano, M.; Kataoka, T.: A Kinetic Study of Propene Polymerization using $MgCl_2$-supported Catalysts. *Makromol.Chem. Rapid Commun*., 1989, vol. 10, pp. 97-102

11 Di Martino, A.; Weickert, G.; McKenna, T. F. L.: Contributions to the Experimental Investigation of the Nascent Polymerisation of Ethene on Supported Catalysts, 1. A Quenched-Flow Apparatus for the Study of Particle Morphology and Nascent Polymer Properties. *Macromol. React. Eng*., 2007, vol. 1, pp. 165–184

12 Chien, J.W.C.; Weber, S.; Hu, Y.: Magnesium Chloride Supported Catalysts for Olefin Polymerization. XIX. Titanium Oxidation States, Catalyst Deactivation and Active Site Structure. *Journal of Polymer Science*, Part A: Polym. Chem., 1989, vol. 27, pp. 1499-1514

13 Busico, V.; Corradini, P.; Ferraro, A.: Propene Polymerization in the Presence of $MgCl_2$-supported Ziegler-Natta Catalysts, 3 – Catalyst Deactivation. *Makromol. Chem*., 1986, vol. 187, pp. 1125-1130

14 Kissin, Y.V.; Rishina, L.A.: Kinetics of Propylene and Ethene Polymerization Reactions with Heterogeneous Ziegler-Natta Catalysts: Recent Results. *Polym. Sci. Series A*, 2008, vol. 50, pp. 1101-1121

15 Kissin, Y.V.; Zhou, Q; Li, H.; Zhang, L.: Active centers in propylene polymerization catalysts of the fourth generation. *Journal of Catalysis*, 2015, vol. 332, pp. 156-163

16 Kissin, Y.V.; Mink, R.I.; Nowlin, T.E.: Ethene Polymerization Reaction with Ziegler-Natta Catalysts. I. Ethene Polymerization Kinetics and Kinetic Mechanism. *Journal of Polymer Science, Part A: Polym. Chem*. 1999, vol. 37, pp. 4255-4272

17 Thushara, K.S.; Ajithkumar, T.G.; Rajamohanaa, P.R.; Gopinath, C.S.: Structural investigations of porous $MgCl_2$–2-butanol molecular adduct as support for olefin polymerization. *Applied Catalysis A: General*, 2014, vol. 469, pp. 267-274

18 Ko, Y.S., Jeon, J.-K.: The Effect of the Composition of Heterogeneous Polymerization Catalyst on Ethene-1-butene Copolymerization. *Catalysis Today*, 2008, vol. 132, pp. 178–181

19 Han-Adebekun, G. C.; Hamba, M.; Ray, W. H.: Kinetic Study of Gas Phase Olefin Polymerization with a TiCl4/MgCl2 Catalyst I. Effect of Polymerization Conditions. *Journal of Polymer Science Part A: Polymer Chemistry*, 1997, vol. 35, pp. 2063-2074

20 Cui, N.; Ke, Y.; Lu, Z.; Wu, Ch.; Hu, Y.: Structure and Properties of Polypropylene Alloy In Situ Blends. *Journal of Applied Polymer Science*, 2006, vol. 100, pp. 4804-4810

21 Shimizu, F., Pater, J.T.M., van Swaaij, P.M., Weickert, G.: Kinetic Study of a Highly Active $MgCl_2$-Supported Ziegler-Natta Catalyst in Liquid Pool Propylene Polymerization. II. The Influence of Alkyl Aluminum and Alkoxysilane on Catalyst Activation and Deactivation. *Journal of Applied Polymer Science*, 2002, vol. 83, pp. 2669-2679

22 Septälä, J.V.; Auer, M.: Factors Affecting Kinetics in Slurry Type Coordination Polymerization. *Prog.Polym. Sci.*, 1990, vol. 15, pp. 149

23 Luo, Z.-H., Wang, W., Su, P.-L.: Modeling of the Propylene Polymerization Catalyzed by Single-/Multi-Active Site Catalyst: A Monte Carlo Study. *Journal of Applied Polymer Science*, 2008, vol. 110, pp. 3360-3367

24 Kissin, Y.V., Rishina L. A., Hydrogen Effects in Propylene Polymerization Reactions with Titanium-Based Ziegler-Natta Catalysts. I. Chemical Mechanism of Catalyst Activation. *Journal of Polymer Science, Part A: Polym. Chem*., 2002, vol. 40, pp. 1353-1365

25 Mori, H., Endo, E., Tashino, K., Terano, M.: Study of Activity Enhancement by Hydrogen in Propylene Polymerization using Stopped-flow and Conventional Metods. *J. Mol. Catal. A: Chem*., 1999, vol. 145, pp. 153-158

26 Busico, V., Cipullo, R., Polzone, C., Talarico, G.: Propene/ethene-[1-13C] Copolymerization as a Tool for Investigating Catalyst Regioselectivity, 2 – The $MgCl_2/TiCl_4$-AlR_3 System. *Macromolecules*, 2003, vol. 36, pp. 2616-2622

27 Chadwick, J.C., Miedema, A., Sudmeijer, O., Hydrogen Activation in Propene Polymerization with MgCl2-supproted Ziegler-Natta Catalysts: The Effect of the External Donor. *Macromol. Chem. Phys*., 1994, vol. 195, pp. 167-172

28 Vestberg, T., Denifl, P., Parkinson, M., Wilén, C.E.: Effects of External Donors and Hydrogen Concentration on Oligomer Formation and Chain End Distribution in Propylene Polymerization with Ziegler-Natta Catalysts. *Journal of Polymer Science, Part A: Polym. Chem*., 2010, vol. 48, pp. 351-358

29 Guyot, A., Spitz, R., Dassaud, J., Gomez, C.: Mechanism of Deactivation and Reactivation of Ziegler-Natta Catalysts for Propene Polymerization. *J. Mol. Catal*., 1993, vol. 82, pp. 29-36

30 Nejad, M.H.; Ferrari, P.; Pennini, G.; Cecchin, G.: Ethylene Homo- and Copolymerization Over MgCl2-TiCl4 Catalysts: Polymerization Kinetics and Polymer Particle Morphology. *Journal of Applied Polymer Science*, 2008, vol. 108, pp. 3388-3402

31 Dusseault J.J.A.; Hsu, Ch.C.J.: $MgCl_2$-Supported Ziegler-Natta Catalysts for Olefin Polymerization: Basic Structure, Mechanism, and Kinetic Behavior. *Journal of Macromolecular Science, Part C: Polymer Reviews*, 1993, vol. 33, pp. 103-145

32 Lim, S.Y., Choung, S.J.: Studies on the Catalytic Deactivation in Propylene Polymerization. *Appl. Catal. A, General I*, 1997, vol. 153, pp. 103-118

33 Kissin, Y.V.: Main Kinetic Features of Ethene Polymerization Reactions with Heterogeneous Ziegler-Natta Catalysts in the Light of a Multicenter Reaction Mechanism. *Journal of Polymer Science, Part A: Polym. Chem*., 2001, vol. 39, pp. 1681-1695

34 Spitz, R., Masson, P., Bobichon, Ch., Guyot, A.: Propene Polymerization with $MgCl_2$ Supported Ziegler Catalysts: Activation by Hydrogen and Ethene*. Makromol. Chem.*, 1988, vol. 189, pp. 1043-1050

35 Meshkova, I.N., Ushakova, T.M., Gul´tseva, N.M.: The Nature of the Promoting Effect of Propylene on Ethene Polymerization over Supported Ziegler-Natta Catalysts. *Polimery,* 1998, vol. 43, pp. 243-246

36 Matsko, M.A., Echevskaya, L.G., Zakharov, V.A., Nikolaeva, M.I., Mikenas, T.B., Vanina, M.P.: Study of Multi-Site Nature of Supported Ziegler-Natta Catalysts in Ethene-Hexene-1 Copolymerization. *Macromol. Symp*., 2009, vol. 282, pp. 157–166

37 Debling, J.A.; Ray, W.H.: Morphological Development of Impact Polypropylene Produced in Gas Phase with a TiCl4/MgCl2 Catalyst: *Journal of Applied Polymer Science*, 2001, vol. 81, pp. 3085-3106

38 Albizzati, E., Giannini, U., Collina, G., Noristi, L., Resconi, L.: Catalysts and Polymerizations, Chapter 2: *Polypropylene Handbook*, Part I., Edited by Moore E.P., Munich: Hanser Publishers: 1996. 419 p. ISBN 3-446-18176-8

39 Kissin, Y.V.: *Isospecific Polymerization of Olefins with Heterogeneous Ziegler-Natta Catalyst*, Springer-Verlager New York Inc.: 1985. 371 p. ISBN 0-387-96105-4

40 Bozik, J.E., Vogel, R.F., Kissin, Y.V., Beach, D.L.: Metallophosphate-Supported Ziegler-Natta Catalysts for Ethene Polymerization, *Journal of Applied Polymer Science*, 1984, vol. 29, pp. 3491-3497

41 Czaja, K., Novokshonova, L.A., Kovaleva, N.J.: Deactivation of Oxide-supported Titanium Catalysts in the Ethene Polymerization Process. *Macromol. Chem. Phys*., 1999, vol. 200, pp. 983-988

42 Skoumal, M.: *Characterization of MgCl2-supported Catalyst and Initial Kinetics Determination in Low-pressure Propene Polymerization*. Ph.D. Thesis. Enschede: University of Twente: 2007. 98 p., ISBN: 978-90-365-2522-0.

43 Al-Haj Ali, M., Betlem, B., Roffel, B., Weickert, G.: Hydrogen response in liquid propylene polymerization: Towards a generalized model. *AIChEJ*, 2006, vol. 52, pp. 1866-1876

44 Maddikeri, R. R., *Characterization of Self-Assembled Functional Polymeric Nanostructures: I. Magnetic Nanostructures from Metallopolymers II. Zwitterionic Polymer Vesicles in Ionic Liquid*: 2013, Dissertations. 694 p. (http://scholarworks.umass.edu/open_access_dissertations)

45 Lodge, T. P.: Block Copolymers: Past Successes and Future Challenges. *Macromol. Chem. and Phys*., 2003, vol. 204, pp. 265–273

46 Ruzette A.V., Leibler L.: http://www.nature.com/nmat/journal/v4/n1/abs/nmat1295.html - a1#a1, L.: Block copolymers in tomorrow's plastics. *Nature Materials*, 2005, vol. 4, pp. 19-31

47 Hamley, I.W., *The Physics of Block Copolymers*. Oxford University Press, 1.edition, 1999, 432 p. ISBN: 9780198502180

48 Lecommandoux, S.; Lazzari, M.; Lui, G.: *An Introduction to Block Copolymer Applications: State-of-the-art and Future Developments: Block Copolymers in Nanoscience*, Edited by Massimo Lazzari, Guojun Liu, and Sébastien Lecommandoux: 2006, WILEY-VCH Verlag, 451 p. ISBN: 978-3-527-31309-9

49 Semenov, A. N.: Contribution to the theory of microphase layering in block-copolymer melts: *Sov. Phys. JETP*, 1985, vol. 61, pp. 733-742

50 He, W-N; Xu, J-T.: Crystallization assisted self-assembly of semicrystalline block copolymers. *Progress in Polymer Science*, 2012, vol. 37, pp. 1350– 1400

51 Soto-Figueroa, C.; Vincente, L.; Rodríguer-Hidalgo, M.R: Thermal Study on Phase Transitions of Block Copolymers by Mesoscopic Simulation, Chapter 22 in *Advances in Chemical Engineering* Edited by Dr Zeeshan Nawaz ISBN 978-953-51-0392-9 Hard cover, 584 pages Publisher InTech Published online 23, March, 2012 Published in print edition March, 2012

52 O'Mahony C. T.; Farrell, R. A.; Goshal, T.; Holmes, J. D.; Morris, M. A.: The Thermodynamics of Defect Formation in Self-Assembled Systems, Chapter 13 in *Thermodynamics - Systems in Equilibrium and Non-Equilibrium* Edited by Dr. Juan Carlos Moreno PirajÃ¡n ISBN 978-953-307-283-8 Hard cover, 306 pages Publisher InTech Published online 10, October, 2011 Published in print edition October, 2011

53 Karger-Kocsis, J.: *Polypropylene structure, blends and composites, vol. 1: Structure and Morphology*, Chapman & Hall, London: 1995. 345 p. ISBN 0-421-58430-1

54 Danesi, S.; Porter, R. S.: Blends of isotactic polypropylene and ethylene-propylene rubbers: rheology, morphology and mechanics. *Polymer*, 1978, vol. 19, pp. 448–457

55 Katayama, K.; Tanase, S.; Ishihara, N.: Considerations on detailed analysis and particle growth in high impact polypropylene particles. *Journal of Applied Polymer Science*, 2011, vol. 122, pp. 632–638

56 Galli P, Haylock J.C: Advances in Ziegler-Natta polymerization - unique polyolefin copolymers, alloys and blends made directly in the reactor. *Makromolekulare Chemie. Macromol.Symp*., 1992, vol. 63, pp. 19-54

57 Xue, Y.; Fan, Y.; Bo, S.; Ji, X.: Characterization of the microstructure of impact polypropylene alloys by preparative temperature rising elution fractionation. *European Polymer Jurnal*, 2011, vol. 47, pp. 1646-1653

58 Chen, Y., Chen, Y., Chen, W., Yang, D.C.: Multilayered Core-Shell Structure of the Dispersed Phase in High-Impact Polypropylene. *Journal of Applied Polymer Science*, 2008, vol. 108, pp. 2379-2385

59 D'Orazio L.; Mancarella, C.; Martuscelli E.; Cecchin, G.; Corrieri, R.: Isotactic polypropylene/ethylene-co-propylene blends: effects of the copolymer microstructure and content on rheology, morphology and properties of injection moulded samples. *Polymer*, 1999, vol. 40, pp. 2745-2757

60 Caballero, M. J.; Suarez, I.; Coto, B.; Grieken, R.; Monrabal, B: Synthesis and Characterization of Ethylene/Propylene Copolymers in the Whole Composition Range. *Macromol. Symp*., 2007, vol. 257, pp. 122-130

61 Jing, T.; Chen, H.; Ning, Y.; Kuang, D.; Qu, G.: Study on morphology of high impact polypropylene prepared by in situ blending. *Journal of Applied Polymer Science*, 2006, vol. 101, pp 1386-1390

62 Tong, C; Chen, Y; Chen, Y; Zhang, X; Yang, D; Zhang, J.: Mass transfer resistance in the production of high impact polypropylene. *Polymer*, 2008, vol. 49, pp. 2974-2978

63 Chen, Y., Chen, Y., Chen, W., Yang, D: Evolution of phase morphology of high impact polypropylene particles upon thermal treatment. *Eur. Polym. J*., 2007, vol. 43, pp. 2999-3008

64 Zhang, Ch., Shangguan, Y., Chen, R., Wu, Y., Chen, F., Zheng, Q, Hu, G.: Morphology, microstructure and compatibility of impact polypropylene copolymer. *Polymer*, 2010, vol. 51 pp. 4969-4977

65 Song, S., Feng, J., Wu, P., Yang Y.: Shear-Enhanced Crystallization in Impact-Resistant Polypropylene Copolymer: Influence of Compositional Heterogeneity and Phase Structure. *Macromolecules*, 2009, vol. 42, pp. 7067–7078

66 Remerie, K.; Groenewold, J.: Morphology formation in polypropylene impact copolymers under static melt conditions: A simulation study. *Journal of Applied Polymer Science*, 2012 vol. 125, pp. 212-223

67 Jang, B. Z., Uhlmann, D.R., Vander Sande, J.B.: Rubber-toughening in polypropylene. *Journal of Applied Polymer Science,* 1985 vol. 30, pp. 2485-504.

68 Mahdavi, H.; Nook, M. E.: Structure and morphology of a commercial high-impact polypropylene in-reactor alloy synthesized using a spherical Ziegler–Natta catalyst. *Polym Int.*, 2010; vol. 59, pp. 1701–1708

69 Mirabella, F. M.: Impact polypropylene copolymers: fractionation and structural characterization. *Polymer,* 1993, vol. 34, pp. 1729-1735

70 Nitta, K-H; Shin, Y-W; Hashiguchi, H.; Tanimato, S.; Terano, M.: Morphology and mechanical properties in the binary blends of isotactic polypropylene and novel

propylene-co-olefin random copolymers with isotactic propylene sequence 1. Ethylene–propylene copolymers. *Polymer*, 2005, vol. 46, pp. 965-975

71 Fan, Z.; Zhang, Y.; Xu, J.; Wang, H.; Feng, L: Structure and properties of polypropylene/poly(ethylene-co-propylene) in-situ blends synthesized by spherical Ziegler-Natta catalyst. *Polymer*, 2001, vol. 42, pp. 5559-5566

72 Tong, C; Lan, Y; Chen, Y; Chen, Y; Yang, D; Yang, X: The functions of crystallizable ethylene-propylene copolymers in the formation of multiple phase morphology of high impact polypropylene. *Journal of Applied Polymer Science*, 2012, vol. 123, pp. 1302-1309

73 Hongjun, C; Xiaolie, L; Dezhu, M; Jianmin, W; Hongsheng, T.: Structure and Properties of Impact Copolymer Polypropylene. I. Chain Structure. *Journal of Applied Polymer Science*, 1999, Vol. 71, pp 93-101

74 Tan, H-S.; Yu Y-Z.; Zhao, L-Y.; Sun, H-Q.: Composition Ascription Analysis of Disperse Phases for Impact Polypropylene Copolymers. *Polymer-Plastics Technology and Engineering*, 2012, vol. 51, pp. 71-74

75 Cheruthazhekatt, S.; Pijpers, T. F. J.; Harding, G. W.; Mathot, V. B. F, Pasch, H: Compositional Analysis of an Impact Polypropylene Copolymer by Fast Scanning DSC and FTIR of TREF-SEC Cross-Fractions. *Macromolecules*, 2012, vol. 45, pp. 5866-5880

76 Cheruthazhekatt, S.; Pijpers, T. F. J.; Harding, G. W.; Mathot, V. B. F, Pasch, H: Multidimensional Analysis of the Complex Composition of Impact Polypropylene Copolymers: Combination of TREF, SEC-FTIR-HPer DSC, and High Temperature 2D-LC. *Macromolecules*, 2012, vol. 45, pp. 2025-2034

77 Tian Z.; Gu, X-P; Feng, L-F; Fan, Z-Q; Hu, G-H: An Atmosphere-Switching Polymerization Process: A Novel Strategy to Advanced Polyolefin Materials. *AIChE Journal*, 2013, vol. 59, pp. 4468-4473

78 Song, S., Feng, J., Wu, P.: Relaxation of shear-enhanced crystallization in impact-resistant polypropylene copolymer: Insight from morphological evolution upon thermal treatment. *Polymer*, 2010, vol. 51, pp. 5267-5275

79 Fu, Z.; Fan, Z.; Zhang, Y.; Xu, J.: Chain structure of polyethylene/polypropylene in-reactor alloy synthesized in gas phase with spherical Ziegler–Natta catalyst. *Polym Int.*, 2004, vol. 53, pp.1169-1175

80 Hongjun; C; Xiaolie; Xiangxu, CH.; L; Dezhu, M; Jianmin, W; Hongsheng, T.: Structure and Properties of Impact Copolymer Polypropylene. II. Phase Structure and Crystalline Morphology. *Journal of Applied Polymer Science*, 1999, Vol. 71, pp. 103-113

81 Tan, H.; Li, L.; Chen, Z.; Song, Y.; Zheng, Q.: Phase morphology and impact toughness of impact polypropylene copolymer. *Polymer,* 2005, vol. 46, pp. 3522-3527

82 Mahdavi, H.; Nook, M. E.: Commercial, high-impact polypropylenes: Composition and chain structure as revealed by temperature-gradient extraction fractionation. *Journal of Applied Polymer Science*, 2012, vol. 125, pp. 1606-1615

83 Tian, Z.; Feng, L-F.; Fan, Z-Q; Hu, G-H: Ethylene−Propylene Segmented Copolymer as an in Situ Compatibilizer for Impact Polypropylene Copolymer: An Assessment of Rheology and Morphology. *Ind. Eng. Chem. Res*., 2014, vol. 53, pp. 11345-11354

84 Nitta, K-H, Kawada, T., Yamahiro, M., Mori, H., Terano, M.: Polypropylene-block-poly(ethene-co-propylene) addition to polypropylene/poly(ethene-co-propylene) blends: morphology and mechanical properties. *Polymer*, 2000, vol. 41, pp. 6765-6771

85 Mori, H.; Yamahiro, M.; Prokhorov, V. V., Nitta, K; Terano, M.: High-Pressure Stopped-Flow Polymerization for Polypropene-block-poly(ethene-co-propene) Having Controlled Molecular Weight: Synthesis and Characterization. *Macromolecules*, 1999, vol. 32, pp. 6008-6018

86 Nitta, K-H; Kawada, T.; Prokhorov, V. V.; Yamahiro, M.; Mori, H.; Terano, M.: Characterization and Properties of Polypropylene-block-poly(ethylene-co-propylene) Synthesized by Short-PeriodPolymerization. *Journal of Applied Polymer Science*, 1999, vol. 74, pp. 958-964

87 Yamahiro M.; Mori, H; Nitta, K.; Terano, M.: Electron donor-induced improvement of the microstructure of polypropene-block-poly(ethene-co-propene) synthesized by a modified stopped-flow polymerization method and correlation with its crystalline morphology. *Polymer,* 1999, vol. 40, pp. 5265-5275

88 Cao, M.; Xu, J-T; Dong, Q.; Fu, Z-S; Fan, Z-Q: Crystallization Kinetics and Morphology of iso-PP/Ethylene-propylene-b-copolymer/ Ethylene-propylene-r-copolymer Ternary Blends. Iranian Polymer Jurnal, 2009, vol. 18, pp. 373-382

89 Chen, R.; Shangguan, Y.; Zhang, Ch.; Chen, F.; Harkin-Jones, E.; Zheng, Q.: Influence of molten-state annealing on the phase structure and crystallization behaviour of high impact polypropylene copolymer. *Polymer*, 2011, vol. 52, pp. 2956-2963

90 Feng, Z.; Dong, L.; Zhang, B.; Fang, Z.; Yang, Y: Investigation of PP-EPR diblock copolymer as compatibilizer for PP/EPT Blend. *Polymer Communications*, 1985, vol. 3, pp. 216-225

91 Yamahiro, M; Miyata, H.; Nitta, K-H: Compatibility of binary blends of polypropylene with ethylene-α-olefin copolymer. *Journal of Applied Polymer Science*, 1996, vol. 62, pp. 87-97

92 Di Martino S., Kelchtermans M.: Determination of the composition of ethylene–propylene–rubbers using ^{13}C-NMR spectroscopy. *Journal of Applied Polymer Science*, 1995, vol. 56, pp. 1781-1787

93 Kakugo, M.; Naito, Y.; Mizunuma, K.; Miyatake, T.: Carbon-13 NMR determination of monomer sequence distribution in ethylene-propylene copolymers prepared with δ-titanium trichloride-diethylaluminum chloride. *Macromolecules*, 1982, vol. 15, pp. 1150-1152

94 Randall, J.C.: Sequence distributions versus catalyst site behavior of in situ blends of polypropylene and poly(ethylene-*co*-propylene). *Journal of Polymer Science Part A*, 1998, vol. 36, pp. 1527-1542

95 Bicerano J.: Crystallization of Polypropylene and Poly(Ethylene Terephthalate). *J. Macromol. Sci. – Rev. In Macromol. Chem. and Phys.*, 1998, vol. C38, pp. 391

96 Teng, H.; Shi, Y. Jin, X.: Novel characterization of the crystalline segment distribution and its effect on the crystallization of branched polyethylene by differential scanning calorimetry. *Journal of Polymer Science Part B: Polymer Physics,* 2002, vol. 40, pp. 2107-2118

97 Sterzynski, T.: *Lamella dimension and distribution: Polypropylene: An A-Z Reference*, Edited by Karger-Kocsis, J., Springer Netherlands: Kluwer Academic Publishers: 1999, 966 p., ISBN 978-94-010-5899-5

98 Bond, E.B.; Spruiell, J.E.: The effects of atacticity, comonomer content, and configurational defects on the equilibrium melting temperature of monoclinic isotactic polypropylene. *Journal of Applied Polymer Science*, 2001, vol. 81, pp. 229-236

99 Clark, E.J.; Hoffman, J.D.: Regime III crystallization in polypropylene. *Macromolecules*, 1984, vol. 17, pp 878-885

100 Varga, J.; Ehrenstein, G.W.: *Beta-modification of isotactic polypropylene*: Polypropylene: An A-Z Reference, Edited by Karger-Kocsis, J., Springer Netherlands: Kluwer Academic Publishers: 1999, 966 p., ISBN 978-94-010-5899-5

101 Tochaček, J.; Jančář, J.; Kalfus, J.; Zbořilová, P.; Buráň, Z.: Degradation of polypropylene impact-copolymer during processing. *Polymer Degradation and Stability*, 2008, vol. 93, pp. 770-775

102 Edwards, M.C: *Gammadot Rheology Testing & Consultancy Services*. Available from: http://www.gammadot.com/

103 Gregor, T., *Experimental investigaton of morphology and thermodynamics of polymeric systems*. 2012, UCT Prague.

104 Gregor, T., et al., *Correlating Micro-CT Imaging with Quantitative Histology*, in *Injury and Skeletal Biomechanics*, T. Goswami, Editor. 2012, InTech.

105 Romans, L.E., *Computed Tomography for Technologists: A Comprehensive Text*. 2010.

106 Ketcham, R.A.; C. W.D., Acquisition, optimization and interpretation of X-ray computed tomographic imagery: applications to the geosciences. *Computed Geoscience*, 2001. Vol. 27: pp. 381–400.

107 Smolná, K; .Gregor, T.; Kosek, J.: Morphological analysis of high-impact polypropylene using X-ray microCT and AFM. *European Polymer Journal*. 2017, vol. 49, pp. 3966-3976

108 Smolná, K; .Gregor, T., Buráň, Z.; Kosek, J.: Formation and Distribution of Rubbery Phase in High Impact Poly(propylene) Particles. *Macromol. Mater. Eng*., 2016, vol. 301, pp. 390−400

109 Calvao, P.S.; Yee, M.; Demarquette, N.R.: Effect of composition on the linear viscoelastic behavior and morphology of PMMA/PS and PMMA/PP blends. *Polymer*, 2005, vol. 46, pp. 2610−2620

110 Graebling, D.; Muller, R.; Palierne, J.: Linear viscoelastic behavior of some incompatible polymer blends in the melt. Interpretation of data with a model of emulsion of viscoelastic liquids. *Macromolecules*, 1993, vol. 26, pp. 320−329

111 Buráň, Z.: *Příprava modelových blokových kopolymerů a jejich vliv na morfologii a vlastnosti* HI PP - Annual Research Report 2014 for the Project TA03011394: PIB: 19.1.2015

112 Keii T., Suzuki E., Tamura M., Murata M., Doi Y.: Propene polymerization with a magnesium chloride-supported ziegler catalyst, 1. Principal kinetics. *Makromol. Chem.*, 1982 vol. 183, pp. 2285-2304

113 Duca, D.D.; Moore, E.P.: *End-Use Properties, Chapter 6: Polypropylene Handbook, Part I.*, Edited by Moore E.P., Munich: Hanser Publishers: 1996. 419 p. ISBN 3-446-18176-8

114 Grůza, J.: *Příprava nových typů polypropylenu na základě reaktorového modelování polymeračního procesu* - Final Research Report for the Project FR-TI1/140: PIB: 30.6.2013

7 LIST OF SYMBOLS AND ABBREVIATIONS

7.1 ABBREVIATIONS:

BCC	– body-centred cubic conformation	
BCP	– block copolymer	
BPR	– butene-propylene rubber	
C2	– ethylene	
C3	– propylene	
Cat.	– catalyst	
DBP	– di-*i*-butyl phthalate	
DTMA	– Dynamic Mechanical Analysis	
DSC	– Differential Scanning Calorimetry	
E	– ethylene	
EB	– ethylene-1-butene copolymer	
EbP	– ethylene-propylene block copolymer	
ED	– external donor	
EH	– ethylene-1-hexene copolymer	
EPR	– ethylene-propylene random copolymer	
EsP	– ethylene-propylene segmented copolymer	
F_a	– xylene insoluble fraction	
F_b	– xylene soluble fraction	
FT-IR	– Fourier transform infrared spectroscopy	
g	– gas phase	
GPC/SEC	– gel permeation chromatography / size exclusion chromatography	
ICP	– impact copolymer polypropylene	
iPP	– isotactic polypropylene	
MFR	– melting flow rate	[g/10min]
MWD	– molecular weight distribution	
NMR	– nuclear magnetic resonance	
P	– Propylene	
PE	– polyethylene	
PP-b-EPR	– polypropylene – block-poly(propylene-co-ethylene) block copolymer	
PTFE	– Polytetrafluoroethylene	
RC	– content of EPR in ICP	
RCC2	– content of ethylene in EPR copolymer	[wt. %]
SF	– stopped-flow	
SEM	– Scanning electron microscope	
SSA	– Successive Self-nucleation Annealing	
TEA	– triethylaluminium	
TEM	– Transmission electron microscopy	
TREF	– temperature rising elution fractionation	
X.S.	– xylene soluble	
ZN	– Ziegler-Natta	
µ-CT	– Computer micro-tomography	

7.2 SYMBOLS:

[A]	– equilibrium concentration of alkylaluminium	[mol/L]
C*	– number of active sites	[mol. %]

C_i^*	– number of i-type active sites	[mol. %]
f_A	– volume fractions of block A	
f_B	– is volume fractions of block B	
G	– Gibbs free energy	
G'	– elastic modulus	[Pa]
G"	– viscous modulus	[Pa]
H	– enthalpy	
H_u, H_i	– heats of fusion for repeating monomer unit	[J.cm^{-3}]
k	– Boltzmann constant	[J/K]
k_a	– activation rate constant	[1/h]
k_d	– deactivation rate constant of active site	[1/h]
k_{di}	– deactivation rate constant of i-type active site	[1/h]
k_{ds}	– deactivation rate constant of stable active sites	[1/h]
k_p	– propagation rate constant	[L/(mol*s)]
K_A	– equilibrium adsorption constant for alkylaluminium	[L/mol]
K_M	– equilibrium adsorption constant for monomer	[L/mol]
K_D	– deactivation constant	[mmol-Ti/m^3]
[M]	– concentration of monomer	[mol/L]
M_n	– number-average molar mass	[g/mol]
M_w	– weight-average molar mass	[g/mol]
M_w/M_n	– polydispersity index	
n	– order of active site deactivation	
N	– degrees of polymerisation of the all block macromolecule	
N_A	– degrees of polymerisation of the block A	
N_B	– degrees of polymerisation of the block B	
p	– pressure	[Pa]
PI	– polydispersity index	
Q_i	– quantity of segment length	[mol/g]
r	– reactivity ratios	
R	– gas constant	[J/K*mol]
R_p	– polymerization rate	[g-PP/(mmol-Ti*h)]
R_{pi}	– polymerization rate of i-type of active site	[g-PP/(mmol-Ti*h)]
$R_p(0)$f	– initial polymerization rate of unstable active site	[g-PP/(mmol-Ti*h)]
$R_p(0)$s	– initial polymerization rate of stable active site	[g-PP/(mmol-Ti*h)]
S	– entropy	
t	– time	[s]
T	– temperature	[°C]
T_g	– glass-transition temperature	[°C]
$T_{m,I}$	– melting temperature	[°C]
V_m	– molar volume	[m^3/mol]
w	– energy	
Y	– polymer yield	[g]
z	– number of neighbouring chains surrounding one block	

7.3 GREEK LETTERS:

δ	– Hildebrand solubility parameter	[Mpa$^{1/2}$]
Δ	– exchange of parameter	
η	– viscosity	[Pa.s]

η^*	– complex viscosity	[Pa.S]
λ	– number-average dispersed phase of growing chains	
ρ	– density	[g/cm^3]
ρ_c	– density of crystals	[g/cm^3]
σ_e	– basal surface energy of polymer crystals	[mJ/m^2]
τ	– average lifetime of growing polymer chain	[s]
χ	– Flory-Huggins interaction parameter	